# The Effects of Polymer Concentration on Turbulent Drag Reduction

# 聚合物濃度對湍流減阻的影響

LEUNG, Chung Yin

梁頌賢

A Thesis Submitted in Partial Fulfilment

of the Requirements for the Degree of

Master of Philosophy

in

Physics

The Chinese University of Hong Kong

August 2011

Thesis/Assessment Committee

Professor CHU, Ming Chung (Chair)
Professor CHING, Shuk Chi Emily (Thesis Supervisor)
Professor LEUNG, Pui Tang (Committee Member)
Professor BENZI, Roberto (External Examiner)

Abstract of thesis entitled:

The Effects of Polymer Concentration on Turbulent Drag Reduction

Submitted by LEUNG, Chung Yin

for the degree of Master of Philosophy

at The Chinese University of Hong Kong in August 2011

In 1948 the phenomenon of turbulent drag reduction by polymers was discovered [B. Toms, Proc. Int'l Rheological Congress 2, 135 (1948)]. It was found that the addition of a small amount of polymers can significantly reduce the frictional drag in wall-bounded turbulent flows. The reduction in drag is characterized by an increase in the fluid throughput under fixed applied pressure gradient, or equivalently, a smaller pressure gradient is required to drive the flow at the same flow rate. This phenomenon has been studied extensively in the past decades but a theory that can give predictions was proposed only recently [I. Procaccia, V.L. L'ov, and R. Benzi, Rev. Mod. Phys. 80, 225 (2008)]. This theory is based on the balance of momentum and energy, and shows that the effect of the polymers can be represented by a position-dependent effective viscosity.

In this thesis, we work out further predictions of this theory that can be tested by experiments. In particular, we have worked out the various effects of polymer concentration for both flexible and rodlike polymers. We have

focused on the pipe geometry for easy comparison with experiments. We have calculated the relation of the friction factor with the Reynolds number and studied how this relation changes with the zero shear viscosity of the polymer solution. The zero-shear viscosity of the polymer solution depends on the concentration of the polymers in the solvent. Using additional experimental knowledge of the concentration dependence of viscosity, we have found how the friction factor relation changes with concentration for the rodlike polymer xanthan gum. We have also calculated how the Reynolds stress profile varies with the concentration of the polymer. Our results reveal a linear dependence of the maximum Reynolds stress on the position of the maximum. This linear dependence is a new theoretical prediction, which can be tested experimentally. We have found that the viscosity dependence of the percentage drag reduction at different Reynolds numbers can be collapsed into a universal curve with different functional forms for flexible and rodlike polymers. We have also compared our results with experimental observations.

# 概要

聚合物湍流減阻這現象於1948年在實驗中被發現 [B. Toms, Proc. Int'l Rheological Congress 2, 135 (1948)]。實驗顯示在液體中添加少量的聚合物可以顯著降低壁面湍流中的摩擦阻力。阻力的減少體現在固定的壓力梯度下流體總平均 流速的增加，或可以更小的壓力梯度來達到同一平均流速。這個現象在過去幾十年被廣泛研究，但有預測性的理論到了最近才被提出[I. Procaccia, V.L. L'ov, and R. Benzi, Rev. Mod. Phys. 80, 225 (2008)]。這理論是基於動量和能量的平衡，並顯示了聚合物的效果可以由一個與位置相關的有效粘度(effective viscosity)來表示。

本論文的目的是用這理論計算出進一步的預測性結果，以求與實驗數據比較。我們已計算出聚合物濃度對柔性和剛性聚合物在湍流減阻的影響。我們的計算集中在管道流方面，以便於與實驗比較。我們計算了摩擦系數(friction factor)與雷諾數的關係和研究這種關係如何隨著聚合物溶液的零剪切粘性改變。聚合物溶液的零剪切粘性與聚合物濃度有關。我們利用實驗量度的粘性與濃度關係求出黃原膠(xanthan gum)溶液裡濃度對摩擦系數的影響。我們還計算了雷諾應力隨位置與聚合物濃度的變化，我們的結果揭示了雷諾應力的最大值與達到最大值的位置符合線性關係。這種線性關係是一個可以被實驗測試的新的理論預測。我們發現在不同雷諾數之下百分比減阻與溶液粘度的關係經過適當的座標轉換之後可以用單一的曲線來描述，而且柔性和剛性聚合物的曲線具有不同的函數形式。我們並將得到的結果與實驗數據比較。

# Acknowledgements

I would like to thank my supervisor, Prof. Emily S. C. Ching for her invaluable support and useful suggestions.

This work is dedicated to all the people who have worked diligently on the highly challenging problem of turbulence.

# Contents

# List of Figures

# Chapter 1

# Introduction

## 1.1 The phenomenon of polymer drag reduction

The phenomenon of polymer drag reduction was discovered in experiment by Toms in 1948 [1]. It was found that the addition of a small amount of polymer can reduce the frictional drag in wall-bounded turbulent flow by up to 80%. Consider the turbulent flow of a fluid in a long pipe of radius $R$. The frictional drag is quantified by the friction factor $f$,

$$f \equiv \frac{\Delta p R}{\rho U_{av}^2 l} \tag{1.1}$$

where $\Delta p$ is the pressure drop across a length $l$ of the pipe, $\rho$ is the fluid density and $U_{av}$ is the bulk velocity averaged over the cross-section of the pipe.

$$U_{av} = \frac{1}{\pi R^2} \int_0^R V(y) 2\pi (R - y) dy \tag{1.2}$$

Here $y$ is the distance from the wall and $V(y)$ is the time average velocity profile.

A drop in the pressure gradient required to drive the flow at a fixed average velocity would mean a decrease in the friction factor. Alternatively, an increase in the average velocity under a fixed pressure gradient would also cause a decrease in the friction factor. While drag reduction was observed originally for flexible polymer, it was later found that rodlike polymers also exhibit such a drag reducing property. In Fig. 1.1, the experimental friction factors of flexible polymers at different concentrations are plotted in the coordinates $1/\sqrt{f}$ against $Re\sqrt{f}$ called the Prandtl-Karman coordinates [2]. The Reynolds number $Re$ is defined using the bulk velocity,

$$Re = \frac{2U_{av}R}{\nu} \tag{1.3}$$

where $\nu$ is the solvent viscosity.

A decrease in the friction factor compared to the Newtonian case without polymer is seen. The amount of drag reduction increases with the polymer concentration and approaches a Maximum Drag Reduction (MDR) asymptote. The experimentally reported friction factor relations of a rodlike polymer is shown in Fig. 1.2 [2].

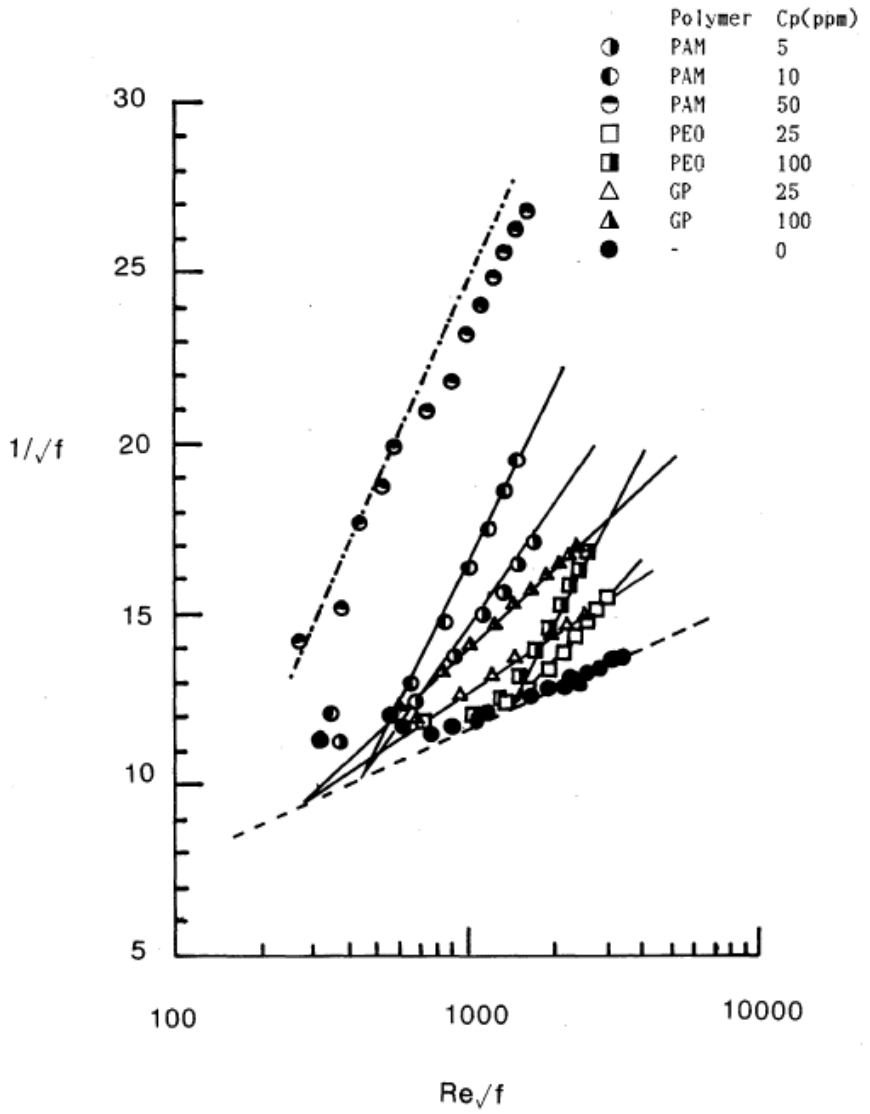


Figure 1.1: Experimental friction factor relation in Prandtl-Karman coordinates for flexible polymers. Taken from Ref. [2].

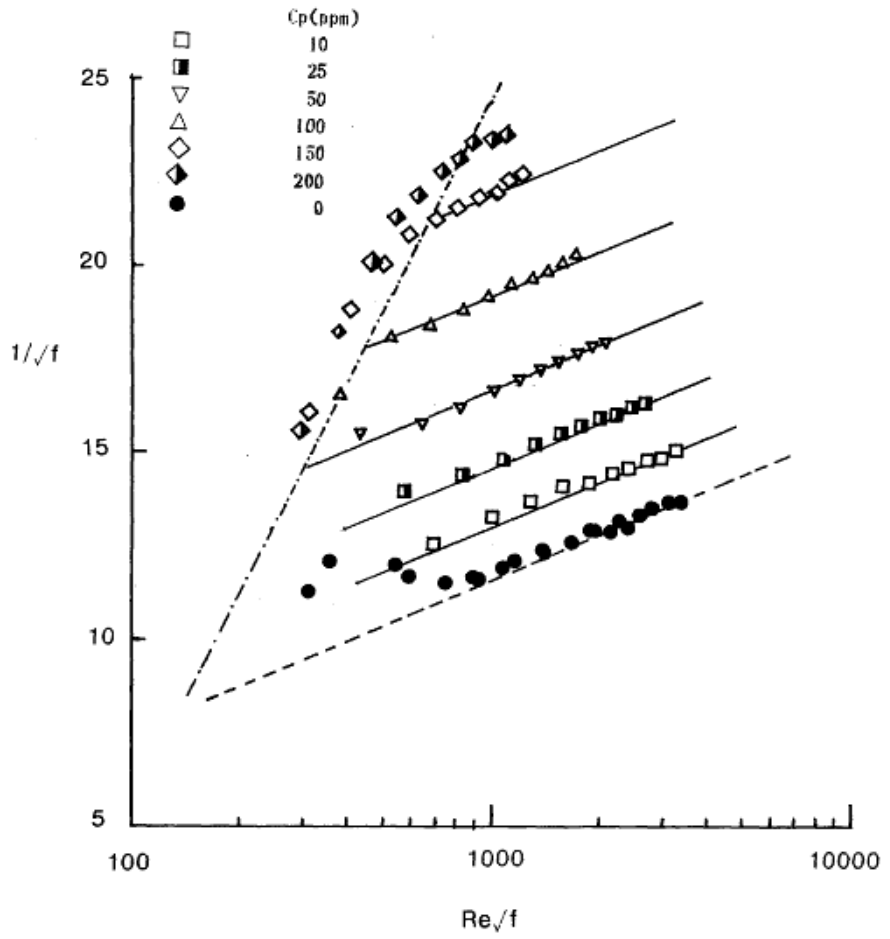


Figure 1.2: Experimental friction factor relation in Prandtl-Karman coordinates for a rodlike polymer. Taken from Ref. [2].

In general, the friction factor relations of flexible and rodlike polymers show different behaviors, but it has been reported in experiments that they approach the same Maximum Drag Reduction asymptote at high polymer concentrations [3]. In other words, there exists two experimentally reported asymptotes for which the drag reduction is bounded. Firstly, there is the Newtonian case without polymer, for which the friction factor relation is

given by the Prandtl-von Karman log law [4],

$$1/\sqrt{f} = 4.0\log(Re\sqrt{f}) - 0.4 \tag{1.4}$$

On the other hand, there is the MDR asymptote approached at high polymer concentration [4].

$$1/\sqrt{f} = 19.0\log(Re\sqrt{f}) - 32.4 \tag{1.5}$$

It has been reported in experiments that there are also log laws for the Newtonian velocity profile when there is no polymer and the MDR asymptote. For the Newtonian case without polymer, there is the von-Karman log law,

$$V^+(y^+) = \kappa_k^{-1}\ln y^+ + B \tag{1.6}$$

Here the velocity and distance from wall are given in terms of the dimensionless units defined using the solvent viscosity $\nu$ and the friction velocity $u_\tau = \sqrt{p' R/2\rho}$ where $p' = \Delta p/l$ is the pressure gradient.

$$y^+ \equiv \frac{yu_\tau}{\nu}, \qquad V^+ \equiv \frac{V}{u_\tau} \tag{1.7}$$

Quantity with the superscript "+" means that it is in the dimensionless unit where every length and velocity scales are normalized according to Eq. (1.7). The von Karman constant $\kappa_k$ and the intercept $B$ are known only through experiments and numerical simulations. The reported experimental values of the constants are $\kappa_k \approx 0.436$ and $B \approx 6.13$ [5]. For the MDR asymptote, there is another log law,

$$V^+(y^+) = \kappa_v^{-1}\ln y^+ + B' \tag{1.8}$$

The Virk constant $\kappa_v$ and the intercept $B'$ have been obtained using Eqs.

(1.1), (1.2) and the experimental relation Eq. (1.5), yielding $\kappa_v^{-1} \approx 11.7$ and $B' \approx -17.0$ [4].

For intermediate polymer concentration, there is no universal log law for the friction factor relation or the mean velocity profile as they depend on the polymer concentration. Experimentally it has been reported that log laws also exist in this regime, with different forms for flexible and rodlike polymers [2, 6]. For flexible polymer, the following log law is reported.

$$1/\sqrt{f} = (4.0 + D)\log(Re\sqrt{f}) + A \tag{1.9}$$

where the slope increment $D$ and the intercept $A$ are constants that depend on the concentration. This type of behavior is illustrated in Fig. 1.1 which has a fan-like structure. For rodlike polymers, the log law was found to be of the following form.

$$1/\sqrt{f} = 4.0\log(Re\sqrt{f}) - 0.4 + \delta \tag{1.10}$$

Here the effective slip $\delta$ is a function of concentration. In Fig. 1.2 the ladder-like feature can be seen. The slope increment $D$ and effective slip $\delta$ have been found to have power law relationships with the concentration [2, 6, 7].

$$D \sim c^{\omega} \tag{1.11}$$

$$\delta \sim c^{\phi} \tag{1.12}$$

There is no general consensus on the value of the scaling exponents $\omega$ and $\phi$ in experiments. For example, Virk found that [6, 7],

$$\omega = 0.5 \tag{1.13}$$

$$\phi = 1 \tag{1.14}$$

On the other hand, Sasaki reported that [2],

$$\omega = 0.80 \tag{1.15}$$

$$\phi = 0.72 \tag{1.16}$$

Apart from the friction factor, another quantity of interest is the Reynolds stress $W$. It is the stress caused by the turbulent fluctuations of fluid momentum and will be defined in Chapter 2. The Reynolds stress has been measured as a function of the distance from wall in experiments [8, 9]. Figure 1.3 shows a typical Reynolds stress profile, an overall decrease in the Reynolds stress can be seen as the concentration is raised. This is in agreement with the theoretical understanding that the MDR asymptote is an edge solution between turbulent and laminar flow [10]. However, currently there is little theoretical prediction on the shape of the Reynolds stress profile and how it depends on concentration. In this thesis we will derive a new prediction on the concentration dependence of the Reynolds stress profile.

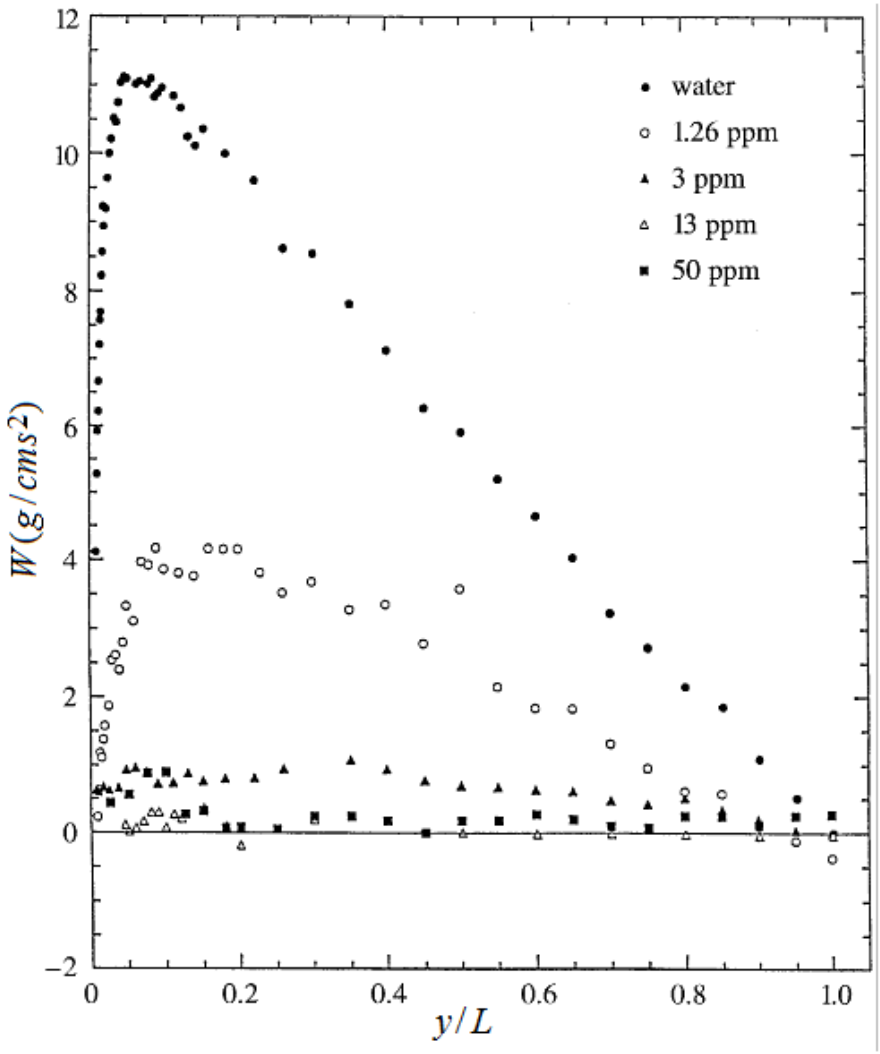


Figure 1.3: Experimental Reynolds stress profile in channel flow at various concentrations for Percol 727, a flexible copolymer of polyacrylamide (PAM) and sodium acrylamide. $L$ is the channel half width. Taken from Ref. [8].

In Section 1.2 of this chapter, some early phenomenological ideas will be reviewed. These ideas concern mainly on understanding the onset of drag reduction and the MDR asymptote. A recent theory of turbulent drag reduction by polymers and the basis of our work will be outlined in Section

1.3. The theory is based on the balance of momentum and energy and shows that the effect of the polymers can be represented by a position-dependent effective viscosity. In Chapter 2 we review the theory and apply it to pipe flow. We use the theory to carry out a systematic study of the concentration dependence of the phenomenon. Our results are presented in Chapters 3 to 7. We have calculated the relation of the friction factor with the Reynolds number and studied how this relation changes with the zero shear viscosity of the polymer solution. The zero-shear viscosity of the polymer solution depends on the concentration of the polymers in the solvent. Using additional experimental knowledge of the concentration dependence of viscosity, we have found how the friction factor relation changes with concentration for the rodlike polymer xanthan gum. We have also calculated how the Reynolds stress profile varies with the concentration of the polymer. Our results reveal a linear dependence of the maximum Reynolds stress on the position of the maximum. This linear dependence is a new theoretical prediction, which can be tested experimentally. We have found that the viscosity dependence of the percentage drag reduction at different Reynolds numbers can be collapsed into a universal curve with different functional forms for flexible and rodlike polymers. We have also compared our results with experimental observations. Besides, we have also revisited the MDR asymptote and shown analytically the reduction of drag in the limit of small concentrations. In Chapter 8 we finish with some concluding remarks and suggestion for future work.

## 1.2 The Phenomenology of drag reduction

Early attempts at understanding polymer drag reduction mainly involve phenomenological descriptions of interactions between the turbulent eddies and the polymer. These ideas focused on understanding the onset and MDR of

drag reduction, but do not describe the detailed mechanism of how the interaction would give rise to drag reduction. Two phenomenological frameworks have been proposed by Lumley and De Gennes, with the former focusing on a comparison of time scales and the latter involving the elastic energy of the polymer. Both frameworks are applicable only to flexible polymers but not rodlike polymers as they rely on the relaxation time and elastic properties of the polymer, which is irrelevant in the case of rodlike polymers.

Lumley proposed [11] that the polymer would be affected by the flow only if the characteristic timescale of the turbulent eddies becomes smaller than the polymer relaxation time. This is known as the Lumley time criterion, Lumley argued that only if this condition is satisfied would the polymer become significantly stretched.

$$\tau_p > T_{flow} \tag{1.17}$$

where $\tau_p$ is the relaxation time of the polymer and $T_{flow}$ is the characteristic time scale of turbulence. For simplicity, assume that there is only one polymer relaxation time given by the Zimm relaxation time,

$$\tau_p = T_Z \equiv \frac{\eta_0 R_G^3}{k_B T} \tag{1.18}$$

where $\eta_0$ is the solvent viscosity, $R_G$ the radius of gyration of the polymer coil, and $k_B T$ the typical thermal energy of the system. On the other hand, the turbulent flow time scale at a length scale $r$ is estimated by dimensional analysis as in the usual phenomenology of turbulence [12].

$$T_{flow} = \frac{r}{U(r)} \tag{1.19}$$

where $U(r)$ is the typical velocity at the length scale $r$, and is related to the energy dissipation rate $\epsilon$ and $r$ by,

$$U(r) = (r\epsilon)^{1/3} \tag{1.20}$$

Eqs. (1.19) and (1.20) implies that $T_{flow} \sim r^{2/3}$, therefore the turbulent time scale decreases when the length scale of turbulence is decreased, so this time criterion holds for all length scales smaller than a certain scale $r^*$ at which the time scale of turbulence equals the polymer relaxation time.

$$\frac{r^*}{U(r^*)} = T_Z \tag{1.21}$$

When the time criterion is satisfied, the stretched polymer produces a significant increase in elongational viscosity [13, 14, 15]. Lumley argued that the increased elongational viscosity would then reduce the drag by suppressing the turbulent fluctuations and increasing the thickness of the buffer layer. However, it is yet unknown how the suppression of turbulent fluctuations or the increased buffer layer thickness may contribute to the reduction in drag. The length scale $(r^*)^+$ is related to the Weissenberg number $We = u_\tau^2 T_Z/\nu$ and the distance from the wall $y^+$ by,

$$(r^*)^+ = \frac{We^{3/2}}{(y^+)^{1/2}} \tag{1.22}$$

The onset condition of drag reduction is understood as the requirement for the Weissenberg number to be sufficiently large such that $r^*$ exceeds the smallest turbulent length scale, making it possible for some eddies to satisfy the time criterion. In the phenomenology of turbulence, the smallest

turbulent length scale is estimated by the Kolmogorov scale defined as [12],

$$r_{kol} = (\frac{\nu^3}{\epsilon})^{1/4} \tag{1.23}$$

Using dimensional analysis, $\epsilon$ in the log layer is approximated as $u_\tau^3/y$. As such the Kolmogorov scale in the dimensionless unit is estimated as,

$$r_{kol}^+ = (y^+)^{1/4} \tag{1.24}$$

Therefore the Kolmogorov scale increases with the position $y^+$. Lumley assumed that the smallest $y^+$ that is relevant lies just outside the viscous sublayer and is of the order one. We remark that this assumption is not entirely obvious as the polymer may well have certain effects inside the viscous sublayer. Using this assumption, the onset condition is approximated by,

$$We \sim O(1) \tag{1.25}$$

Maximum drag reduction occurs when the polymer concentration is sufficiently large and the Weissenberg number is large enough for eddies of the largest size to satisfy the time criterion. In this case the following condition has to be satisfied,

$$We \approx Re_\tau \tag{1.26}$$

where $Re_\tau = R^+$ is the friction Reynolds number.

In the phenomenology of De Gennes [16], he identified the elastic property of the polymer as the major factor in drag reduction and suggested that the polymer would affect the energy cascade substantially only when its elastic energy becomes comparable to the turbulent kinetic energy. The idea is that this elastic energy criterion is more stringent than the time criterion,

and therefore will be the effective criterion for drag reduction. De Gennes used the following estimation of the elastic free energy per unit volume for a polymer in good solvents originally derived by Pincus [17].

$$F_{el} = c_p k_B T \lambda^{5/2} = G\lambda^{5/2} \tag{1.27}$$

where $c_p$ is the number concentration of the polymer, $G \equiv c_p k_B T$ and $\lambda$ is the fractional molecular elongation of the polymer. De Gennes further assumed $\lambda$ to be of the following form.

$$\lambda(r) = (\frac{r^*}{r})^n \tag{1.28}$$

where $n$ is an unknown parameter between 0 and 2.

At a certain length scale $r^{**}$, the elastic energy of the polymer would be equal to the turbulent kinetic energy estimated by $\rho U^2(r^{**})$.

$$G(\frac{r^*}{r^{**}})^{5n/2} = \rho U^2(r^{**}) \tag{1.29}$$

When the length scale decreases, the elastic energy increases and the turbulent kinetic energy $\rho U^2(r) \sim r^{2/3}$ decreases. Therefore the elastic energy would be higher than the turbulent energy for length scales smaller than $r^{**}$. Sreenivasan and White have applied the idea of De Gennes to pipe flow and derived the functional form of $r^{**}$ [18]. Using the estimate $\epsilon \approx u_\tau^3/y$ and Eqs. (1.20), (1.22) and (1.29), $r^{**}$ can be expressed as,

$$\begin{aligned} (r^{**})^+ &= (\frac{Gy^+}{\rho u_\tau^2 We})^\gamma [\frac{We^{3/2}}{(y^+)^{1/2}}] \\ \gamma &\equiv (5n/2 + 2/3)^{-1} \end{aligned} \tag{1.30}$$

The onset of drag reduction happens when $r^{**}$ is larger than the Kol-

mogorov scale given in Eq. (1.23). Since the elastic energy depends on the polymer concentration, $r^{**}$ is dependent on both the polymer concentration and Weissenberg number, and there will be an onset concentration for each Weissenberg number. This is in contrast to Lumley's result in which the onset depends only on the Weissenberg number. From Eqs. (1.24) and (1.30) it is seen that both $(r^{**})^+$ and $r^+_{kol}$ depends on $y^+$. Sreenivasan and White argued that the onset of drag reduction is given by the comparison of $(r^{**})^+$ and $r^+_{kol}$ at a constant $y^+$, yielding the following scaling relationship at onset.

$$\frac{G_0}{\rho u_\tau^2} \sim We^{1-3/2\gamma} \tag{1.31}$$

where $G_0$ is the value of $G$ at onset.

The scaling behavior in Eq. (1.31) has been fitted [18] to the available experimental data [18, 19, 20, 21] by using $\gamma$ as the fitting parameter in Fig. 1.4. The prediction of a power law according to Eq. (1.31) is reasonably satisfied, albeit with some variation in $\gamma$. The scaling exponent of $-5/2$ best captures the general trend of the experimental data shown, giving $\gamma \approx 3/7$ and therefore $n \approx 2/3$.

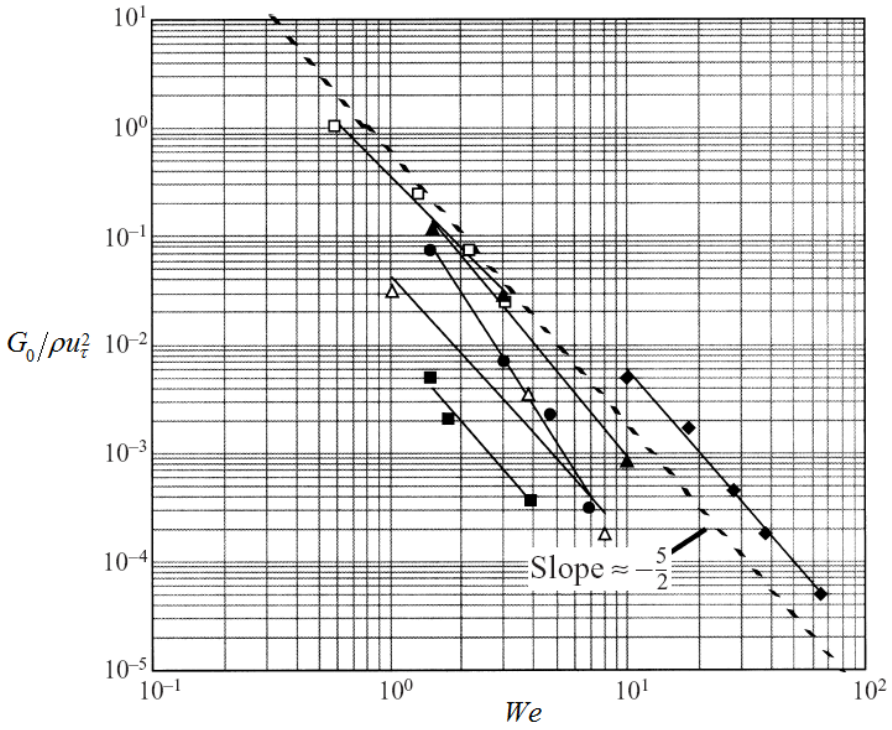


Figure 1.4: Available experimental data for $G_0/\rho u_\tau^2$ against $We$. The dashed line corresponds to a scaling exponent of $-5/2$. The data are from the following sources and with different number of monomers $N$. Nadolink [19]: $N = 6.1\times10^4$ (solid rhombus), $7\times10^4$ (solid triangle) and $2.3\times10^4$ (empty triangle); Berman [20]: $N = 1.4\times10^5$ (empty square); Patterson and Abernathy [21]: $N = 1.8\times10^5$ (solid circle); Sreenivasan and White [18]: $N = 1.1\times10^5$ (solid square). Figure taken from Ref. [18].

It was hypothesized that saturation at high concentration may happen at the critical concentration $c_m = 1/R_G^3$ at which the polymer coils start to touch each other.

$$G_m = c_m k_B T = k_B T/R_G^3 = \eta_0/T_Z \tag{1.32}$$

where Eq. (1.18) has been used. From the definition $We \equiv T_Z u_\tau^2/\nu_s$, the saturation condition is acquired.

$$\frac{G_m}{\rho u_\tau^2} = We^{-1} \tag{1.33}$$

where $G_m$ is the value of $G$ when the drag reduction approaches the MDR asymptote.

Sreenivasan and White has compared [18] Eq. (1.33) to experimental data [3, 7, 18, 21, 22, 23] of the MDR asymptote , with the results shown in Fig. 1.5. It seems to overestimate the concentration required for MDR.

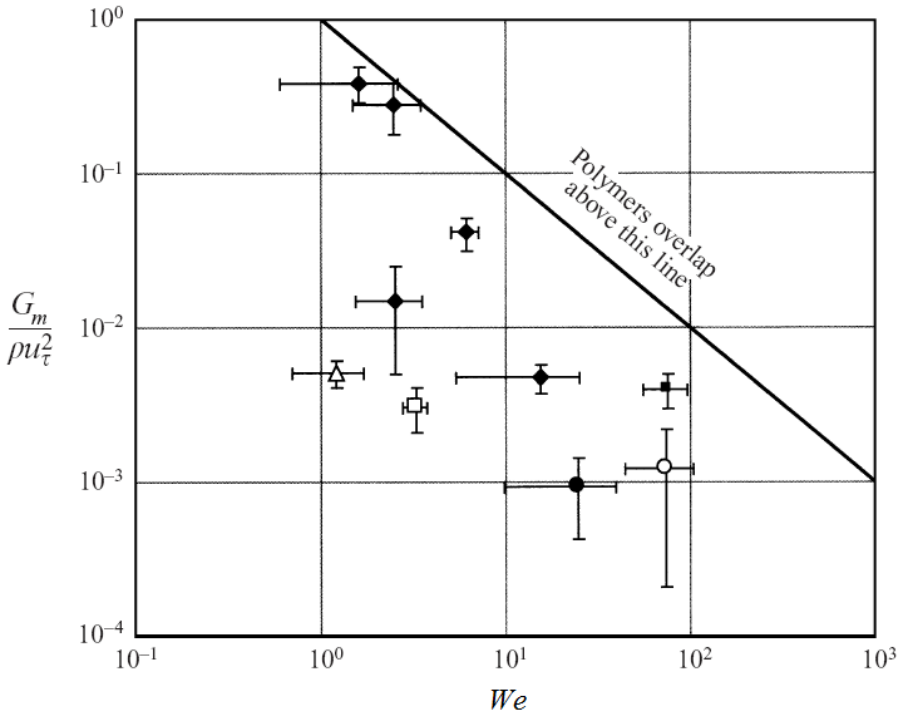


Figure 1.5: Experimental data for MDR asymptote with $G_m/\rho u_\tau^2$ against $We$. The straight line represents Eq. (1.33). The data are from the following sources: Sreenivasan and White [18] (empty triangle); Patterson and Abernathy [21] (empty square); Virk [3] (solid rhombus); Virk (virk1971b) [22]; Gampert and Wagner [23] (empty circle); Virk and Baher (virk1970) [7]. Figure taken from Ref. [18].

Lee and Akhavan has compared Eq. (1.33) to DNS data [24] as shown in Fig. 1.6 which also shows an overestimation. Based on the DNS results, Lee and Akhavan suggested that the saturation data has the following relationship instead,

$$\frac{G_m}{\rho u_\tau^2} = (1-\beta)We^{-1} \tag{1.34}$$

with $\beta = 0.98$.

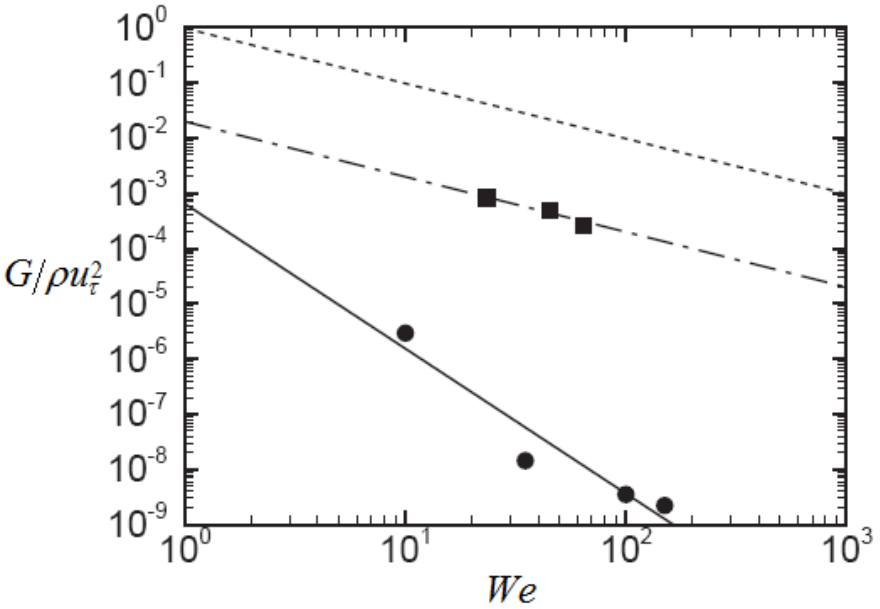


Figure 1.6: DNS data with $G_0/\rho u_\tau^2$ at onset (circle) and $G_m/\rho u_\tau^2$ at saturation (square) against $We$. The solid line is a fitting with $G_0/\rho u_\tau^2 \sim We^{-5/2}$. The dashed line is Eq. (1.33) and the dash-dotted line Eq. (1.34). Taken from Ref. .

Lee and Akhavan argued that based on the modeling of flexible polymers and some approximations, the MDR relationship in Eq. (1.34) can be obtained.

In this section we have reviewed some early phenomenological ideas. These ideas produced very limited predictions on the onset of drag reduction such as the power law relationship in Eq. (1.31), and have nothing concrete to say about the MDR asymptote. Furthermore, they have not explained how the reduction in drag can be brought about by the interaction between the polymer and the flow. Moreover, they are not directly applicable to rodlike polymers which are also known to reduce drag, and do not provide predictions for the velocity profile and friction factor. More recently, a theory

has been developed that can provide these predictions.

## 1.3 A recent theory

Recently, a theory has been developed for polymer drag reduction and has been applied to channel flow [25, 10, 26, 27, 28]. Starting from the Navier-Stokes equations with an additional contribution of stress from the polymer and approximating the polymer stress, it has been shown that two balance equations can be obtained by a procedure of Reynolds decomposition which decompose the velocity into the mean and fluctuating parts. The two balance equations correspond to the momentum and energy balance of the system. After applying appropriate approximations, it has been found that the effect of the polymer is given by a position dependent effective viscosity. The effect of polymer concentration is parametrized by the polymer contribution to the solution zero-shear viscosity. Analytical expressions have been obtained for the mean shear rate and the Reynolds stress for the Newtonian and MDR case, and have been shown to correspond to log laws as observed in experiments [25, 10]. Velocity profiles at intermediate concentrations have been calculated by solving the set of equations numerically [27].

Our work is to use the theory to conduct a systematic study of the concentration dependence of the phenomenon. Following the same ideas of the theory that has been used in the study of channel flow, we have applied the theory to pipe flow. Furthermore, earlier work [25, 28, 27] have focused on the region where the distance from the wall is much smaller than the width of the channel or in our case the radius of the pipe. In our present work one of the quantity of interest is the friction factor. To calculate this quantity, one has to integrate the mean velocity over the entire cross-section of the pipe. As a result, the term $y^+/R^+$ must be kept in the equations. Further-

more, in previous works the analytical expressions of the mean shear rate and Reynolds stress were given separately for the Newtonian case with no polymer and MDR limit. Using the theory, we have written a single set of explicit equations for the general case that will give back the Newtonian and MDR expressions when the appropriate limit is taken.

# Chapter 2

# Review of a recent theory of drag reduction

## 2.1 The balance equations

When polymers are added to the solvent, there is an additional stress tensor $\mathbf{\Sigma}$ contributed by the polymer. Therefore the equations of motion would be the Navier-Stokes equations with a polymer stress term $\Sigma$. The form of the polymer stress is not known exactly and has to be modeled.

$$\frac{\partial \mathbf{U}}{\partial t} + \mathbf{U}\cdot\nabla\mathbf{U} = -\nabla p + \nu\nabla^2\mathbf{U} + \nabla\cdot\mathbf{\Sigma} \tag{2.1}$$

where the fluid density $\rho$ is taken to be unity for simplicity.

It has been shown that the momentum and turbulent energy balance equations are important in understanding drag reduction [25]. The two balance equations will be derived in this section. Define $x$, $r$ and $\theta$ to be the lengthwise, radial and azimuthal directions. Therefore the radial distance from the wall is $y = R - r$. Let the $i-th$ component of the fluid velocity be

$U_i$. For a sufficiently long pipe, the velocity statistics depends only on the radial distance from the centre, $r$, or equivalently the distance from the wall $y$. In addition, the mean flow will be along the $x$ direction. As a result, the fluid velocity can be decomposed as the sum of its mean $V(y)$ and turbulent fluctuation $u_i(\mathbf{r}, t)$,

$$\mathbf{U}(\mathbf{r}, t) = V(y)\hat{\mathbf{x}} + \mathbf{u}(\mathbf{r}, t) \tag{2.2}$$

Such a procedure of decomposing a quantity into the mean and the fluctuation is called the Reynolds decomposition.

Likewise, the shear rate tensor $\mathbf{S} \equiv (\nabla \mathbf{U})^T$ and the polymer stress tensor $\mathbf{\Sigma}$ can be decomposed as,

$$\mathbf{S} = \mathbf{S_0} + \mathbf{s} \tag{2.3}$$

where $\mathbf{S_0} = S_0 \hat{\mathbf{x}}\hat{\mathbf{y}}$ with $S_0 = dV(y)/dy$

$$\mathbf{\Sigma} = \mathbf{\Sigma_0} + \sigma \tag{2.4}$$

Consider the continuity equation and the $x$ component Eq. (2.1),

$$\frac{\partial U_x}{\partial x} + \frac{1}{r}\frac{\partial}{\partial r}(rU_r) + \frac{1}{r}\frac{\partial U_\theta}{\partial \theta} = 0 \tag{2.5}$$

$$\frac{\partial U_x}{\partial t} + U_x\frac{\partial U_x}{\partial x} + U_r\frac{\partial U_x}{\partial r} + \frac{U_\theta}{r}\frac{\partial U_x}{\partial \theta} = -\frac{\partial p}{\partial x} + \nu\nabla^2 U_x + (\nabla \cdot \Sigma)_x \tag{2.6}$$

Before applying the Reynolds decomposition, rewrite Eq. (2.6) by the following three equations stemming from the product rule of differentiation,

$$U_x\frac{\partial U_x}{\partial x} = \frac{\partial U_x^2}{\partial x} - U_x\frac{\partial U_x}{\partial x} \tag{2.7}$$

$$\frac{U_\theta}{r}\frac{\partial U_x}{\partial \theta} = \frac{1}{r}\frac{\partial U_x U_\theta}{\partial \theta} - \frac{U_x}{r}\frac{\partial U_\theta}{\partial \theta} \tag{2.8}$$

$$U_r\frac{\partial U_x}{\partial r} = \frac{1}{r}\frac{\partial}{\partial r}(rU_xU_r) - \frac{U_x}{r}\frac{\partial}{\partial r}(rU_r) \tag{2.9}$$

As a result, Eq. (2.6) is rewritten as,

$$\begin{aligned}\frac{\partial U_x}{\partial t}+\frac{\partial U_x^2}{\partial x}+\frac{1}{r}\frac{\partial}{\partial r}(rU_xU_r) &+ \frac{1}{r}\frac{\partial U_xU_\theta}{\partial \theta}-U_x[\frac{\partial U_x}{\partial x}+\frac{1}{r}\frac{\partial U_\theta}{\partial \theta}+\frac{1}{r}\frac{\partial}{\partial r}(rU_r)] \\ &= -\frac{\partial p}{\partial x}+\nu\nabla^2U_x+(\nabla\cdot\Sigma)_x \end{aligned} \tag{2.10}$$

By Eq. (2.5), the last term on the LHS of Eq. (2.10) vanishes, giving

$$\frac{\partial U_x}{\partial t}+\frac{\partial U_x^2}{\partial x}+\frac{1}{r}\frac{\partial}{\partial r}(rU_xU_r)+\frac{1}{r}\frac{\partial U_xU_\theta}{\partial \theta}=-\frac{\partial p}{\partial x}+\nu\nabla^2U_x+(\nabla\cdot\Sigma)_x \tag{2.11}$$

Applying Reynolds decomposition to Eq. (2.5) and (2.11) and taking average, noting that the statistics depends only on $r$ (or equivalently $y=R-r$),

$$\frac{1}{r}\frac{\partial}{\partial r}(r\langle U_r\rangle)=0 \tag{2.12}$$

$$\frac{DV(r)}{Dt}=-\frac{\partial p}{\partial x}-\frac{1}{r}\frac{\partial}{\partial r}(r\langle u_xu_r\rangle)+\nu\nabla^2V(r)+(\nabla\cdot\Sigma)_x \tag{2.13}$$

where $\frac{D}{Dt}=\frac{\partial}{\partial t}+V(r)\frac{\partial}{\partial x}+\langle U_r\rangle\frac{\partial}{\partial r}$ and $V(r)=\langle U_x\rangle$. Equation (2.12) is equivalent to the condition that $r\langle U_r\rangle$ is a constant for all $r$. The no-slip boundary condition at the wall means that $R\langle U_r\rangle=0$ at the wall, therefore $\langle U_r\rangle=0$ for all $r$. As a result,

$$\frac{D}{Dt}=\frac{\partial}{\partial t}+V(r)\frac{\partial}{\partial x} \tag{2.14}$$

Plugging Eq. (2.14) into Eq. (2.13), it is evident that the LHS of Eq. (2.13) vanishes.

$$0=-r\frac{dp}{dx}-\frac{d}{dr}(r\langle u_xu_r\rangle)+\nu\frac{d}{dr}(r\frac{dV(r)}{dr})+\frac{\partial(r\langle\Sigma_{xr}\rangle)}{\partial r} \tag{2.15}$$

Equation (2.15) can be rewritten as,

$$r\frac{dp}{dx} = \frac{d(\tau(r)r)}{dr} \tag{2.16}$$

where the total shear stress $\tau(r) = -\langle u_x u_r \rangle + \nu(\frac{dV(r)}{dr}) + \langle \Sigma_{xr} \rangle$. Integrating Eq. (2.16) with respect to $r$, noting that $\tau(r = 0) = 0$ because it is anti-symmetric to the centre-line,

$$\tau(r) = \frac{r}{2}\frac{dp}{dx} \tag{2.17}$$

Therefore shear stress at the wall $\tau_w$ is,

$$\tau_w \equiv -\tau(R) = \frac{p^{'}R}{2} \tag{2.18}$$

Therefore in pipe flow, the friction velocity can also be written as,

$$u_\tau = \sqrt{\tau_w} \tag{2.19}$$

By integrating Eq. (2.15) with respect to $r$, the momentum balance equation is found,

$$\frac{p^{'}r}{2} = -\langle u_x u_r \rangle + \nu\frac{d}{dr}V(r) + \langle \Sigma_{xr} \rangle \tag{2.20}$$

Writing Eq. (2.20) in terms of the variable $y$ and defining the Reynolds stress $W \equiv -\langle u_x u_y \rangle$ and the mean shear rate $S_0 \equiv dV/dy$.

$$\nu S_0 + W + \langle \Sigma_{xy} \rangle = \frac{p^{'}R}{2}(1 - \frac{y}{R}) = \tau_w(1 - \frac{y}{R}) \tag{2.21}$$

The shear rate and the stresses can be transformed to dimensionless units

by rescaling all velocity and length scales according to Eq. (1.7),

$$\begin{aligned} S_0^+ &= \frac{\nu S_0}{u_\tau^2} \\ W^+ &= \frac{W}{u_\tau^2} \\ \Sigma_{ij}^+ &= \frac{\Sigma_{ij}}{u_\tau^2} \end{aligned} \tag{2.22}$$

In this set of dimensionless units, Eq. (2.21) is rewritten as,

$$S_0^+ + W^+ + \langle \Sigma_{xy}^+ \rangle = (1 - \frac{y^+}{Re_\tau}) \tag{2.23}$$

The energy balance eqaution can be obtained in a similar fashion. It can be derived by making a dot product with the velocity fluctuation **u** on both sides of Eq. (2.1) and then taking average. The result is given by,

$$\begin{aligned} WS_0 &= \frac{\partial}{\partial y}\langle \frac{u^2 u_y}{2} + u_y p - \sigma_{iy} u_i - \nu \partial_y (\frac{u^2}{2}) \rangle \\ &\quad + \nu \langle s_{ij} s_{ij} \rangle + \langle \sigma_{ij} s_{ij} \rangle \end{aligned} \tag{2.24}$$

where $s_{ij} = \partial_j u_i$.

The first term on the RHS of Eq. (2.24) is the spatial flux of the energy, and has been assumed to be negligible in the log layer.

$$WS_0 = \nu \langle s_{ij} s_{ij} \rangle + \langle \sigma_{ij} s_{ij} \rangle \tag{2.25}$$

The energy balance equation can also be written in dimensionless units.

$$W^+ S_0^+ = \langle s_{ij}^+ s_{ij}^+ \rangle + \langle \sigma_{ij}^+ s_{ij}^+ \rangle \tag{2.26}$$

The balance equations (2.23) and (2.26) forms the basis for further discus-

sions. In particular, it is necessary to estimate the relevant averaged terms $\langle \sigma_{xy}^{+} \rangle$, $\langle s_{ij}^{+} s_{ij}^{+} \rangle$ and $\langle \sigma_{ij}^{+} s_{ij}^{+} \rangle$. These approximations are described in Section 2.2.

## 2.2 Estimating the average terms

To proceed from the general balance equations (2.23) and (2.26), the average terms in these equations have to be estimated. Starting with non-polymeric terms, the first term on the RHS of the energy balance equation Eq. (2.25) is the viscous dissipation of the energy. The dissipation has been estimated [25] using the phenomenology of turbulence.

$$\nu \langle s_{ij} s_{ij} \rangle \sim \nu (\frac{a}{y})^2 K(y) + \frac{b K^{3/2}}{y} \tag{2.27}$$

where $K \equiv \langle |\mathbf{u}|^2 \rangle / 2$ is the turbulent kinetic energy. The first term in the RHS of Eq. (2.27) is the dissipation when the viscous effects are dominant. The second term is important when the Reynolds number is large and the flow is turbulent, where the viscous dissipation equals the turbulent energy flux down the cascade of scales and is approximated as the turbulent kinetic energy divided by the eddy turnover time $y/\sqrt{K}$.

The turbulent kinetic energy was experimentally found to be proportional to the Reynolds stress $W^{+}$,

$$K^{+} = \frac{W^{+}}{c^2} \tag{2.28}$$

Experiments have shown that $c$ has a value of around 0.5 for Newtonian flow without polymer and 0.25 for MDR flow [3, 9].

The difference between flexible and rodlike polymers will be accounted for when the average polymeric terms in equations (2.23) and (2.26) are

estimated [28, 26, 25, 29]. The treatments for flexible and rodlike polymers will be given in the following.

### 2.2.1 Average terms for flexible polymers

Flexible polymers are commonly modeled by the FENE-P model (Finitely Extensible Nonlinearly Elastic model with the Peterlin closure) [30], in which a polymer is approximated as a dumbbell connected by a Non-linearly Elastic spring that has a Finite maximum Extension. The P refers to the closure suggested by Peterlin. Denote $\mathbf{n}$ to be the end-to-end distance of the polymer normalized by the equilibrium length of the polymer. Then the conformation tensor describing the extent of stretching of the polymers is defined as,

$$\Re_{ab} \equiv \overline{n_a n_b} \tag{2.29}$$

where the average is carried out over the polymer conformations. The Peterlin function is defined as,

$$P(r,t) = (\rho_m^2 - 1)/(\rho_m^2 - \Re_{kk}) \tag{2.30}$$

where $\rho_m$ is the maximum value of the end-to-end length of the polymer. $\Re_{kk}$ is the end-to-end length of the polymer (the indices are summed over). In the FENE-P model, the components of the polymer stress tensor $\mathbf{\Sigma}$ is given by [30],

$$\Sigma_{ab} = \frac{\nu_p}{\tau_p}[P(r,t)\Re_{ab} - \delta_{ab}] \tag{2.31}$$

where $\nu_p$ is the polymeric contribution to the solution viscosity for infinitesimal shear and the average is over the turbulent fluctuations. It has been reported that in most numerical simulations $P\Re_{ab}$ is usually much greater

than one [28], therefore the polymer stress tensor can be approximated as,

$$\Sigma_{ab} \approx \frac{\nu_p}{\tau_p} P \Re_{ab} \tag{2.32}$$

The conformation tensor is governed by the following equation,

$$\frac{D}{Dt}\Re_{ab} = \frac{\partial U_a}{\partial r_k}\Re_{kb} + \Re_{ak}\frac{\partial U_b}{\partial r_k} - \frac{1}{\tau_p}[P(r,t)\Re_{ab}] \tag{2.33}$$

where $D/Dt$ is the substantial time derivative.

The term $\langle \Sigma_{xy} \rangle$ in the momentum balance Eq. (2.21) can be written in terms of the conformation tensor as,

$$\langle \Sigma_{xy} \rangle = \frac{\nu_p}{\tau_p} \langle P \Re_{xy} \rangle \tag{2.34}$$

By Eq. (2.34) and recalling that the statistics only depends on $y$, Eq. (2.33) can be averaged to give,

$$\langle P\Re_{xy} \rangle / \tau_p = -\partial_y \langle U_y \Re_{xy} \rangle + \langle \Re_{xk} \partial_k U_y \rangle + \langle \Re_{yk} \partial_k U_x \rangle \tag{2.35}$$

By approximating the average of the product as the product of the averages, the leading order term in Eq. (2.35) is given by,

$$\langle P\Re_{xy} \rangle = \tau_p S_0 \mathcal{R}_{yy} \tag{2.36}$$

where $\mathcal{R}_{ab} \equiv \langle \Re_{ab} \rangle$. It has been checked using DNS that when the Weissenberg number is large, the approximation is satisfactory [28].

Plugging this result back into Eq. (2.34), the averaged $xy$ component of

the polymer stress can be approximated.

$$\langle \Sigma_{xy} \rangle \approx \nu_p \mathcal{R}_{yy} S_0 \tag{2.37}$$

The momentum balance equation can then be expressed as,

$$(\nu + \nu_p \mathcal{R}_{yy}) S_0 + W = \tau_w (1 - \frac{y}{R}) \tag{2.38}$$

In dimensionless units, it reads

$$\nu_{eff} S_0^+ + W^+ = 1 - \frac{y^+}{R^+} \tag{2.39}$$

The effective viscosity $\nu_{eff}$ is given by,

$$\nu_{eff} = 1 + \tilde{\nu} \mathcal{R}_{yy} \tag{2.40}$$

where $\tilde{\nu} = \nu_p / \nu$.

Proceeding to the energy balance Eq. (2.25), the term $\langle s_{ij} s_{ij} \rangle$ has already been approximated in Eq. (2.27), so it remains to estimate the term $\langle \sigma_{ij} s_{ij} \rangle$. The physical meaning of $\langle \sigma_{ij} s_{ij} \rangle$ is the dissipation of the turbulent energy as a result of the stretching of polymer. The total dissipation of energy brought about by the polymer can be obtained from Eqs. (2.30) and (2.33).

$$E_p = \frac{\nu_p}{2\tau_p^2} \langle P^2 \Re_{kk} \rangle \tag{2.41}$$

The total disspation of energy due to polymer is the sum of the dissipation of turbulent energy and mean energy. The balance equation for the mean energy is the same as the momentum balance energy, but with an additional factor of $S_0$. Therefore the polymer contribution to the dissipation of mean energy

is given by the polymer contribution to the momentum balance multiplied by $S_0$, $\langle P\Re_{xy}\rangle S_0\nu_p/\tau_p$. Subtracting this from the total polymeric energy dissipation yields the polymeric turbulent energy dissipation,

$$\epsilon_p = \langle\sigma_{ij}s_{ij}\rangle = \frac{\nu_p}{2\tau_p^2}\langle P^2(\Re_{xx}+\Re_{yy}+\Re_{zz})\rangle - \frac{\nu_p}{\tau_p}\langle P\Re_{xy}\rangle \tag{2.42}$$

It has been shown [28] that in Eq. (2.42) there is a cancelation of terms due to the following equation,

$$\langle P^2\Re_{xx}\rangle = 2\langle P\Re_{xy}\rangle S_0\tau_p \tag{2.43}$$

Equation (2.43) can be understood by the relation of the components of the conformation tensor at high Weissenberg number, $\langle P\Re_{xx}\rangle \sim We\mathcal{R}_{xy}$. Therefore Eq. (2.42) can be simplified to,

$$\langle\sigma_{ij}s_{ij}\rangle = \frac{\nu_p}{2\tau_p^2}\langle P^2(\Re_{yy}+\Re_{zz})\rangle \tag{2.44}$$

The terms $\mathcal{R}_{yy}$ and $\mathcal{R}_{zz}$ have been shown by DNS to have very similar values. As a result, Eq. (2.44) can be further written as,

$$\langle\sigma_{ij}s_{ij}\rangle \approx \frac{\nu_p}{\tau_p^2}\langle P^2\Re_{yy}\rangle \tag{2.45}$$

The correlation term on the RHS of Eq. (2.44) can be further estimated by approximating the average of the product by the product of the averages,

$$\frac{\nu_p}{\tau_p^2}\langle P^2\Re_{yy}\rangle \approx \frac{\nu_p}{\tau_p^2}\langle P\rangle^2\langle\Re_{yy}\rangle \tag{2.46}$$

Identifying $\tau_p/P$ as the effective relaxation time, it must be of the order of the typical turbulent time scale of $y/\sqrt{K}$ in order for coil-stretch transition

to occur, without which the polymer would not interact strongly with the flow. With the approximation $\sqrt{K}/y \sim \langle P \rangle / \tau_p$ and Eq. (2.46), $\langle \sigma_{ij} s_{ij} \rangle$ is estimated as,

$$\langle \sigma_{ij} s_{ij} \rangle \approx \nu_p \mathcal{R}_{yy} \frac{K}{y^2} \tag{2.47}$$

By Eqs. (2.25), (2.27) and (2.47), the energy balance equation becomes,

$$WS = (\nu + \nu_p \mathcal{R}_{yy}) K (\frac{a}{y})^2 + b \frac{K^{3/2}}{y} \tag{2.48}$$

In dimensionless units,

$$W^+ S^+ = \nu_{eff} K^+ (\frac{a}{y^+})^2 + b \frac{(K^+)^{3/2}}{y^+} \tag{2.49}$$

To provide the basis for a testable theory, $\mathcal{R}_{yy}$ needs to be related to other variables. Such a relation has been established as [27, 28],

$$\mathcal{R}_{yy} \approx \frac{\sqrt{K^+}}{S^+ y^+} \tag{2.50}$$

Therefore the effective viscosity $\nu_{eff}$ is given by,

$$\nu_{eff} = 1 + \tilde{\nu} \frac{\sqrt{K^+}}{S^+ y^+} \tag{2.51}$$

To summarize, by comparing the relative magnitude of the different contributions to the average terms in the balance equations and approximating the term $\sqrt{K}/y$ by $P/\tau$ by considering a coil-stretch transition at large Weissenberg number, the polymer has been shown to produce a effective viscosity that depends on the position.

### 2.2.2 Average terms for rodlike polymers

The theory of drag reduction for rodlike polymer has been presented in Ref. [26], showing that the idea of a position dependent effective viscosity is also applicable in this case. The procedure of estimating the average terms in the balance equations for rodlike polymer will be reviewed in the following.

For rodlike polymer, the polymer stress tensor is given by [31],

$$\Sigma_{ab} = 6\nu_p n_a n_b (n_i n_j S_{ij}) \tag{2.52}$$

Or in terms of the conformation tensor,

$$\Sigma_{ab} = 6\nu_p \Re_{ab} (\Re_{ij} S_{ij}) \tag{2.53}$$

The equation of motion of the conformation tensor is given by,

$$\frac{D\Re_{ab}}{Dt} = S_{ai}\Re_{ib} + S_{bi}\Re_{ia} - 2S_{ij}\Re_{ij}\Re_{ab} \tag{2.54}$$

Consider the momentum balance equation, the average term $\langle \Sigma_{xy} \rangle$ can be obtained from Eq. (2.53) and the equation $S_{ab} = S_0 \delta_{ax}\delta_{by} + s_{ab}$,

$$\langle \Sigma_{xy} \rangle = 6\nu_p [S_0 \langle \Re_{xy}^2 \rangle + \langle \Re_{xy}\Re_{ij}s_{ij} \rangle] \tag{2.55}$$

To obtain the term $\langle \Re_{xy}^2 \rangle = \langle n_x^2 n_y^2 \rangle$ in Eq. (2.55), approximate the average of the product as the product of the averages and note that $n_x \approx 1$.

$$\Re_{xy}^2 = \Re_{xx}\Re_{yy} \approx \Re_{yy} \tag{2.56}$$

By Eq. (2.56), the first term on the RHS of Eq. (2.55) can be estimated

as,

$$6\nu_p S_0 \langle \Re_{xy}^2 \rangle \approx \nu_p \mathcal{R}_{yy} S_0 \tag{2.57}$$

It has been argued in Ref. [26] that by Reynolds decomposition of Eq. (2.54) and a careful analysis of the leading order terms, the second term in Eq. (2.55) can be shown to be of the same order as the first term. Using this estimation, the momentum balance equation can be written as,

$$\nu S_0 + \nu_p \mathcal{R}_{yy} S_0 + W = \tau_w (1 - \frac{y}{R}) \tag{2.58}$$

Or in dimensionless units,

$$S_0^+ + \frac{\nu_p}{\nu} \mathcal{R}_{yy} S_0^+ + W^+ = (1 - \frac{y^+}{R^+}) \tag{2.59}$$

This result can be written more simply by the introduction of an effective viscosity $\nu_{eff}$,

$$\nu_{eff} S_0^+ + W^+ = (1 - \frac{y^+}{R^+}) \tag{2.60}$$

where $\nu_{eff}$ is given also by Eq. (2.40).

Similar to the flexible polymer case, the term $\langle \sigma_{ij} s_{ij} \rangle$ needs to be estimated. It can be expressed as,

$$\langle \sigma_{ij} s_{ij} \rangle = 6\nu_p \langle s_{ij} \Re_{ij} (S_0 \Re_{xy} + s_{kl} \Re_{kl}) \rangle \tag{2.61}$$

It has been reported that by expanding Eq. (2.61) into a series in the small parameter $n_y \sim n_z$ according to the expansion $n_x \approx 1 - \frac{1}{2}(n_y^2 + n_z^2)$ and a delicate cancellation of terms, $\langle \sigma_{ij} s_{ij} \rangle$ can be approximated by,

$$\langle \sigma_{ij} s_{ij} \rangle \approx \nu_p \mathcal{R}_{yy}(y) K(y) / y^2 \tag{2.62}$$

By Eqs. (2.25), (2.27) and (2.62),

$$WS_0 = \nu K(\frac{a}{y})^2 + \frac{b(K^+)^{3/2}}{y} + \nu_p \mathcal{R}_{yy}\frac{K}{y^2} \tag{2.63}$$

Writing Eq. (2.63) in dimensionless units and with the effective viscosity $\nu_{eff}$,

$$W^+S_0^+ = \nu_{eff}K^+(\frac{a}{y^+})^2 + \frac{b(K^+)^{3/2}}{y^+} \tag{2.64}$$

where $\nu_{eff} = 1 + \tilde{\nu}\mathcal{R}_{yy}$

Since $\mathcal{R}_{yy} \sim \mathcal{R}_{xy}^2$ and $S_0\mathcal{R}_{xy} \sim \sqrt{K}/y$, $\mathcal{R}_{yy}$ can be written as,

$$\mathcal{R}_{yy} \sim \frac{K}{(S_0 y)^2} \tag{2.65}$$

Therefore the effective viscosity for rodlike polymers is given by,

$$\nu_{eff} = 1 + \tilde{\nu}\frac{K^+}{(S_0^+ y^+)^2} \tag{2.66}$$

In this section the theory for rodlike polymer has been reviewed, showing that rodlike polymer also produces a position dependent effective viscosity that depends on $\mathcal{R}_{yy}$ in the same linear manner as flexible polymer. The difference between flexible polymer and rodlike polymer is the functional form of $\mathcal{R}_{yy}$, with $\mathcal{R}_{yy} \sim \sqrt{K}/S_0 y$ for flexible polymer and $\mathcal{R}_{yy} \sim K/(S_0 y)^2$ for rodlike polymer. In Section 2.3 the method of solving the set of equations containing the effective viscosity will be reviewed.

## 2.3 Solving the balance equations

With the average terms in the balance equations estimated, the balance equations can be solved to give expressions of $S_0^+$ and $W^+$. This has been carried

out in Refs. [10, 25] for the Newtonian case without polymer and the MDR asymptote. The velocity profiles at intermediate polymer concentrations have been calculated numerically in Ref. [27].

We first derive the general set of equations for $W^+$ and $S_0^+$, with care taken in preserving the term $y^+/R^+$.

The position dependence of the effective viscosity $\tilde{\nu}$ is conveniently discussed by defining a slope $\alpha$ of the effective viscosity profile [10].

$$\nu_{eff} = 1 + \alpha[y^+ - \Delta] \tag{2.67}$$

where $\Delta$ is the thickness of the viscous sublayer and is a function of $\alpha$. In general, the effective viscosity is not linear so $\alpha$ is a function of $y^+$.

The functional form of $\Delta(\alpha)$ has been derived in Ref. [10] using the symmetry of Eqs. (2.21) and (2.25) under the transformation to a new set of variables. The resulting functional form is given by,

$$\Delta(\alpha) = \frac{\delta^+}{1 - \alpha\delta^+} \tag{2.68}$$

The inclusion of the term $y^+/R^+$ in the balance equations does not affect the functional form of $\Delta(\alpha)$, therefore the result in Eq. (2.68) carries over to the present case.

By Eq. (2.67), Eqs. (2.60) and (2.64) can be written as,

$$[1 + \alpha(y^+ - \Delta)]S_0^+ + W^+ = 1 - \frac{y^+}{R^+} \tag{2.69}$$

$$W^+ S_0^+ = [1 + \alpha(y^+ - \Delta)]K^+(\frac{a}{y^+})^2 + \frac{b(K^+)^{3/2}}{y^+} \tag{2.70}$$

Inside the viscous sublayer ($y^+ < \Delta$), $S_0^+ = 1$, therefore Eq. (2.70) can be further simplified by fitting the boundary solution at $y^+ = \Delta$ which should

give $S_0^+ = 1$. Using Eq. (2.28), Eq. (2.70) can be rewritten as,

$$S_0^+ = [1 + \alpha(y^+ - \Delta)](\frac{a}{cy^+})^2 + \frac{\sqrt{W^+}}{(c^3/b)y^+} \tag{2.71}$$

Approaching the boundary of the viscous sublayer from the outside ($y^+ \to \Delta$), the limits are $S_0^+ \to 1$ and $W^+ \to 0$. Therefore Eq. (2.71) gives a relation between $\Delta$, $a$ and $c$.

$$\Delta = a/c \tag{2.72}$$

Putting the results together,

$$S_0^+ = [1 + \alpha(y^+ - \Delta)](\frac{\Delta}{y^+})^2 + \frac{\sqrt{W^+}}{\kappa_c y^+} \tag{2.73}$$

where $\kappa_c = c^3/b = a^3/\Delta^3 b$. The values of $\kappa_c$ at zero polymer concentration and at the MDR asymptote are given by $\kappa_k$ and $\kappa_v$ respectively.

Now consider the region far from the viscous sublayer, i.e. $y^+ \gg \Delta$. The set of equations become,

$$[1 + \alpha y^+]S_0^+ + W^+ = 1 - \frac{y^+}{R^+} \tag{2.74}$$

$$S_0^+ = [1 + \alpha y^+](\frac{\Delta}{y^+})^2 + \frac{\sqrt{W^+}}{\kappa_c y^+} \tag{2.75}$$

Eqs. (2.74) and (2.75) give a quadratic equation of $y^+ S_0^+$ in the form,

$$\kappa_c^2(y^+S_0^+)^2 + y^+S_0^+(\alpha + \frac{1}{y^+})(1 - 2\kappa_c^2\Delta^2) + [\kappa_c^2(\alpha + \frac{1}{y^+})^2\Delta^4 - 1 + \frac{y^+}{R^+}] = 0 \tag{2.76}$$

Solving the quadratic equation yields the following solution.

$$\begin{aligned} y^+S_0^+ &= (\alpha+\frac{1}{y^+})\Delta^2 - \frac{(\alpha+\frac{1}{y^+})}{2\kappa_c^2} \\ &\quad + \frac{1}{\kappa_c}\sqrt{(\frac{\alpha+\frac{1}{y^+}}{2\kappa_c})^2+1-\frac{y^+}{R^+}-(\alpha+\frac{1}{y^+})^2\Delta^2} \end{aligned} \tag{2.77}$$

From Eq.(2.75), there is also an expression for $W^+$,

$$\sqrt{W^+} = -\frac{(\alpha+\frac{1}{y^+})}{2\kappa_c} + \sqrt{(\frac{\alpha+\frac{1}{y^+}}{2\kappa_c})^2+1-\frac{y^+}{R^+}-(\alpha+\frac{1}{y^+})^2\Delta^2} \tag{2.78}$$

The velocity profiles have been calculated for flexible and rodlike polymers in Ref. [27]. The equations have been solved numerically to provide concrete results for the mean velocity profile. To obtain $S_0^+$ and $W^+$, Eqs. (2.77) and (2.78) are inconvenient to be used directly because $\alpha$ depends on $y^+$ and $\tilde{\nu}$ in a complicated way, therefore a scheme has been developed for solving these equations [27].

From Eq. (2.68) and (2.72), $\alpha$ can be expressed in terms of $\delta^+$, $c$ and $a$.

$$\alpha = \frac{1}{\delta^+}(1-\frac{\delta^+c}{a}) \tag{2.79}$$

Then with Eq. (2.67), the effective viscosity becomes,

$$\nu_{eff} = 1+\frac{1}{\delta^+}(1-\frac{\delta^+c}{a})[y^+-\frac{a}{c}] \tag{2.80}$$

This equation can be manipulated to give a quadratic equation in $c$.

$$\frac{\delta^+y^+}{a}c^2 + [\delta^+(\nu_{eff}-2)-y^+]c + a = 0 \tag{2.81}$$

Solving for $c$ gives,

$$c = \frac{a}{2}[\frac{1}{\delta^+} + \frac{(2-\nu_{eff})}{y^+}] + \frac{a}{2\delta^+}\sqrt{1 - \frac{2\nu_{eff}\delta^+}{y^+} + \frac{(2-\nu_{eff})^2(\delta^+)^2}{(y^+)^2}} \tag{2.82}$$

Next a variable $A$ is introduced such that,

$$K^+ = A^2(S_0^+ y^+)^2 \tag{2.83}$$

where

$$A^2 = (\frac{\nu_{eff}-1}{\tilde{\nu}})^2 \tag{2.84}$$

for flexible polymers, and

$$A^2 = \frac{\nu_{eff}-1}{\tilde{\nu}} \tag{2.85}$$

for rodlike polymers.

With Eq. (2.28) and (2.83), the set of equations become,

$$\nu_{eff}S_0^+ + c^2A^2(S_0^+y^+)^2 = 1 - \frac{y^+}{R^+} \tag{2.86}$$

$$c^2S_0^+ = \nu_{eff}(\frac{a}{y^+})^2 + bAS_0^+ \tag{2.87}$$

To solve for $\nu_{eff}$, $S_0^+$ can be eliminated from the equations, first by observing that Eq. (2.87) leads to,

$$S_0^+ = \frac{\nu_{eff}}{(y^+)^2}\frac{a^2}{(c^2-bA)} \tag{2.88}$$

Substituting Eq. (2.88) into Eq. (2.86) provides an equation for $\nu_{eff}$,

$$\nu_{eff}^2(\frac{a}{y^+})^2(c^2-bA) + c^2A^2\nu_{eff}^2(\frac{a^2}{y^+})^2 = (1-\frac{y^+}{R^+})(c^2-bA)^2 \tag{2.89}$$

Equation (2.89) can be solved to get $\nu_{eff}(y^+)$ for different values of $\tilde{\nu}$. Then

$S_0^+$ can be obtained from Eq. (2.88). By integrating $S_0^+$ over $y^+$, $V^+(y^+)$ is obtained.

The constants $a$ and $b$ are fixed by the empirical von-Karman log law for the Newtonian case without polymer. The Newtonian case corresponds to $\nu_{eff} = 1$ and therefore $\alpha = 0$. From Eq. (2.77), $S_0^+$ is found to be,

$$\begin{aligned} S_0^+ &= (\frac{1}{y^+})^2[(\delta^+)^2 - \frac{1}{2\kappa_k^2}] \\ &\quad + \frac{1}{\kappa_k (y^+)^2}\sqrt{(y^+)^2(1-\frac{y^+}{R^+}) - (\delta^+)^2 + (2\kappa_k)^{-2}} \end{aligned} \tag{2.90}$$

where $\kappa_k = a^3/(\delta^+)^3 b$ and $\delta^+$ is the dimensionless thickness of the viscous sublayer in the Newtonian case where there is no polymer.

While Eq. (2.90) cannot be directly integrated to give an expression in terms of elementary functions and numerical integration has to be used, it can be simplified by considering the near wall region $y^+ \ll R^+$. By taking this approximation, Eq. (2.90) can be readily integrated to give the mean velocity profile. This has been done in Ref. [25] with the resulting velocity profile given by,

$$V^+ = \kappa_k^{-1} \ln Y(y^+) + B - \Theta(y^+) \tag{2.91}$$

where the functions are defined as,

$$\begin{aligned} Y(y^+) &\equiv \frac{1}{2}[y^+ + \sqrt{(y^+)^2 - (\delta^+)^2 + (2\kappa_k)^{-2}}] \\ \Theta(y^+) &\equiv \frac{2\kappa_k^2(\delta^+)^2 + 4\kappa_k[Y(y^+) - y^+] - 1}{2\kappa_k^2 y^+} \\ B &\equiv 2\delta^+ - \kappa_k^{-1}\ln[\frac{e(1+2\kappa_k\delta^+)}{4\kappa_k}] \end{aligned}$$

Note that in the limit $y^+ \gg \delta^+$, $Y(y^+) \to y^+$ and $\Theta(y^+) \to 0$. As a result,

the von-Karman log law is recovered,

$$V^+(y^+) = \kappa_k^{-1} \ln y^+ + B \tag{2.92}$$

Since the von-Karman constant $\kappa_k = a^3/b(\delta^+)^3$ in the theory and it is known from experiments that $\delta^+ \approx 6$, the experimental values [5] of $\kappa_k \approx 0.436$ and $B \approx 6.13$ were used to fix the parameters $a$ and $b$. The best fitted values are given by $a \approx 3$ and $b \approx 0.321$.

In the following we describe how we obtained the friction factor relations from the velocity profiles. From Eq. (1.1), the friction factor $f$ can be obtained by first averaging the mean velocity profile $V^+(y^+)$ over the whole cross-section of the pipe to get the average velocity $U_{av}^+$, which is related to $f$ by,

$$\frac{1}{\sqrt{f}} = \frac{1}{\sqrt{2}} U_{av}^+ \tag{2.93}$$

From Eqs. (2.93) and (1.2) we decompose the integral into a sum of integrals over the viscous sublayer and outside the viscous sublayer. However, a complication with numerical calculation of the velocity profile is the instability of the root-finding algorithm at small $y^+$, which means that the velocity is not easily obtained for some small $y^+$ slightly larger than the width of the viscous sublayer $\Delta$ (note that $\Delta = \delta^+$ for Newtonian flow without polymer). Therefore we introduce an additional constant $y_0^+$ that is the smallest $y^+$ outside the viscous sublayer at which the velocity can be reliably computed. Also recall that inside the viscous sublayer $V^+ = y^+$. As a result,

$$\frac{1}{\sqrt{f}} = \frac{\sqrt{2}}{(R^+)^2}\left[\int_0^{\Delta} y^+(R^+ - y^+)dy^+ + \int_{\Delta}^{y_o^+} \Delta \ln\left(\frac{y^+}{\Delta}\right)(R^+ - y^+)dy^+ + \int_{y_0^+}^{R^+} V^+(R^+ - y^+)dy^+\right] \tag{2.94}$$

The first two integrals in Eq. (2.94) are straightforward, giving

$$\begin{aligned}\frac{1}{\sqrt{f}} &= \frac{\sqrt{2}}{(R^+)^2}\{-\frac{\Delta^3}{3}+\Delta(R^+-\frac{\Delta}{4})+\frac{\Delta^2 R^+}{2} \\ &\quad + y_0^+[-R^+ + \frac{y_0^+}{4} + (R^+ - \frac{y_0^+}{2})\ln(\frac{y_0^+}{\Delta})] \\ &\quad + \int_{y_0^+}^{R^+} V^+(R^+ - y^+)dy^+\} \end{aligned} \tag{2.95}$$

The remaining integral on the RHS of Eq. (2.95) can be computed once we know the velocity profile. Furthermore, $Re\sqrt{f}$ is related to $R^+$ by a constant factor,

$$Re\sqrt{f} = 2\sqrt{2}R^+ \tag{2.96}$$

Therefore the Prandtl-Karman coordinates of $1/\sqrt{f}$ against $Re\sqrt{f}$ is just $1/\sqrt{f}$ against $2\sqrt{2}R^+$, and can be plotted once we know the value of $f$ for different $R^+$. Results of the velocity profiles and the friction factor relations will be presented in Chapter 5.

# Chapter 3

# Behavior near the maximum drag reduction asymptote

Earlier studies have identified the MDR asymptote as the edge solution of turbulence where $W^+$ becomes zero and that it corresponds to the maximum amount of drag reduction [10]. In this section we will show that while the zero $W^+$ solution is approached at high polymer concentration, it does not correspond exactly to the maximum velocity profile obtained by treating $\alpha$ as a free parameter. The discrepancy is due to the constraint imposed by the $y^+$ dependence of $\alpha$ at a fixed $\tilde{\nu}$. The difference is very small in the constant $\kappa_c$ case considered in Fig. 3.1, but becomes more noticeable when the $\alpha$ dependence of $\kappa_k$ is taken into account. In addition, $W^+$ and $S^+$ also depend on the position when the term $y^+/R^+$ is preserved. In the following we will first show that the high polymer concentration limit corresponds to the $W^+ = 0$ limit, and then we will proceed to show the non-equivalence between the $W^+ = 0$ solution and the maximum solution of the shear rate (and therefore also the maximum of the velocity).

From Eqs. (2.51), (2.66) and (2.67), there are two equations connecting

$\alpha$ to $\tilde{\nu}$ for flexible and rodlike polymer respectively,

$$\alpha[y^+ - \Delta] = \tilde{\nu}\frac{\sqrt{K^+}}{S_0^+ y^+} \tag{3.1}$$

for flexible polymer. And,

$$\alpha[y^+ - \Delta] = \tilde{\nu}\frac{K^+}{(S_0^+ y^+)^2} \tag{3.2}$$

for rodlike polymer.

From Eqs. (2.28) and (2.72), the term $K^+$ can be expressed in terms of $W^+$ by,

$$K^+ = \frac{W^+}{c^2} = \frac{W^+\Delta^2}{a^2} \tag{3.3}$$

From Eq. (2.75) it is clear that for $y^+ \gg \Delta$,

$$y^+ S_0^+ = (\alpha + \frac{1}{y^+})\Delta^2 + \frac{\sqrt{W^+}}{\kappa_c} \tag{3.4}$$

where $\sqrt{W^+}$ is given by Eq. (2.78). As a result,

$$\frac{\sqrt{K^+}}{S_0^+ y^+} = \frac{\Delta\sqrt{W^+}}{a[(\alpha + 1/y^+)\Delta^2 + \sqrt{W^+}/\kappa_c]} \tag{3.5}$$

Putting the results back into Eqs.(3.1) and (3.2), taking care that $\Delta$ should be neglected when compared to $y^+$ for consistency, we finally arrive at,

$$\tilde{\nu} = \frac{a[(\alpha + 1/y^+)\Delta^2 + \sqrt{W^+}/\kappa_c]}{\Delta\sqrt{W^+}}\alpha y^+ \tag{3.6}$$

for flexible polymer. And,

$$\tilde{\nu} = \frac{a^2[(\alpha + 1/y^+)\Delta^2 + \sqrt{W^+}/\kappa_c]^2}{\Delta^2 W^+}\alpha y^+ \tag{3.7}$$

for rodlike polymer.

$\tilde{\nu}$ has been written in a functional form as $\tilde{\nu} = \tilde{\nu}(\alpha, y^+, R^+)$. This should be understood as giving an implicit function of $\alpha$ in the form $\alpha = \alpha(\tilde{\nu}, y^+, R^+)$ because it is $\tilde{\nu}$ that is being controlled. Therefore it is now clear that $\alpha$ should not be treated as a free parameter. Later we will show that the maximum drag reduction limit obtained by maximizing $S_0^+$ using $\alpha$ as a free parameter does not correspond to the high polymer concentration limit.

From Eqs.(3.6) and (3.7), it is obvious that $\tilde{\nu} = 0$ (no polymer) corresponds to $\alpha = 0$, which is also evident considering that the effective viscosity equals one for the Newtonian case where there is no polymer. Now consider the maximum drag reduction limit where $\tilde{\nu} \to \infty$, therefore,

$$\frac{1}{\tilde{\nu}} = \frac{\Delta\sqrt{W^+}}{a[(\alpha + 1/y^+)\Delta^2 + \sqrt{W^+}/\kappa_c]\alpha y^+} \to 0 \tag{3.8}$$

for flexible polymer.

$$\frac{1}{\tilde{\nu}} = \frac{\Delta^2 W^+}{a^2[(\alpha + 1/y^+)\Delta^2 + \sqrt{W^+}/\kappa_c]^2\alpha y^+} \to 0 \tag{3.9}$$

for rodlike polymer.

Physically, $\Delta$ and $W^+$ must be finite, and $\alpha$ must also be bounded as $\sqrt{W^+}$ is positive. Therefore, Eqs.(3.8) and (3.9) implies that $W^+ \to 0$ in the high concentration limit for both flexible and rodlike polymer. However, the rate of decay of $W^+$ is different in the two cases. Consider very small $W^+$, Eqs.(3.8) and (3.9) become,

$$\frac{1}{\tilde{\nu}} = \frac{\Delta\sqrt{W^+}}{a[(\alpha + 1/y^+)\Delta^2\kappa_c]\alpha y^+} \tag{3.10}$$

for flexible polymer.

$$\frac{1}{\tilde{\nu}} = \frac{\Delta^2 W^+}{a^2[(\alpha + 1/y^+)\Delta^2\kappa_c]^2\alpha y^+} \tag{3.11}$$

for rodlike polymer.

The $\tilde{\nu}$ dependence of $W^+$ is different for flexible and rodlike polymer, with

$$W^+ \sim \frac{1}{\tilde{\nu}^2} \tag{3.12}$$

for flexible polymer.

$$W^+ \sim \frac{1}{\tilde{\nu}} \tag{3.13}$$

for rodlike polymer.

Therefore it is clear that $W^+$ decays faster with $\tilde{\nu}$ in flexible polymer when $\tilde{\nu}$ is very large. While currently there is insufficient experimental data on the Reynolds stress at high polymer concentrations to test the different $\tilde{\nu}$ dependence of $W^+$ quantitatively, the scaling behaviors are reproduced self-consistently from the theory in Section 6 by solving the equations.

In the following the solution for $\alpha$ at which $W^+ = 0$ is derived, which corresponds to the high concentration limit. This solution will be contrasted to the solution for which $S_0^+(y^+)$ attains maximum at every $y^+$ by adjusting $\alpha(y^+)$. The differene between the two solutions stems from the fact that the requirement for a constant $\tilde{\nu}$ implies constraint on the function $\alpha(y^+)$.

From Eqs. (2.77) and (2.78), assuming at the MDR limit $\alpha$ is sufficiently large such that $\alpha y^+ \gg 1$, the following expressions for $S^+$ and $W^+$ can be obtained.

$$y^+ S^+ = \alpha\Delta^2(\alpha) - \frac{\alpha}{2\kappa_c^2} + \frac{1}{\kappa_c}\sqrt{(\frac{\alpha}{2\kappa_c})^2 + 1 - \frac{y^+}{R^+} - \alpha^2\Delta^2(\alpha)} \tag{3.14}$$

$$\sqrt{W^+} = -\frac{\alpha}{2\kappa_c} + \sqrt{(\frac{\alpha}{2\kappa_c})^2 + 1 - \frac{y^+}{R^+} - \alpha^2\Delta^2(\alpha)} \tag{3.15}$$

The MDR asymptote has been considered for the region $y^+ \ll R^+$ in Ref. [10]. In this region Eqs. (3.14) and (2.78) can be simplified to

$$y^+ S_0^+ = \alpha\Delta^2(\alpha) + \sqrt{W^+}/\kappa_C \tag{3.16}$$

$$\sqrt{W^+} = -\frac{\alpha}{2\kappa_c} + \sqrt{(\frac{\alpha}{2\kappa_c})^2 + 1 - \alpha^2\Delta^2(\alpha)} \tag{3.17}$$

In the original analysis in Ref. [10], $\alpha$ was treated as a free parameter and $\kappa_c$ assumed to be a constant. $\sqrt{W^+}$ and $y^+S_0^+$ have been plotted as functions of $\alpha$. The results are shown in Fig. 3.1.

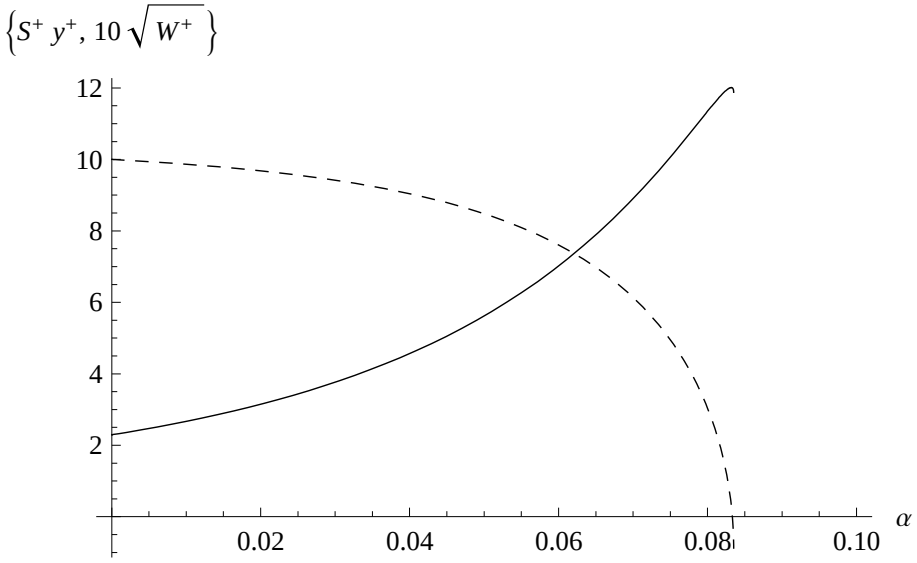


Figure 3.1: $y^+S_0^+$ (solid) and $10\sqrt{W^+}$ (dashed) against $\alpha$ for constant $\kappa_c = 0.436$.

In Fig. 3.1, the maximum of $y^+S_0^+$ lies very close to the zero of $W^+ = 0$, which happens at $\alpha = 1/\Delta(\alpha)$, implying $\alpha = 1/2\delta^+$ and $\Delta(\alpha) = 2\delta^+$. Physically, it means that the maximum drag reduction (thus maximum $y^+S_0^+$)

happens at an edge solution ($W^+ = 0$) where turbulence cannot be supported when $\alpha$ is further increased. Substituting the solution into Eq. (3.16) and integrate over $y^+$, one obtains the MDR log-law for the mean velocity,

$$V^+(y^+) \approx 12 \ln y^+ - 17.8 \tag{3.18}$$

Equation (3.18) agrees well with the empirical log-law in Eq. (1.8).

However, from the definition $\kappa_c = c^3(\alpha)/b$, $\kappa_c$ is clearly a function of $\alpha$ and cannot be treated as a constant. Furthermore, $\alpha$ actually depends on $y^+$ and is not a free parameter. We would like to take these effects into explicit account. We would also like to consider the case where $y^+$ can be comparable to $R^+$, so the term $y^+/R^+$ in Eqs. (3.14) and (3.15) will be kept.

In Fig. 3.1, the maximum of $y^+S_0^+$ is very near the zero of $W^+ = 0$, but closer inspection reveals that the maximum point of $y^+S_0^+$ actually does not coincide exactly with the root of $W^+ = 0$, and the discrepancy (the difference in the $\alpha$ value for these two conditions) is larger if we consider $\kappa_c$ to be dependent on $\alpha$, while for the constant $\kappa_c = 0.436$ they are extremely close, with the maximum of $y^+S_0^+$ happening at $\alpha_m \approx 0.08318$ and $W^+ = 0$ achieved at $\alpha_0 = 1/12 \approx 0.08333$. It can be proved that the two solutions do not match exactly; first taking the derivative of Eq. (3.16) with respect to $\alpha$,

$$\frac{\partial(y^+S_0^+)}{\partial\alpha} = \Delta^2(\alpha) + 2\alpha\Delta(\alpha)\Delta'(\alpha) + \frac{\partial_\alpha\sqrt{W^+}}{\kappa_c} - \frac{\sqrt{W^+}}{\kappa_c^2}\kappa_c'(\alpha) \tag{3.19}$$

$\Delta'(\alpha)$ is easily obtained by direct differentiation,

$$\Delta'(\alpha) = \frac{\partial}{\partial\alpha}\left(\frac{\delta^+}{1-\alpha\delta^+}\right) = \frac{(\delta^+)^2}{(1-\alpha\delta^+)^2} = \Delta^2(\alpha) \tag{3.20}$$

$\partial_\alpha W^+$ can be obtained from Eq. (3.15) by,

$$\partial_\alpha \sqrt{W^+} = \frac{(-\frac{1}{2\kappa_c} + \frac{\alpha}{2\kappa_c^2}\kappa_c'(\alpha))\sqrt{W^+} - \alpha\Delta^2(1+\alpha\Delta)}{\sqrt{(\frac{\alpha}{2\kappa_c})^2 + 1 - \frac{y^+}{R^+} - \alpha^2\Delta^2(\alpha)}} \tag{3.21}$$

Plugging Eqs. (3.20) and (3.21) back into Eq. (3.19) gives,

$$\frac{\partial(y^+S_0^+)}{\partial\alpha} = \frac{\sqrt{W^+}[\Delta^2(1+2\alpha\Delta) - \frac{1}{2\kappa_c^2} + \frac{\alpha}{2\kappa_c^3}\kappa_c'(\alpha)] - \frac{\alpha\Delta^2}{2\kappa_c}}{\sqrt{(\frac{\alpha}{2\kappa_c})^2 + 1 - \frac{y^+}{R^+} - \alpha^2\Delta^2(\alpha)}} - \frac{\sqrt{W^+}}{\kappa_c^2}\kappa_c'(\alpha) \tag{3.22}$$

In Eq. (3.22), we have not specified the functional form of $\kappa_c(\alpha)$ as we are going to demonstrate that the difference between the $W^+ = 0$ solution and the maximum $S^+$ solution exists irrespective of the specific form of $\kappa_c(\alpha)$ used. At $W^+ = 0$, according to Eq. (3.17), the square root in the denominator of Eq. (3.22) becomes $\alpha/(2\kappa_c)$, and

$$[\frac{\partial(y^+S_0^+)}{\partial\alpha}]_{W^+=0} = -\Delta^2(\alpha_0) \tag{3.23}$$

where $\alpha_0$ is the root for $W^+ = 0$. We remark that Eq. (3.23) is valid for any $\alpha$ dependence of $\kappa_c$. The meaning of Eq. (3.23) is that when $W^+ = 0$, the slope of $y^+S_0^+$ against $\alpha$ must have a finite negative value, therefore $W^+ = 0$ does not occur at the same $\alpha$ value as the maximum of $S_0^+$. From the definition of $\kappa_c$, its $\alpha$ dependence is obtained.

$$\kappa_c = \frac{a^3}{\Delta^3 b} = (\frac{1-\alpha\delta^+}{\delta^+})^3\frac{a^3}{b} \tag{3.24}$$

With Eq. (3.14), (3.15) and (3.24), the maximum point of $y^+S_0^+$ and the root of $W^+ = 0$ can be found. The former was done by numerical maximization while the latter can be derived analytically with ease, giving

an explicit functional form. Defining $x \equiv y^+/R^+$, and from Eq. (3.15), $W^+ = 0$ is equivalent to,

$$1 - x - \alpha^2\Delta^2 = 0 \tag{3.25}$$

Equation (3.25) forms a quadratic equation for $\alpha$,

$$x(\delta^+)^2\alpha^2 + 2\delta^+(1-x)\alpha - (1-x) = 0 \tag{3.26}$$

Solving Eq. (3.25) gives $\alpha_0$,

$$\alpha_0 = \frac{1}{\delta^+ x}[\sqrt{1-x} - (1-x)] \tag{3.27}$$

For the region far from the centre of the pipe, $x \ll 1$, therefore

$$\alpha_0 \approx \frac{1}{\delta^+ x}[1 - \frac{x}{2} - 1 + x] = \frac{1}{2\delta^+} \tag{3.28}$$

Next we proceed to the maximization of $y^+S_0^+$, but before that we would like to visualize the relationship between the $W^+ = 0$ solution and the maximum $y^+S_0^+$ solution by plotting $\sqrt{W^+}$ (Eq. (3.15)) and $y^+S_0^+$ (Eq. (3.14)) as a function of $\alpha$ for different $x$ as a parameter. These are plotted with $x$ ranging from 0 to 1 from Figs. 3.2 to 3.7. Looking at the figures, we first observe that differing from the constant $\kappa_c$ case, the maximum $y^+S_0^+$ position is visibly different from the $W^+ = 0$ position, with both solution shifting to the smaller $\alpha$ side when $x$ is increased while keeping a relative difference of around 10%. The increase in the difference between the two solutions is caused by the $\alpha$ dependence of $\kappa_c$. While the two solutions are different in both the constant $\kappa_c$ case and the $\alpha$ dependent $\kappa_c$ case, the magnitude of the difference depends on the functional form of $\kappa_c$. The simultaneous shifting

can be understood by noting in Eq. (3.23), the $\alpha$ derivative of $y^+S_0^+$ has a value of some typical $-\Delta^2(\alpha)$ at the root of $W^+ = 0$ for any $x$, therefore it is expected that the maximum position of $y^+S_0^+$ will shift with $W^+ = 0$.

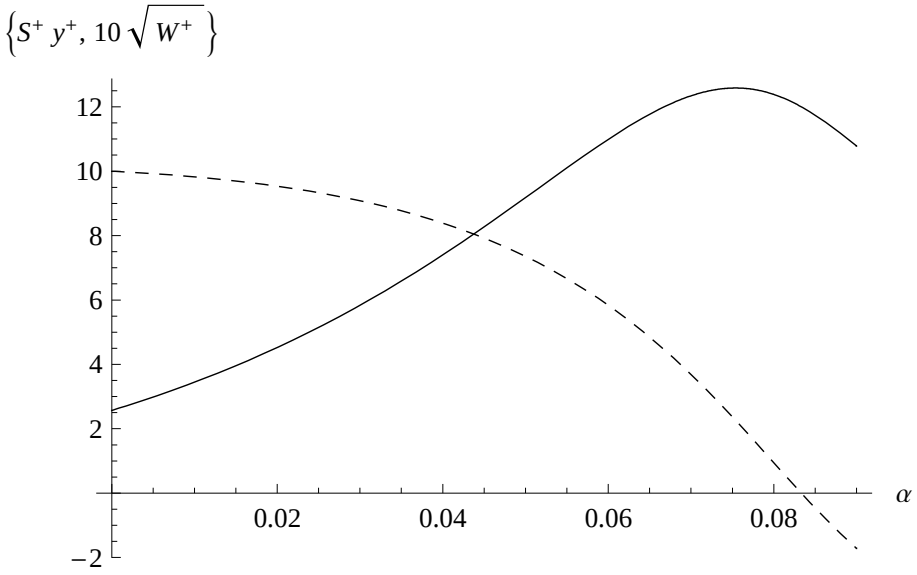


Figure 3.2: $y^+S_0^+$ (solid) and $10\sqrt{W^+}$ (dashed) against $\alpha$ by Eq. (3.15) and (3.14) with $\kappa_c = a^3/(\Delta^3 b)$ and $x = 0$.

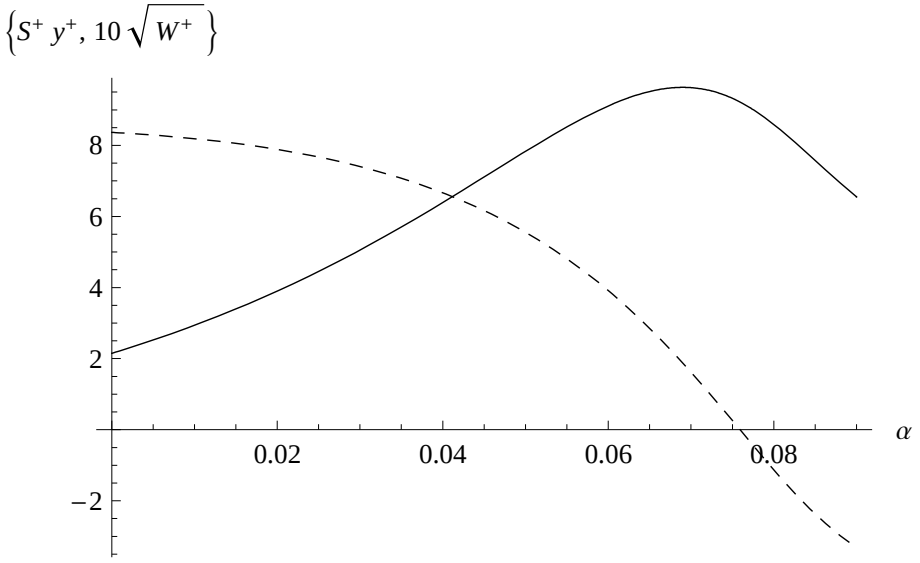


Figure 3.3: $y^+S_0^+$ (solid) and $10\sqrt{W^+}$ (dashed) against $\alpha$ by Eq. (3.15) and (3.14) with $\kappa_c = a^3/(\Delta^3 b)$ and $x = 0.3$.

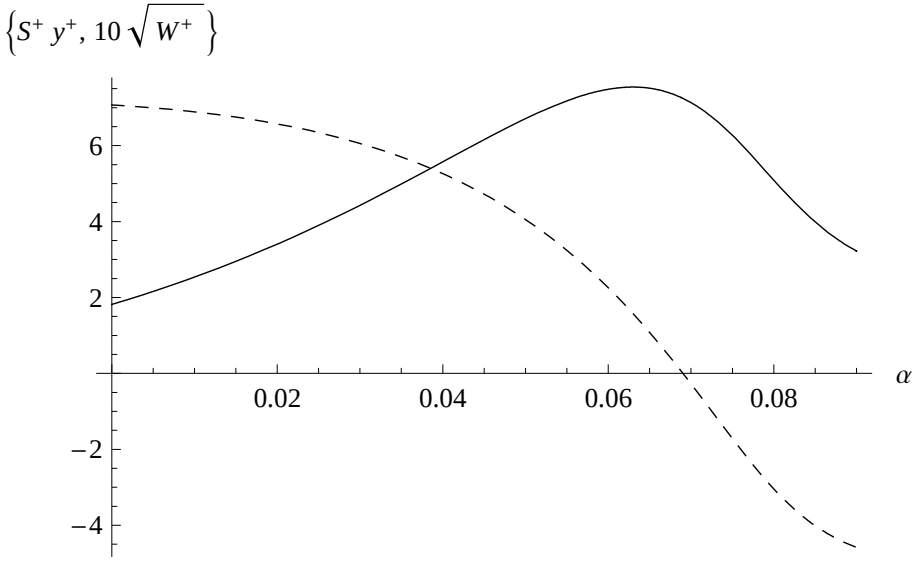


Figure 3.4: $y^+S_0^+$ (solid) and $10\sqrt{W^+}$ (dashed) against $\alpha$ by Eq. (3.15) and (3.14) with $\kappa_c = a^3/(\Delta^3 b)$ and $x = 0.5$.

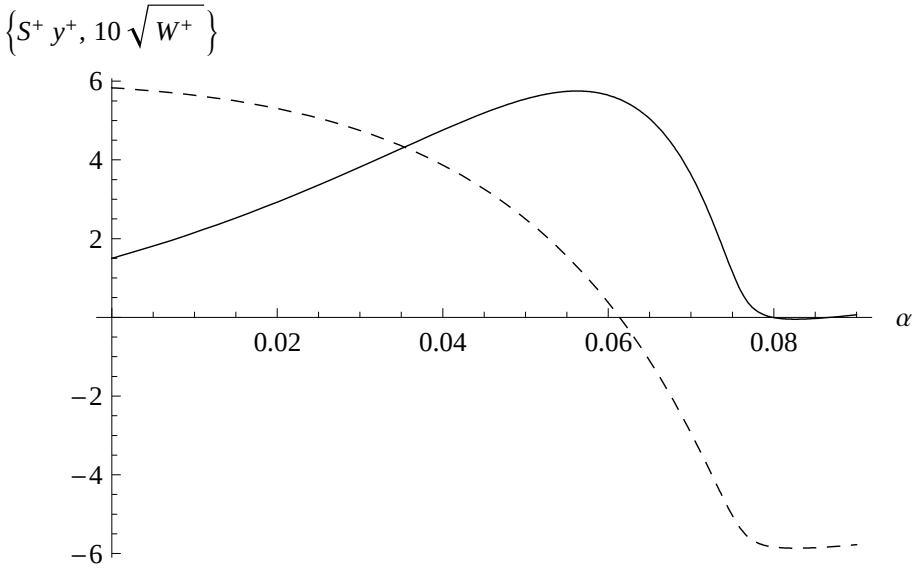


Figure 3.5: $y^+S_0^+$ (solid) and $10\sqrt{W^+}$ (dashed) against $\alpha$ by Eq. (3.15) and (3.14) with $\kappa_c = a^3/(\Delta^3 b)$ and $x = 0.66$.

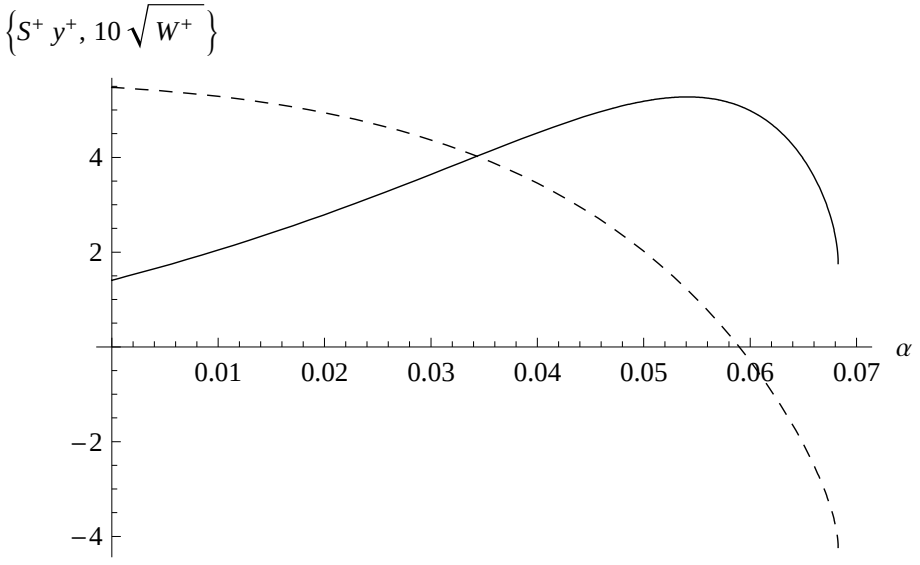


Figure 3.6: $y^+S_0^+$ (solid) and $10\sqrt{W^+}$ (dashed) against $\alpha$ by Eq. (3.15) and (3.14) with $\kappa_c = a^3/(\Delta^3 b)$ and $x = 0.7$.

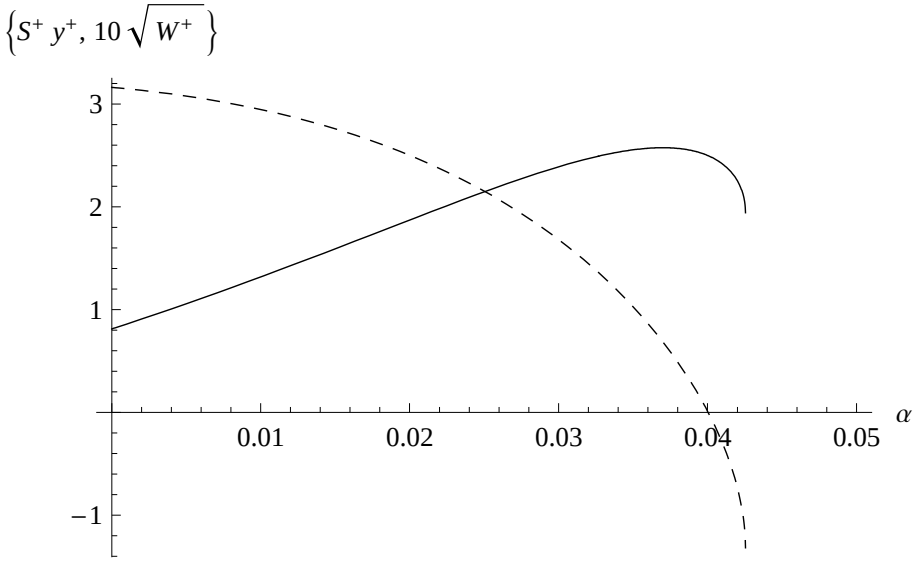


Figure 3.7: $y^+S_0^+$ (solid) and $10\sqrt{W^+}$ (dashed) against $\alpha$ by Eq. (3.15) and (3.14) with $\kappa_c = a^3/(\Delta^3 b)$ and $x = 0.9$.

We first do a numerical maximization of $y^+S_0^+$ to obtain the maximum point $\alpha_m$, and then use Eq. (3.27) to compute $\alpha_0$ which is the root of $W^+ = 0$. The results are presented in Fig. 3.8. It is seen that $\alpha_0$ is always larger than $\alpha_m$, but the gap between them closes up when $x$ approaches to 1. Similarly, the profile for $y^+S_0^+$ for the condition $W^+ = 0$ and maximum $y^+S_0^+$ can also be found. The profiles are shown in Fig. 3.9. Previously we have argued that the high concentration limit corresponds to $W^+ = 0$. The reason why it does not correspond to the maximum $y^+S^+$ profile obtained here is that for the latter $\tilde{\nu}$ cannot be a constant, which is unphysical for a polymer solution of fixed concentration. In other words, the maximum velocity profile obtained by treating $\alpha$ as a free parameter does not satisfy the constraint of a fixed $\tilde{\nu}$. The non-constant behavior of $\tilde{\nu}$ in such a case is shown in Figs. 3.10 and 3.11 for flexible and rodlike polymers respectively.

Therefore there are two velocity profiles each corresponding to $W^+ =$

0 and maximum $S_0^+$ (equivalent to maximizing $y^+S_0^+$ because we find the maximum $y^+S_0^+$ at each $x = y^+/R^+$). The velocity profile can then be integrated to calculate the friction factor relation. These will be compared to the theoretical velocity profile and friction factor results at high concentration in Section 5.2 to show that at high concentration the $W^+ = 0$ limit is indeed approached.

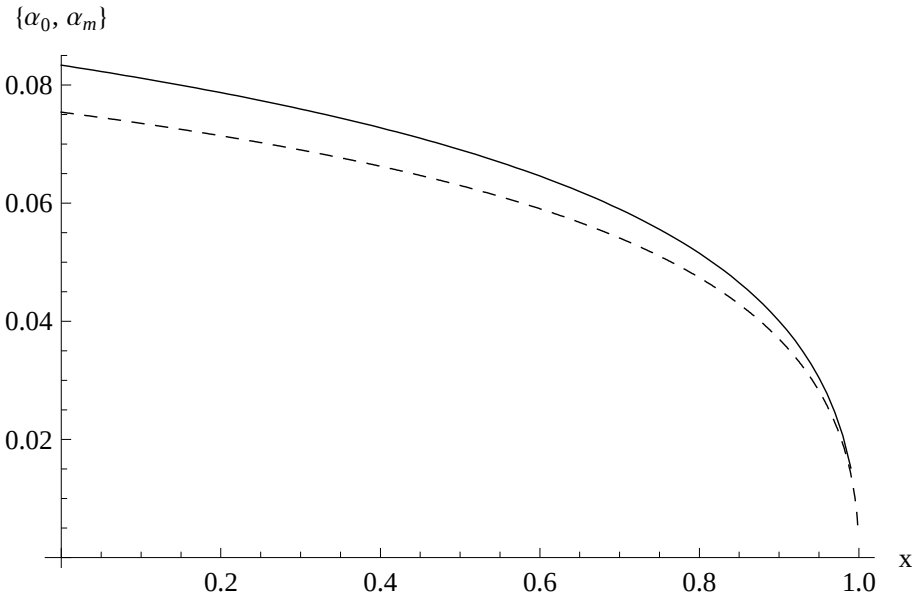


Figure 3.8: $\alpha_0$ (solid) and $\alpha_m$ (dashed) as functions of $x$.

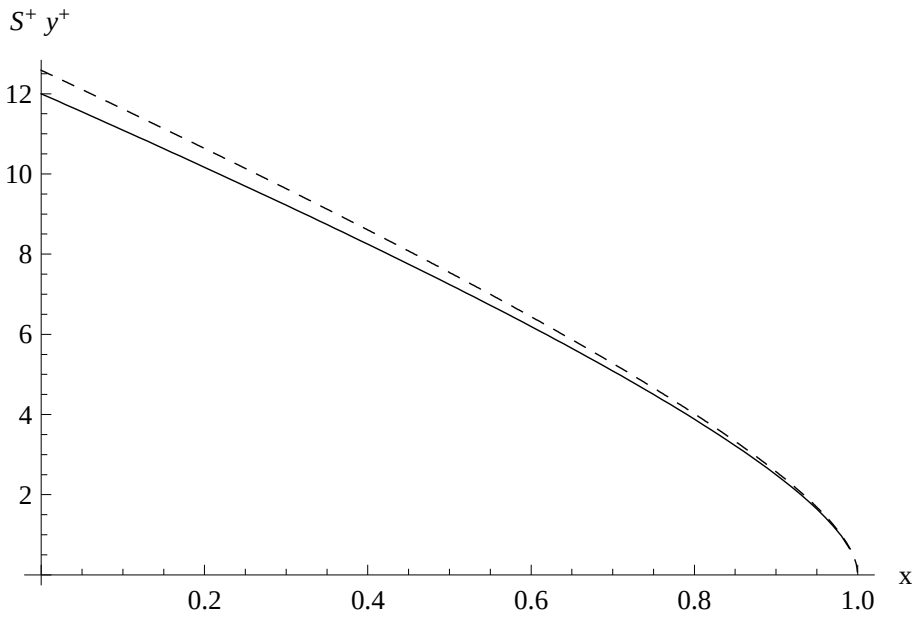


Figure 3.9: $y^+S_0^+$ for $W^+ = 0$ (solid) and the maximum $y^+S_0^+$ (dashed) as functions of $x$.

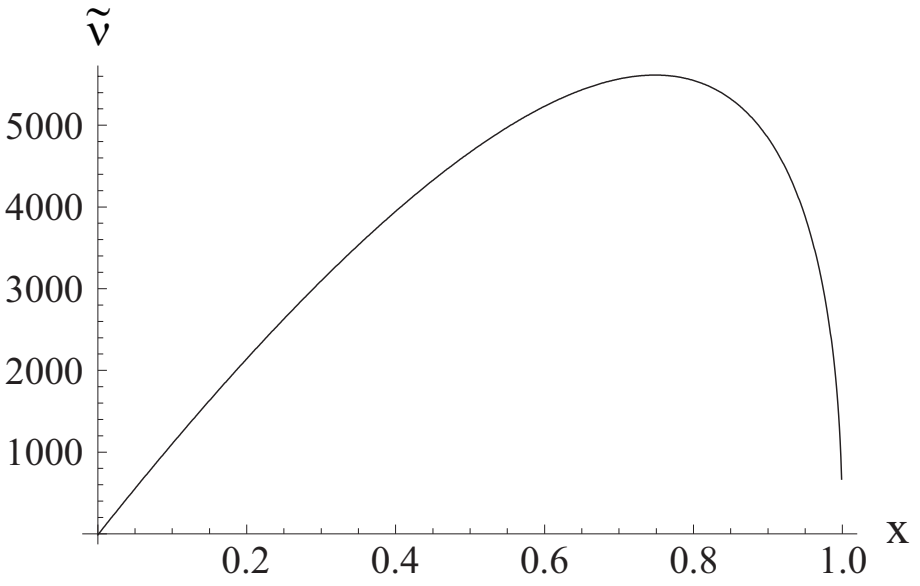


Figure 3.10: $\tilde{\nu}(x)$ of the maximum $y^+S_0^+$ solution for flexible polymer.

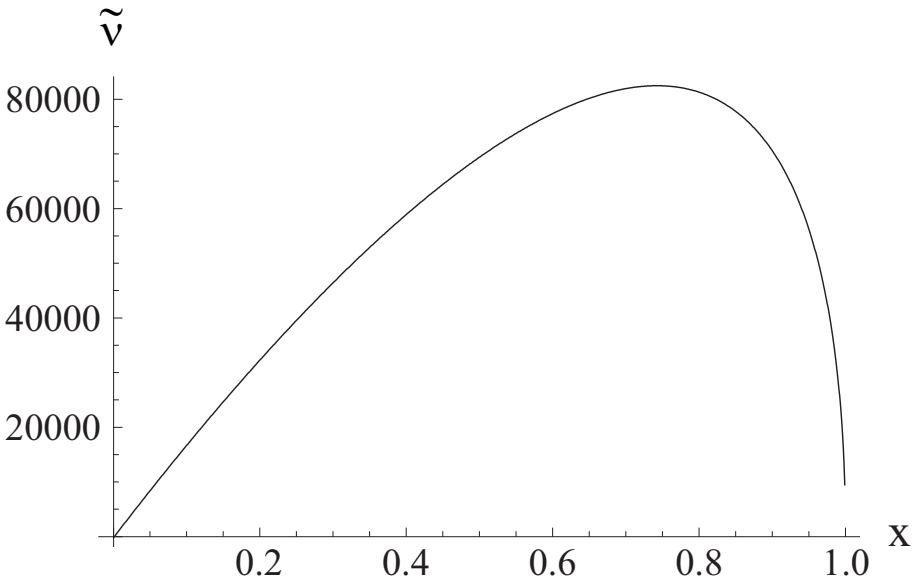


Figure 3.11: $\tilde{\nu}(x)$ of the maximum $y^+S_0^+$ solution for rodlike polymer.

# Chapter 4

# Reduction of drag at small concentrations

This section aims to show analytically that there is indeed a reduction in drag when polymer is added. For simplicity, we consider the case of low polymer concentration (small $\tilde{\nu}$). In this case the change in the mean shear rate $S_0^+$ due to the polymer can be approximated by the first order correction when $\tilde{\nu}$ is increased from zero to a small value. Although there is no direct expression of $S_0^+$ in terms of $\tilde{\nu}$, this expansion can still be carried out by treating $\alpha$ as an implicit function of $\tilde{\nu}$. More specifically,

$$S_0^+(\alpha(\tilde{\nu}, y^+)) = S^+_{0(\alpha=0)}(y^+) + \tilde{\nu}(\frac{\partial S_0^+}{\partial \alpha})_{0(\alpha=0)}(\frac{\partial \alpha}{\partial \tilde{\nu}})_{\tilde{\nu}=0} + O(\tilde{\nu}^2) \tag{4.1}$$

From Eq.(3.4), taking the partial derivative with respect to $\alpha$,

$$y^+(\frac{\partial S_0^+}{\partial \alpha}) = \Delta^2 + 2(\alpha + \frac{1}{y^+})\Delta\partial_\alpha\Delta + \frac{\partial_\alpha\sqrt{W^+}}{\kappa_c} - \frac{\sqrt{W^+}(\partial_\alpha\kappa_c)}{\kappa_c^2} \tag{4.2}$$

The derivatives of $\Delta$ and $\kappa_c$ can be easily evaluated,

$$\partial_\alpha \Delta = \frac{\partial}{\partial \alpha}(\frac{\delta^+}{1-\alpha\delta^+}) = \frac{(\delta^+)^2}{(1-\alpha\delta^+)^2} = \Delta^2 \tag{4.3}$$

$$\partial_\alpha \kappa_c = \frac{\partial}{\partial \alpha}(\frac{a^3}{\Delta^3 b}) = -\frac{3a^3}{b\Delta^2} = -3\kappa_c\Delta \tag{4.4}$$

As a result, the derivative becomes,

$$y^+(\frac{\partial S_0^+}{\partial \alpha}) = \Delta^2 + 2(\alpha + \frac{1}{y^+})\Delta^3 + \frac{3\sqrt{W^+}\Delta}{\kappa_c} + \frac{\partial_\alpha \sqrt{W^+}}{\kappa_c} \tag{4.5}$$

The term $\partial_\alpha \sqrt{W^+}$ is evaluated by partial differentiation of Eq.(2.78).

$$\begin{aligned} \partial_\alpha \sqrt{W^+} &= -\frac{1}{2\kappa_c} - \frac{3\Delta(\alpha + 1/y^+)}{2\kappa_c} \\ &\quad + \frac{1}{\sqrt{\xi}}\{(\frac{\alpha + 1/y^+}{2\kappa_c})[\frac{1}{2\kappa_c} + \frac{3\Delta(\alpha+1/y^+)}{2\kappa_c}] - \\ &\quad (\alpha + 1/y^+)\Delta^2[1 + (\alpha + 1/y^+)\Delta]\} \end{aligned} \tag{4.6}$$

where $\xi = (\frac{\alpha+1/y^+}{2\kappa_c})^2 + 1 - \frac{y^+}{R^+} - (\alpha + \frac{1}{y^+})^2\Delta^2$. Putting the result of Eq.(4.6) into Eq.(4.5),

$$\begin{aligned} y^+(\frac{\partial S_0^+}{\partial \alpha}) &= \Delta^2\Theta(\alpha, y^+, 2) - \frac{1}{2\kappa_c^2}\Theta(\alpha, y^+, 6) \\ &\quad + \frac{1}{\kappa_c\sqrt{\xi}}\{\frac{\alpha + 1/y^+}{(2\kappa_c)^2}\Theta(\alpha, y^+, 6) \\ &\quad - (\alpha + 1/y^+)\Delta^2\Theta(\alpha, y^+, 4) + 3\Delta(1 - \frac{y^+}{R^+})\} \end{aligned} \tag{4.7}$$

where $\Theta(\alpha, y^+, n) \equiv [1 + n(\alpha + 1/y^+)\Delta]$.

We proceed to calculate the value of the derivative at $\alpha = 0$. For $\alpha = 0$,

$$\Theta(\alpha = 0, y^+, n) = 1 + n\frac{\Delta}{y^+} \approx 1 \tag{4.8}$$

since we are considering $y^+ \gg \Delta$.

Therefore for $\alpha = 0$,

$$\begin{aligned}(\frac{\partial S_0^+}{\partial \alpha})_{\alpha=0} &= \frac{1}{y^+}[(\delta^+)^2 - \frac{1}{2\kappa_k^2}] \\ &+ \frac{1}{2\kappa_k^2 y^+\sqrt{1+(1-y^+/R^+)(2\kappa_k y^+)^2}} \end{aligned} \tag{4.9}$$

To complete the expansion, we will need $\partial\alpha/\partial\tilde{\nu}$. It will be obtained by first calculating $\partial\tilde{\nu}/\partial\alpha$ and then taking the reciprocal. Recall that we have previously derived expressions of $\tilde{\nu}$ for flexible and rodlike polymer,

$$\tilde{\nu} = \frac{a[(\alpha+\frac{1}{y^+})\Delta^2 + \frac{\sqrt{W^+}}{\kappa_c}]}{\Delta\sqrt{W^+}}\alpha y^+ \tag{4.10}$$

for flexible polymer. And,

$$\tilde{\nu} = \frac{a^2[(\alpha+\frac{1}{y^+})\Delta^2 + \frac{\sqrt{W^+}}{\kappa_c}]^2}{\Delta^2 W^+}\alpha y^+ \tag{4.11}$$

for rodlike polymer.

We first deal with the flexible polymer case, differentiating $\tilde{\nu}$ with respect to $\alpha$,

$$\begin{aligned}\frac{\partial\tilde{\nu}}{\partial\alpha} &= \frac{a[(\alpha+\frac{1}{y^+})\Delta^2 + \frac{\sqrt{W^+}}{\kappa_c}]}{\Delta\sqrt{W^+}}y^+ \\ &+ \frac{a[\Delta^2 + 2(\alpha+1/y^+)\Delta^3 + \partial_\alpha\sqrt{W^+}/\kappa_c + 3\Delta\sqrt{W^+}/\kappa_c]}{\Delta\sqrt{W^+}}\alpha y^+ \\ &- \frac{a[(\alpha+\frac{1}{y^+})\Delta^2 + \frac{\sqrt{W^+}}{\kappa_c}][\Delta^2\sqrt{W^+} + \Delta(\partial_\alpha\sqrt{W^+})]}{(\Delta\sqrt{W^+})^2}\alpha y^+ \end{aligned} \tag{4.12}$$

The second and third term in the RHS of Eq.(4.12) becomes zero when $\alpha = 0$ because $W^+(\alpha = 0) \neq 0$ outside the viscous sublayer, while $\Delta$ and

the derivative of $W^+$ are well behaved at $\alpha = 0$. Therefore the derivative at $\alpha = 0$ simplifies to,

$$(\frac{\partial \tilde{\nu}}{\partial \alpha})_{\alpha=0} = \frac{ay^+}{\delta^+ \kappa_k} = \frac{by^+}{c_N^2} \tag{4.13}$$

where $c_N \approx 0.5$ is the Newtonian value of $c$ where there is no polymer.

Proceeding to the rodlike polymer case, observe that in Eq.(4.10) and (4.10), the difference in the expressions of $\tilde{\nu}$ for flexible and rodlike polymer is that the coefficient before $\alpha y^+$ for rodlike polymer is the square of the flexible case. So for rodlike polymer,

$$(\frac{\partial \tilde{\nu}}{\partial \alpha})_{\alpha=0} = (\frac{a}{\delta^+ \kappa_k})^2 y^+ = \frac{b^2}{c_N^4} y^+ \tag{4.14}$$

Finally, combining the results, the first order coefficient of the Taylor expansion of $S_0^+$ with respect to the point $\tilde{\nu} = 0$ is,

$$\begin{aligned} (\frac{\partial S_0^+}{\partial \tilde{\nu}})_{\tilde{\nu}=0} &= (\frac{\partial S_0^+}{\partial \alpha})_{\alpha=0} (\frac{\partial \alpha}{\partial \tilde{\nu}})_{\tilde{\nu}=0} \\ &= \frac{\zeta}{(y^+)^2} \{ [(\delta^+)^2 - \frac{1}{2\kappa_k^2}] + \frac{1}{2\kappa_k^2 \sqrt{1 + (1 - y^+/R^+)(2\kappa_k y^+)^2}} \} \end{aligned} \tag{4.15}$$

where $\zeta = \delta^+ \kappa_k / a$ for flexible polymer and $\zeta = (\delta^+ \kappa_k / a)^2$ for rodlike polymer.

$\zeta$ and the second term inside the curly bracket in Eq.(4.15) are obviously positive, while the first term $[(\delta^+)^2 - \frac{1}{2\kappa_k^2}] \approx 32.70$ is also positive. As a result, an small increase of $\tilde{\nu}$ from $\tilde{\nu} = 0$ causes an increase in $S_0^+$, in other words, a reduction in drag. Furthermore, for flexible polymer $\zeta \approx 0.779$ and for rodlike polymer $\zeta \approx 0.607$, so the reduction in drag for flexible polymer is greater than rodlike polymer even for the same $\alpha(y^+)$ profile. Care should be taken when interpreting this result, because major difference in drag reducing power is also caused by the different functional forms of $\alpha(y^+)$ for flexible and rodlike polymers at a given $\tilde{\nu}$, as observed in Chapter 3.

# Chapter 5

# Velocity profiles and friction factor relations

## 5.1 Newtonian flow without polymer

We consider Newtonian flow without polymer in this section, Eq. (2.90) cannot be integrated to give an expression in terms of elementary functions as long as the term $y^+/R^+$ is kept, therefore numerical integration was used instead. We present two velocity profiles in Fig. 5.1, one computed from a numerical integration of Eq. (2.90 with $R^+ = 10000$ and the other directly from Eq. (2.91). Also present in the graph is the von-Karman log law Eq. (2.92). From the graph it can be concluded that at $R^+ = 10000$ the log law is satisfied at around $200 < y < 1000$.

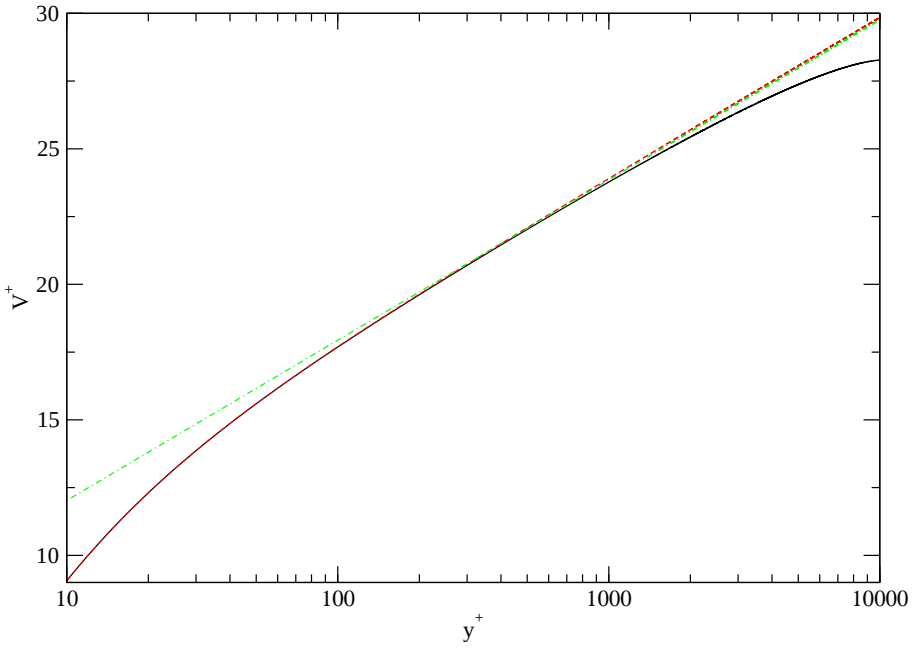


Figure 5.1: Newtonian velocity profiles where there is no polymer. The solid black curve is the velocity profile from Eq. (2.90), in which the $y^+/R^+$ term is kept and $R^+ = 10000$. The dashed red curve has that term dropped and corresponds to the velocity profile of Eq. (2.91). The dash-dotted green curve is the von-Karman log law Eq. (2.92). Notice how the red curve starts to deviate from the black curve when $y^+$ becomes comparable with $R^+$, and that the von-Karman log law (green curve) deviates from the red curve when $y^+$ is not too large compared to $\delta^+$.

The friction factor relation for pipe flow and channel flow are presented in Fig. 5.2 in Prandtl-Karman coordinates ($1/\sqrt{f}$ vs $Re\sqrt{f}$). From Fig. 5.2 it is seen that there is a reasonably straight region of the friction factor relation at large $Re\sqrt{f}$ for both pipe and channel flow, indicating the existence of a log law region. The effect of keeping the $y^+/R^+$ term in the balance equations can be observed by comparing the friction factor relation for pipe

flow with the full expression (solid curve), and the one with $y^+/R^+$ neglected (dotted curve). From the comparison it is concluded that the finite $R^+$ merely shifts the entire friction factor relation curve slightly lower, without causing significant change in the shape of the curve.

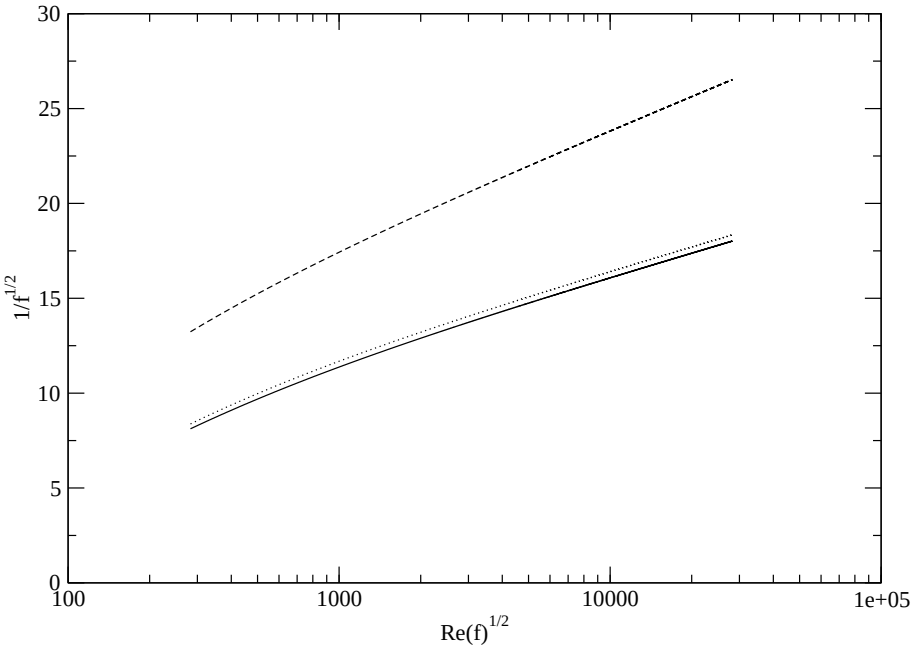


Figure 5.2: Friction factor relations for pipe flow (solid) and channel flow (dashed). The channel flow curve is above the pipe flow curve and therefore has a higher flow rate. Also presented (dotted) is the friction factor relation for pipe flow in which $R^+$ is taken to be infinity, i.e. the $y^+/R^+$ term in the balance equations is neglected.

## 5.2 Flow at high polymer concentration

Previously we have shown that the high polymer concentration limit corresponds to the condition $W^+ = 0$ rather than the maximum $y^+S^+$ profile. In

this subsection we confirm this by comparing results from the two solutions to numerical results at high $\tilde{\nu}$.

The velocity profiles for flexible and rodlike polymers at high polymer concentrations are shown in Figs. 5.3 and (5.4). It is clear that the velocity profiles for both flexible and rodlike polymers at high concentration approaches the $W^+ = 0$ profile rather than the maximum $S_0^+$ profile, with the flexible polymer approaching much faster than its rodlike counterpart, evident from the fact that the $\tilde{\nu} = 10^5$ curve for flexible polymer coincides with the $W^+ = 0$ profile, while for rodlike polymer the profile deviates from the MDR even for $\tilde{\nu}$ as high as $5 \times 10^6$. The velocity profiles overshoot the MDR for some intermediate $\tilde{\nu}$ and then stabilizes back to the MDR. For flexible polymer the velocity profile starts to drop at around $\tilde{\nu} = 5000$, and for rodlike polymer at around $\tilde{\nu} = 50000$. The corresponding friction factor relations are plotted in Figs. 5.5 and 5.6. From the two graphs we see that the $W^+ = 0$ condition matches the friction factor relations at high concentration for high $Re\sqrt{f}$ and $\tilde{\nu}$. The discrepancy at lower $Re\sqrt{f}$ is to be expected because the MDR asymptote is only approached for sufficiently large Reynolds number. The friction factor relations also overshoot the MDR and drop again when $\tilde{\nu}$ is further increased. The $\tilde{\nu}$ at which the maximum occurs differ from the value for the velocity profile we have considered, because in Figs. 5.3 and 5.4 we only considered the large $y^+$ region while the friction factor concerns the whole pipe. In fact, the velocity profiles cross each other at lower $y^+$, and it is the area under the curve that determines the friction factor. For the friction factor relation, the maximum curve occurs at around $\tilde{\nu} = 1000$ for flexible polymer and $\tilde{\nu} = 10000$ for rodlike polymer. It is worth noting that both values are about one-fifth of that for the velocity profile, and the ratio between the values of the flexible and the rodlike cases remains unchanged.

We conclude that the theory predicts that the condition $W^+ = 0$ is what is being approached at the high concentration MDR limit, and the amount of drag reduction may not be a monotonic function of polymer concentration. This result is in contrast to the traditional view that the high concentration limit corresponds to the maximum amount of drag reduction. The existence of a maximum amount of drag reduction at finite concentration has been reported in some experiments and DNS studies [24, 32, 33]. To avoid confusion of the terminology, the high polymer concentration limit will still be denoted as the MDR asymptote in the present work.

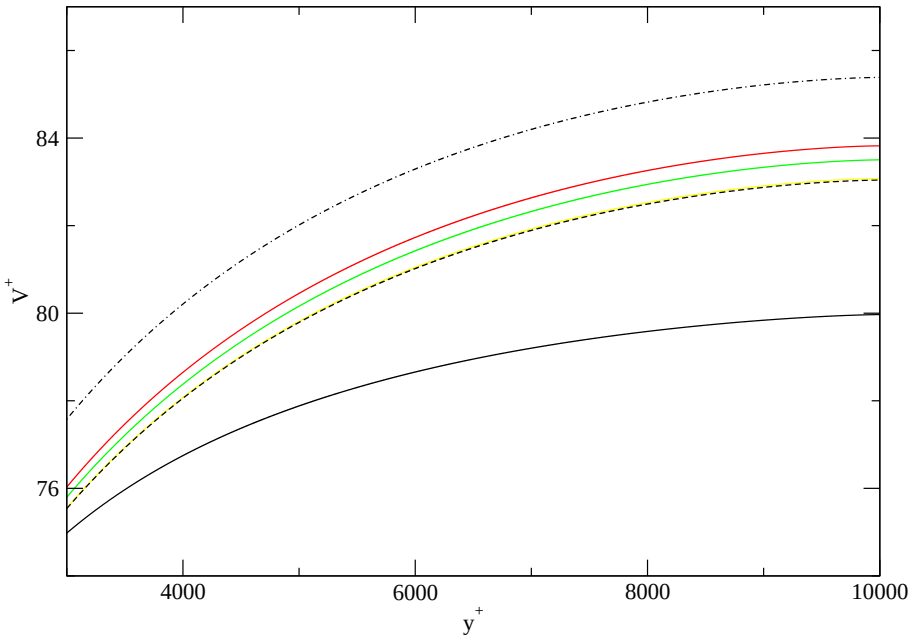


Figure 5.3: Velocity profiles ($R^+ = 10000$) for flexible polymer (solid curves), $\tilde{\nu} = 500$ (black), 5000 (red), 10000 (green), $10^5$ (yellow). Dashed curve is the $W^+ = 0$ profile, and dash-dotted curve the maximum $S^+$ profile. Note that the $\tilde{\nu} = 100000$ curve almost coincides with the $W^+$=0 curve.

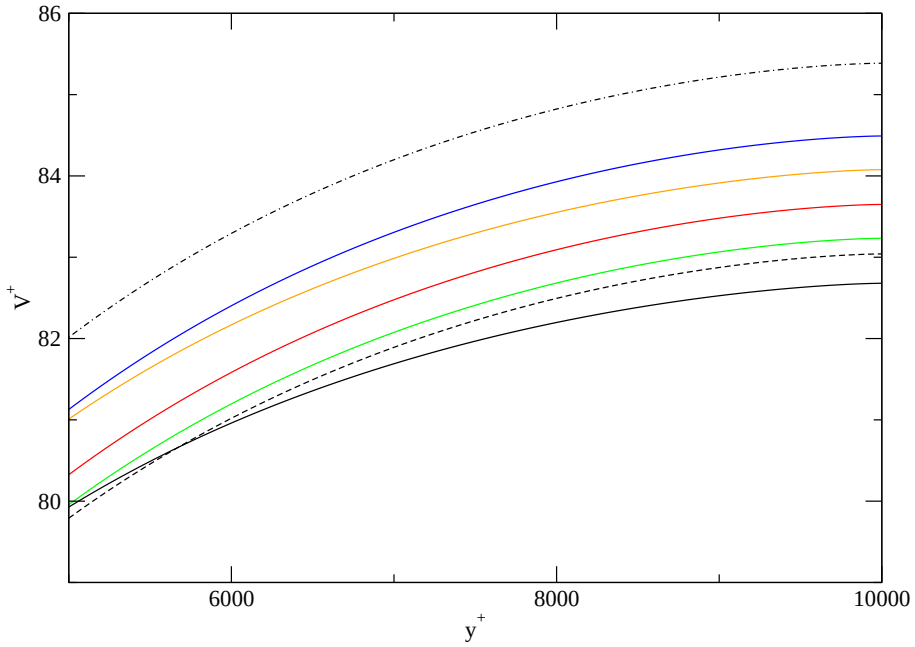


Figure 5.4: Velocity profiles ($R^+ = 10000$) for rodlike polymer (solid curves), $\tilde{\nu} = 5000$ (black), 10000 (orange), 50000 (blue), $5 \times 10^5$ (red), $5 \times 10^6$ (green). Dashed curve is the $W^+ = 0$ profile, and dash-dotted curve the maximum $S^+$ profile. The high $\tilde{\nu}$ profiles appraoch the $W^+ = 0$ profile, but at a much slower rate than the flexible case.

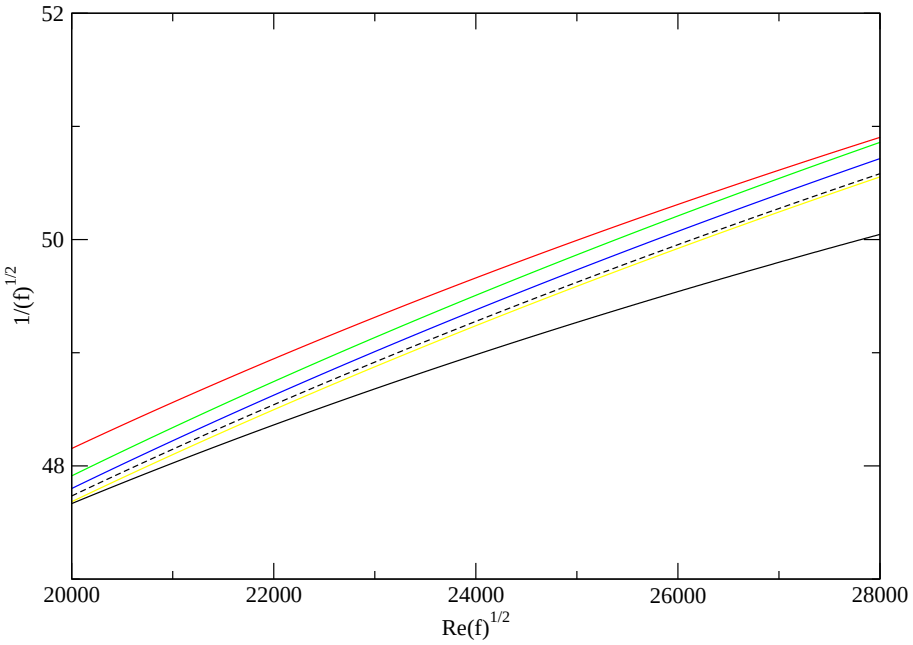


Figure 5.5: Friction factor relations for flexible polymer (solid curves), $\tilde{\nu} =$ 500 (black), 1000 (red), 5000 (green), 10000 (blue), $10^5$ (yellow). Dashed curve is the $W^+ = 0$ friction factor relation.

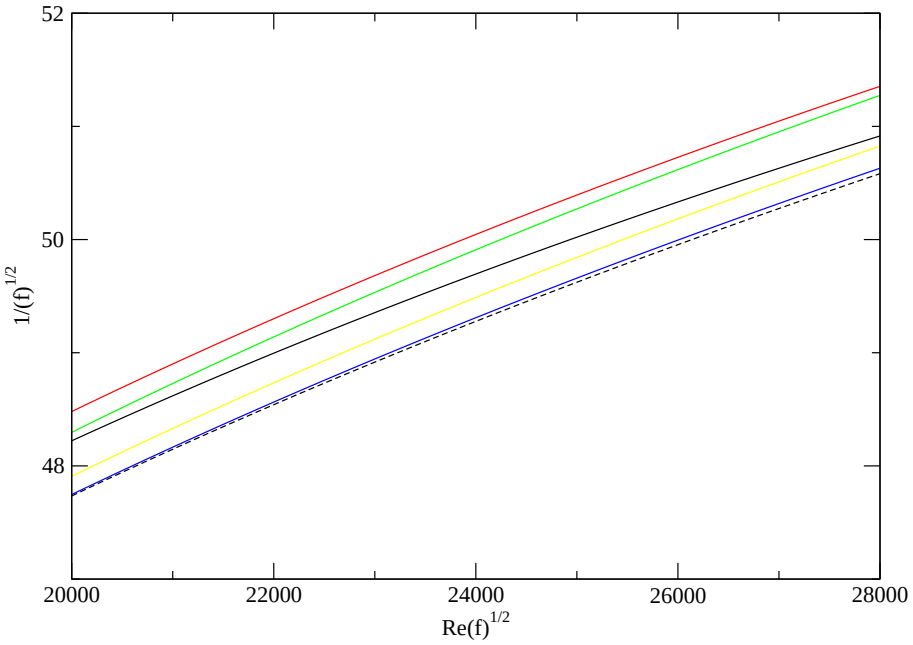


Figure 5.6: Friction factor relations for rodlike polymer (solid curves), $\tilde{\nu} =$ 5000 (black), 10000 (red), 50000 (green), $5 \times 10^5$ (yellow), $5 \times 10^6$ (blue). Dashed curve is the $W^+ = 0$ friction factor relation.

## 5.3 Flow at intermediate concentration

This section presents the results of the velocity profiles and friction factors obtained for pipe flow by solving Eq. (2.89) numerically. To check for self consistency, we show the results at very low concentrations and compare them with the Newtonian values obtained by integrating Eq. (2.90). In Fig. 5.7, the velocity prifles at very low concentrations of flexible polymers are plotted together with the Newtonian profile without polymer. It can be observed that when the concentration is lowered, the profile indeed approaches the Newtonian case with no polymer. A similar trend is observed in Fig. 5.8

with rodlike polymer, and with the profiles much closer to the Newtonian case for the same $\tilde{\nu}$. However, caution should be used when trying to determine the relative strength of drag reduction between flexible and rodlike polymers based on this observation. The reason is that the dependence of $\tilde{\nu}$ on concentration is related to the detailed polymer properties, which is different for different polymers.

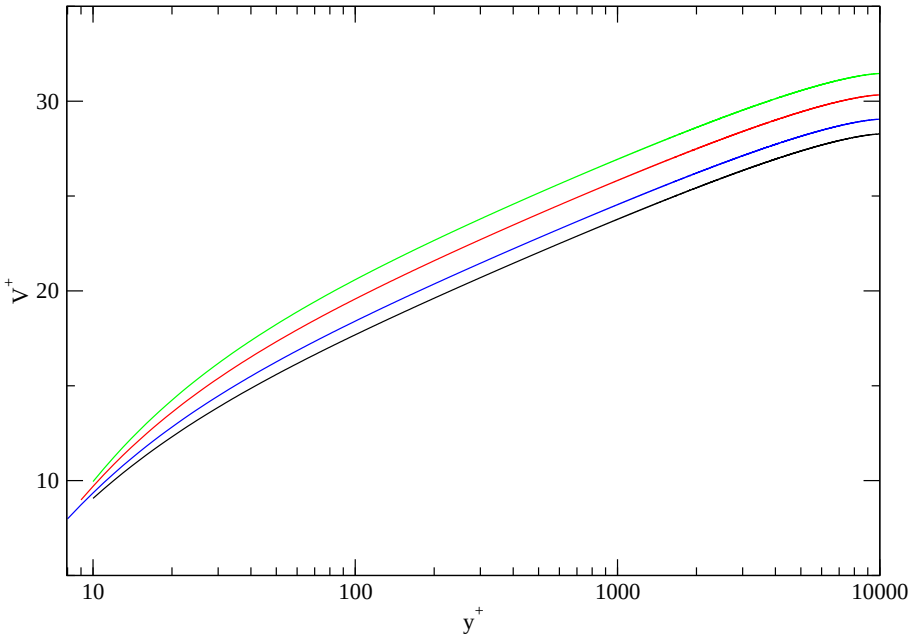


Figure 5.7: Velocity profile for the Newtonian case without polymer (black), $\tilde{\nu} = 0.1$ (blue), 0.3 (red) and 0.5 (green) with flexible polymer ($R^+ = 10000$).

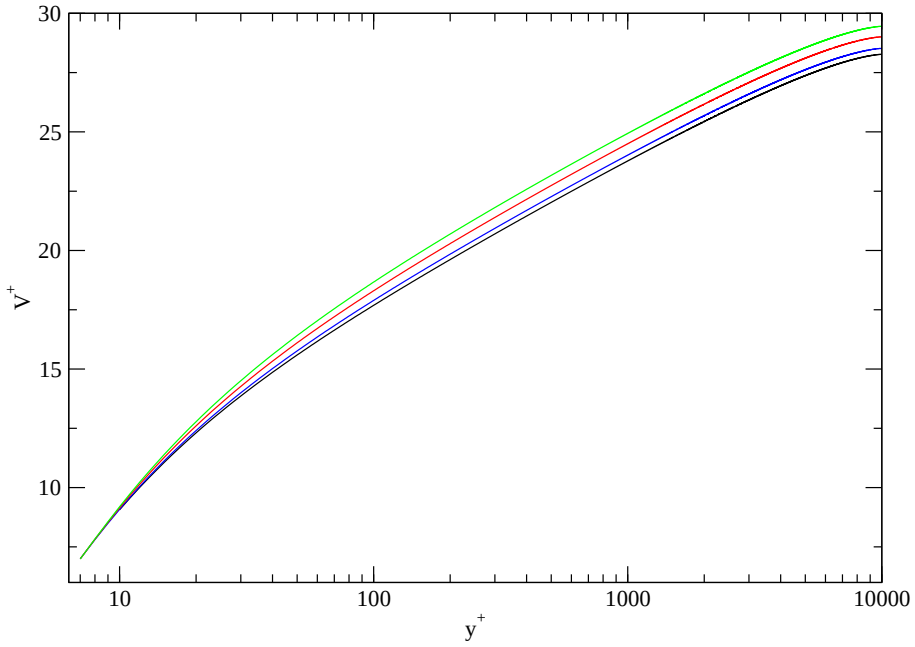


Figure 5.8: Velocity profile for the Newtonian case without polymer (black), $\tilde{\nu} = 0.1$ (blue), 0.3 (red) and 0.5 (green) with rodlike polymer ($R^+ = 10000$).

Next we present a panoramic view of the drag reducing behavior by showing the velocity profiles and friction factors for a wide range of $\tilde{\nu}$ for flexible and rodlike cases. Figures 5.9 and 5.10 shows the velocity profiles for various $\tilde{\nu}$ for flexible and rodlike polymers respectively. Vrik has proposed [4] the elastic sublayer model for flexible polymers in which the velocity profile follows the MDR asymptote for $y^+$ below some critical value, and crosses over back to a region that is parallel to the Newtonian profile without polymer called the Newtonian plug. We check the validity of this model for flexible polymer and rodlike polymer with the data shown in Figs. 5.9 and 5.10. To aid our visualization, we subtract the velocity profiles at different $\tilde{\nu}$ from the MDR profile. This results in Figs. 5.11 and 5.12 for flexible and rodlike polymers respectively. From Fig. 5.11, it can be observed that the subtracted

velocity profiles are close to zero for a range of small $y^+$, indicating that the velocity profiles follow the MDR. This region grows when the concentration is increased, as described by the elastic sublayer model. On the other hand, Fig. 5.12 shows that the velocity profiles of rodlike polymer deviate from the MDR very early on, unless the concentration is very high, where the profiles will follow the MDR for almost the entire pipe. Therefore at low $y^+$ the elastic sublayer model is satisfied by flexible polymer but not rodlike polymer. To investigate the existence of a Newtonian plug, the velocity profiles are subtracted by the Newtonian profile without polymer and shown in Figs. 5.13 and 5.14. Newtonian plugs are observed in both flexible and rodlike cases, characterized by a relatively flat area at high $y^+$. However, there is noticeable deviation from a flat plateau, which is more significant for higher concentration. In addition, the transition from the MDR region to the Newtonian plug for flexible polymer is not sharp as described in the elastic sublayer model.

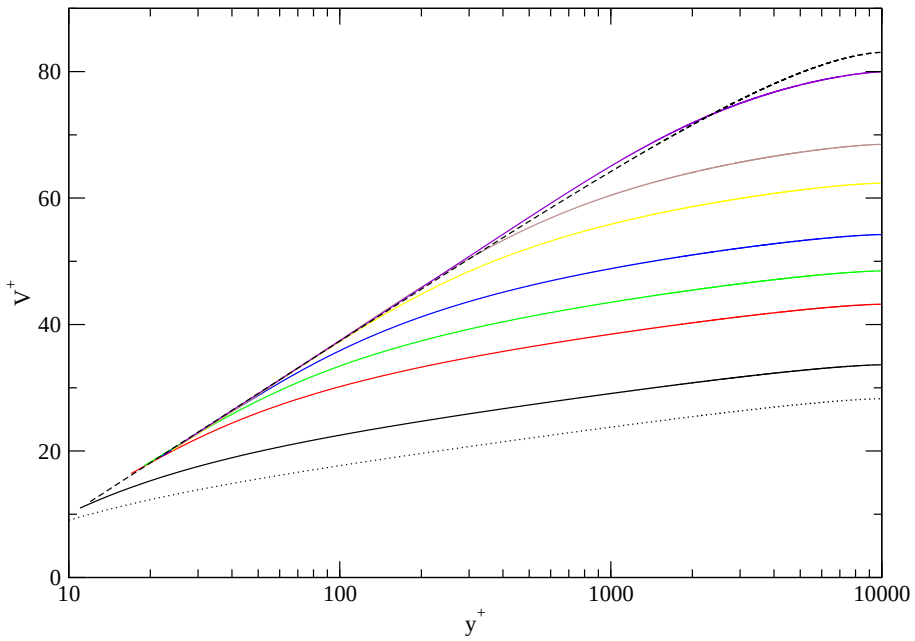


Figure 5.9: Velocity profiles for flexible polymer for $\tilde{\nu} = 0$ (Dotted), 1 (black), 5 (red), 10 (green), 20 (blue), 50 (yellow), 100 (brown) and 500 (violet). The dashed line is the MDR profile.

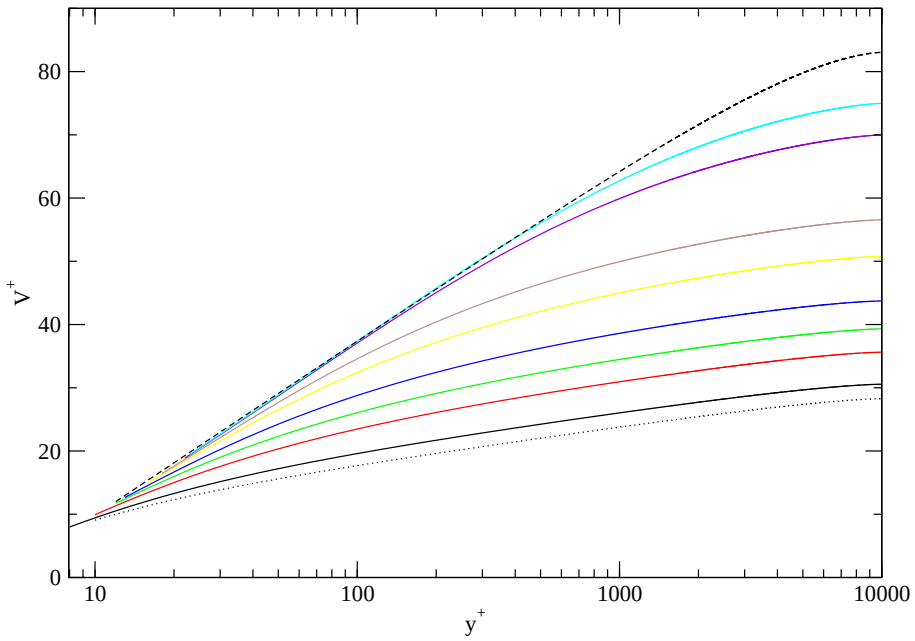


Figure 5.10: Velocity profiles for rodlike polymer for $\tilde{\nu} = 0$ (Dotted), 1 (black), 5 (red), 10 (green), 20 (blue), 50 (yellow), 100 (brown), 500 (violet) and 1000 (cyan). The dashed line is the MDR profile.

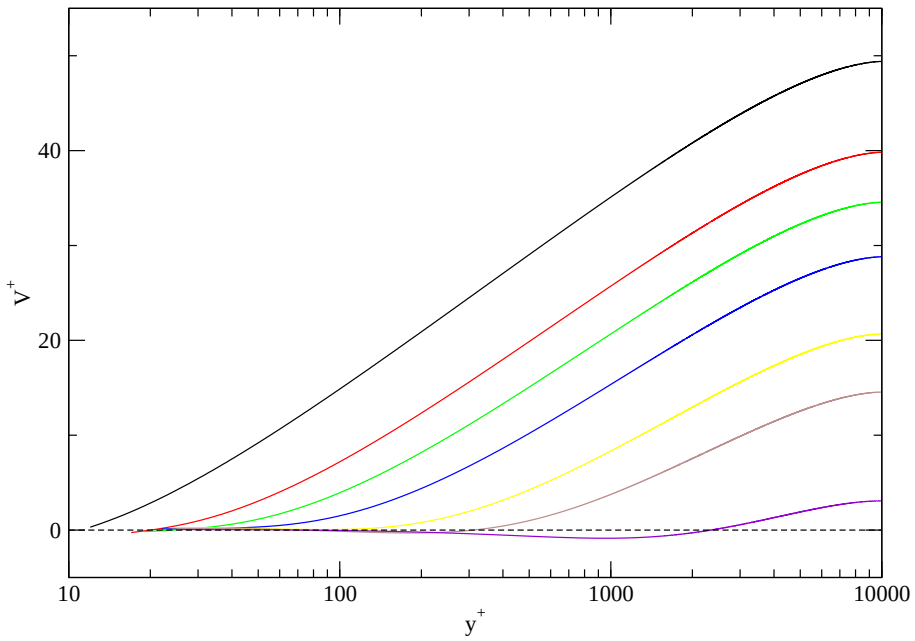


Figure 5.11: Velocity difference between the MDR profile and profiles for flexible polymer with different $\tilde{\nu}$. Positive value means that the velocity is below the MDR. Profiles for $\tilde{\nu} = 1$ (black), 5 (red), 10 (green), 20 (blue), 50 (yellow), 100 (brown) and 500 (violet). The dashed line is the MDR profile which is a horizontal line with an intercept of zero in this representation.

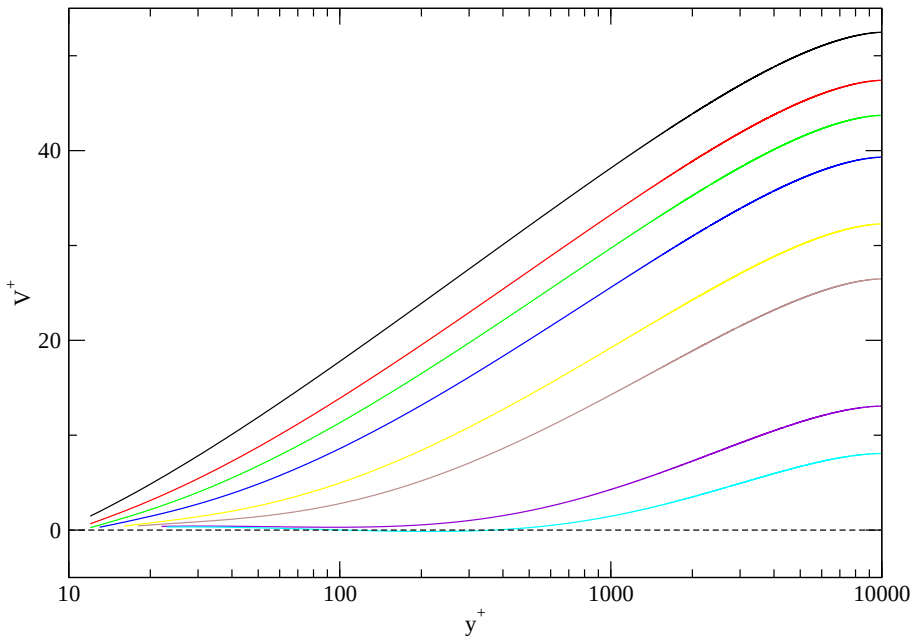


Figure 5.12: Velocity difference between the MDR profile and profiles for rodlike polymer with different $\tilde{\nu}$. Positive value means that the velocity is below the MDR. Profiles for $\tilde{\nu} = 1$ (black), 5 (red), 10 (green), 20 (blue), 50 (yellow), 100 (brown), 500 (violet) and 1000 (cyan). The dashed line is the MDR profile which is a horizontal line with an intercept of zero in this representation.

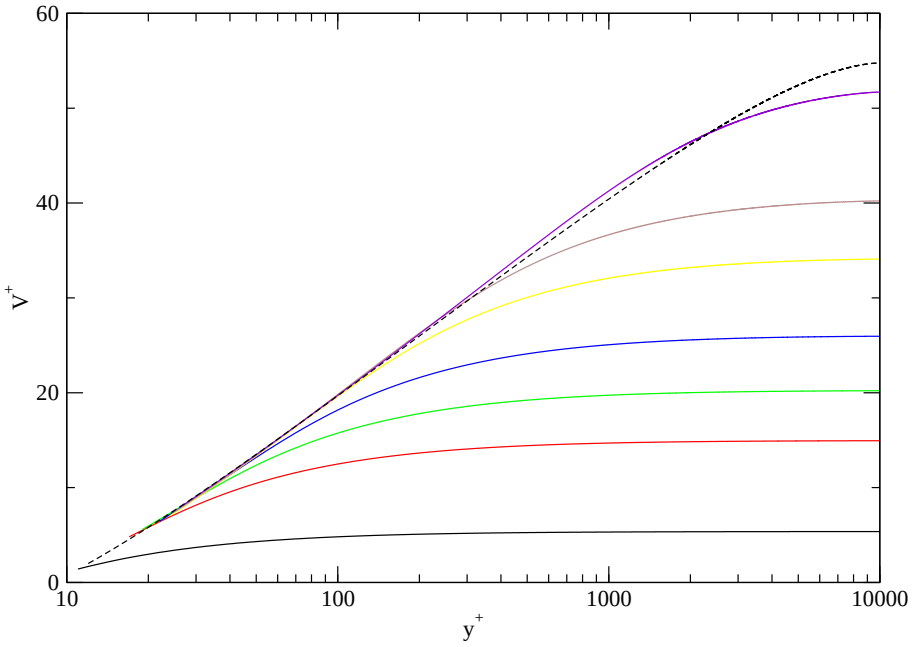


Figure 5.13: Velocity profiles for flexible polymer with different $\tilde{\nu}$ subtracted by the Newtonian profile without polymer. Profiles for $\tilde{\nu} = 1$ (black), 5 (red), 10 (green), 20 (blue), 50 (yellow), 100 (brown) and 500 (violet). The dashed line is the MDR profile.

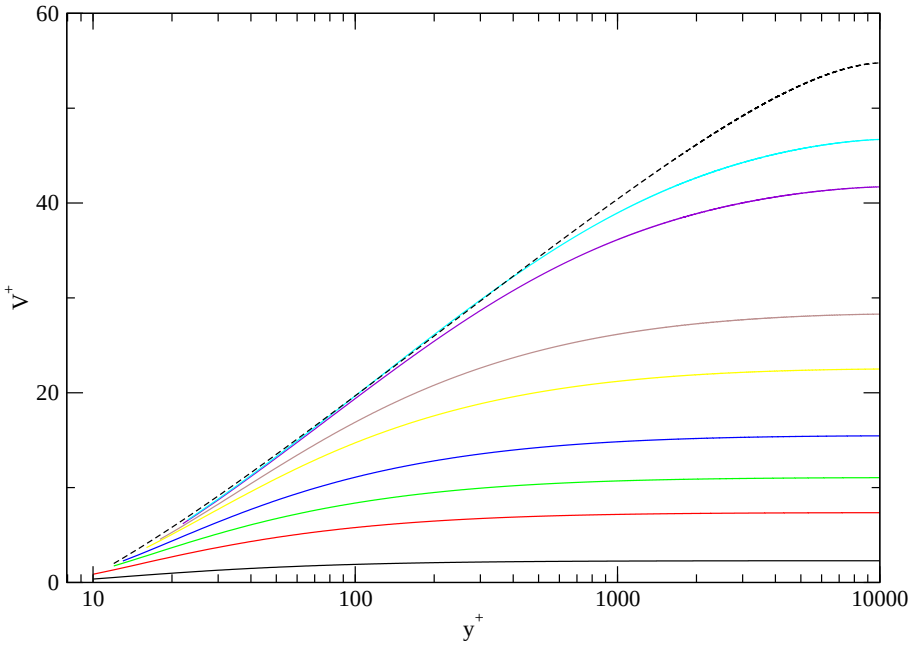


Figure 5.14: Velocity profiles for rodlike polymer with different $\tilde{\nu}$ subtracted by the Newtonian profile without polymer. Profiles for $\tilde{\nu} = 1$ (black), 5 (red), 10 (green), 20 (blue), 50 (yellow), 100 (brown), 500 (violet) and 1000 (cyan). The dashed line is the MDR profile.

The friction factors are presented in Prandtl-Karman coordinates ($1/\sqrt{f}$ vs $Re\sqrt{f}$) for flexible case and rodlike case in Figs. 5.15 and 5.16 respectively.

Recall that in Chapter 1 we quoted the experimental results [2, 6] that the friction factor relations follow different log laws. For flexible polymers,

$$1/\sqrt{f} = (4.0 + D)\log(Re\sqrt{f}) + A \tag{5.1}$$

On the other hand, for rodlike polymers,

$$1/\sqrt{f} = 4.0\log(Re\sqrt{f}) - 0.4 + \delta \tag{5.2}$$

where the slope increment $D$ and effective slip $\delta$ have power law relationships with the polymer concentration.

$$D \sim c^{\omega} \tag{5.3}$$

$$\delta \sim c^{\phi} \tag{5.4}$$

According to Figs. 5.15 and 5.16, our results do not show any profound qualitative difference between the flexible and rodlike case at high $Re\sqrt{f}$. However, the flexible case does seem to show a larger change in slope due to change in $\tilde{\nu}$ at the lower end of $Re\sqrt{f}$. We check the quality of fitting by log laws for flexible and rodlike polymers, which are plotted in Figs. 5.17 and 5.18. In Fig. 5.17 the friction factor relations of flexible polymer at several $\tilde{\nu}$ are plotted with the Newtonian profile without polymer. While they do not follow log laws for the entire range of $Re\sqrt{f}$, we comment that in experiments the log laws are observed over about one decade of $Re\sqrt{f}$. Therefore we separate the graph into three regions: $300 < Re\sqrt{f} < 1000$, $1000 < Re\sqrt{f} < 10000$ and $10000 < Re\sqrt{f} < 30000$. We then fit log laws to them separately, forming the dashed red lines in the figure. As seen from Fig. 5.17, the fitting is satisfactory in most of the regions while the deviations seem to increase with concentration. Similar procedures are conducted in Fig. 5.18. Again, the fittings by Eq. (1.9) are acceptable. There are slighly smaller deviations in the central region, but this is probably due to rodlike polymers causing less drag reduction than flexible polymers at the same $\tilde{\nu}$.

The slope increment $D$ and effective slip $\delta$ as a function of $\tilde{\nu}$ can be extracted from Figs. 5.15 and 5.16 respectively. To obtain results that can be directly compared to the available experimental relations in Eqs. (5.3) and (5.4), we need to know the concentration dependence of the viscosity

parameter $\tilde{\nu}$. However, the form of the relation depends on the concentration range, and for the extremely dilute regime relevant to drag reduction, the available experimental data is inconsistent. Therefore we would like to first study the $\tilde{\nu}$ dependence of the slope increment and effective slip. For the flexible case, we fit log laws to two different regions of Fig. 5.15, $300 < Re\sqrt{f} < 1000$(circles in Fig. 5.19) and $10000 < Re\sqrt{f} < 30000$(crosses), and then obtain the slope for each $\tilde{\nu}$. This slope is then subtracted by the corresponding slope of the Newtonian case without polymer we derived in Section 5.1 to get the slope increment $D$. For the rodlike case, we observe that the friction factor relation curves becomes roughly parallel at high $Re\sqrt{f}$. Therefore we first subtract $1/\sqrt{f}$ by its polymer free Newtonian counterpart at high $Re\sqrt{f}$ to obtain the effective slip $\delta$, represented by circles in Fig. 5.20. Secondly, we fit log law to the Newtonian profile without polymer at $10000 < Re\sqrt{f} < 30000$ and then fit log laws with the same slope fixed at the Newtonian value to the other friction factor relations to obtain the intercept, yielding the effective slip $\delta$ (crosses in Fig. 5.20). In Fig. 5.19 for flexible polymer, the slope increment fitted in the two regions are significantly different at low $\tilde{\nu}$, the slope increment at the higher $Re\sqrt{f}$ region is smaller and saturates slower for increasing $\tilde{\nu}$. In Fig. 5.20 for rodlike polymer the effective slip obtained by the two methods are very close, and saturate at around $\tilde{\nu} = 1000$.

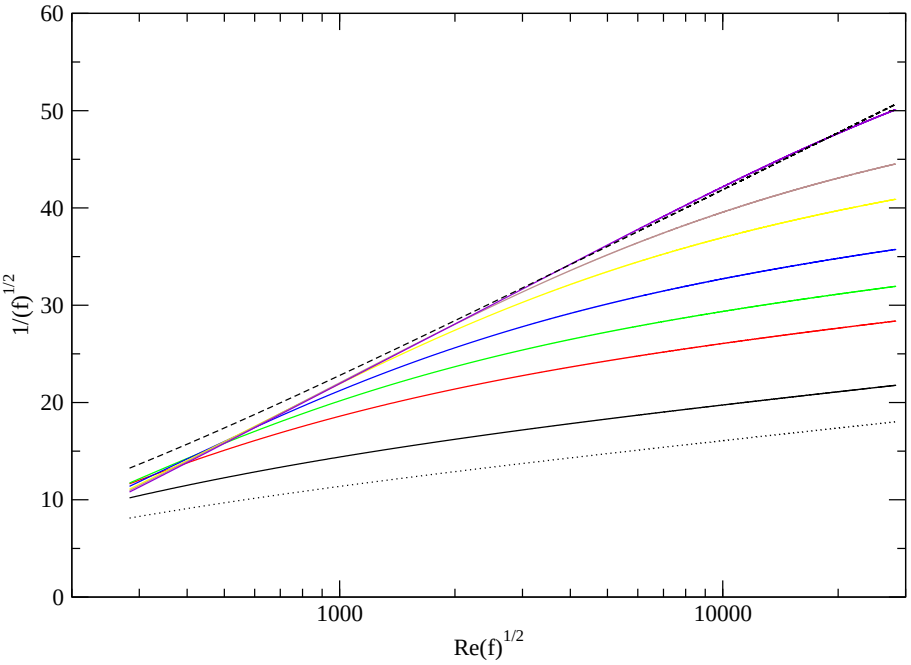


Figure 5.15: Friction factor relations for flexible polymer with different $\tilde{\nu}$. Relations for $\tilde{\nu} = 1$ (black), 5 (red), 10 (green), 20 (blue), 50 (yellow), 100 (brown), 500 (violet) and the MDR(dashed).

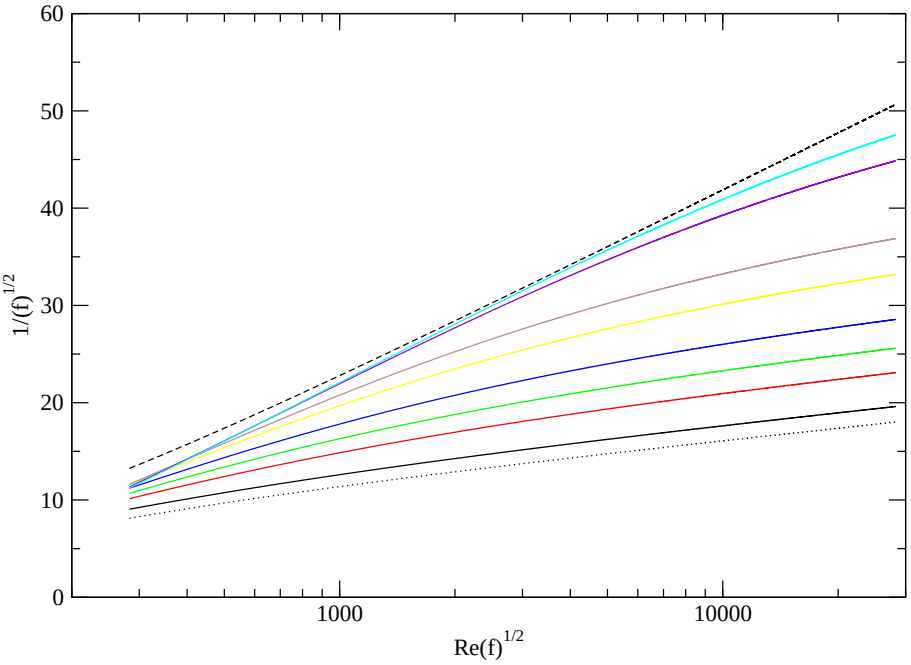


Figure 5.16: Friction factor relations for rodlike polymer with different $\tilde{\nu}$. Relations for $\tilde{\nu} = 1$ (black), 5 (red), 10 (green), 20 (blue), 50 (yellow), 100 (brown), 500 (violet), 1000 (cyan) and the MDR(dashed).

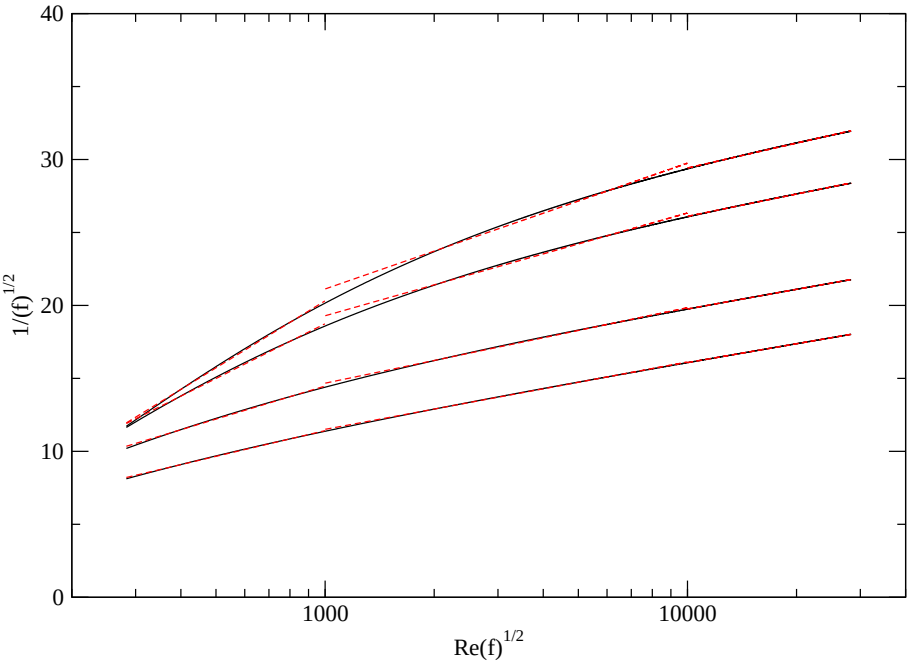


Figure 5.17: Fittings of friction factor relations for flexible polymer with different $\tilde{\nu}$. From bottom to top, $\tilde{\nu} = 0$, 1, 5, 10. Dashed red lines are fittings by log laws applied to three regions separately, $300 < Re\sqrt{f} < 1000$, $1000 < Re\sqrt{f} < 10000$ and $10000 < Re\sqrt{f} < 30000$.

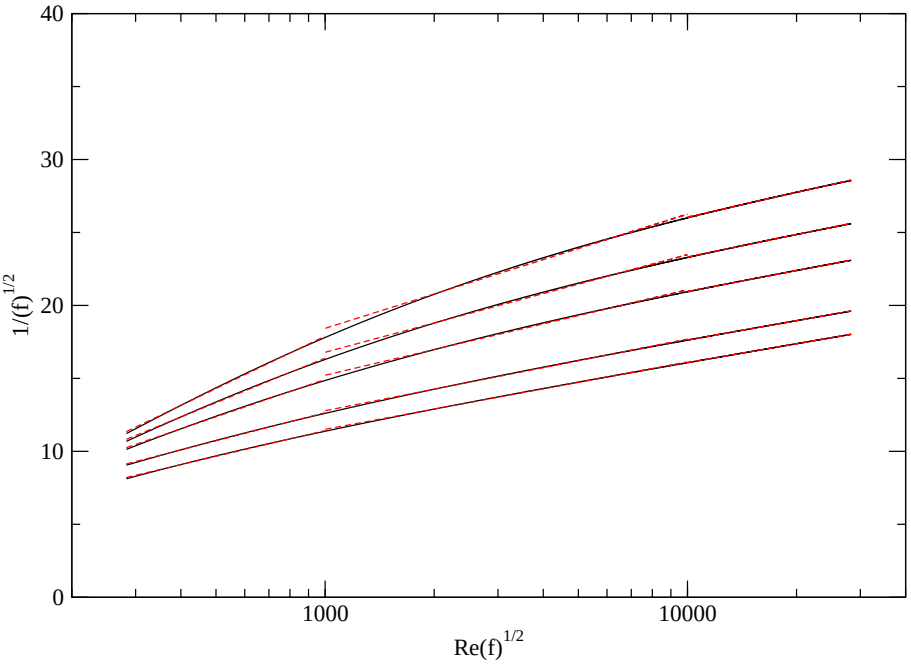


Figure 5.18: Fittings of friction factor relations for rodlike polymer with different $\tilde{\nu}$. From bottom to top, $\tilde{\nu} = 0$, 1, 5, 10, 20. Dashed red lines are fittings by log laws applied to three regions separately, $300 < Re\sqrt{f} < 1000$, $1000 < Re\sqrt{f} < 10000$ and $10000 < Re\sqrt{f} < 30000$.

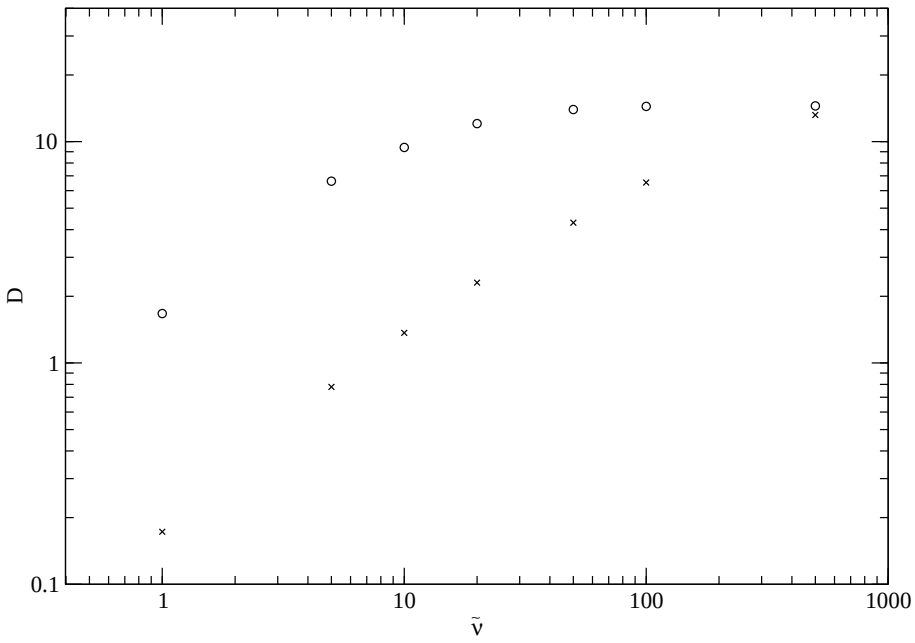


Figure 5.19: The slope increment $D$ as a function of $\tilde{\nu}$. Circles are computed from slopes at $300 < Re\sqrt{f} < 1000$, and crosses from slopes at $10000 < Re\sqrt{f} < 30000$.

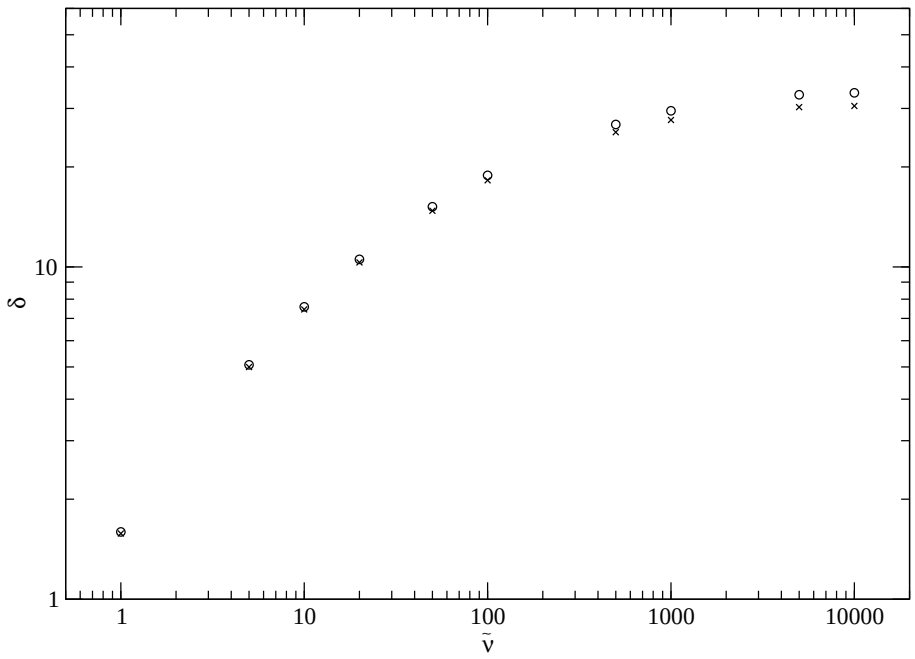


Figure 5.20: The effective slip $\delta$ as a function of $\tilde{\nu}$. Circles are obtained from subtracting the friction factor relations by the Newtonian profile without polymer. Crosses are obtained by fitting lines with the slope of the Newtonian case without polymer at $10000 < Re\sqrt{f} < 30000$ for the intercepts.

As an example of obtaining the concentration dependence from the theory, we present preliminary results using an experimental viscosity-concentration relationship for the rodlike polymer xanthan gum reported in Ref. [34],

$$\tilde{\nu} = 0.011147c^{1.422} \tag{5.5}$$

The resulting friction factor relations at various concentrations are shown in Fig. 5.21.

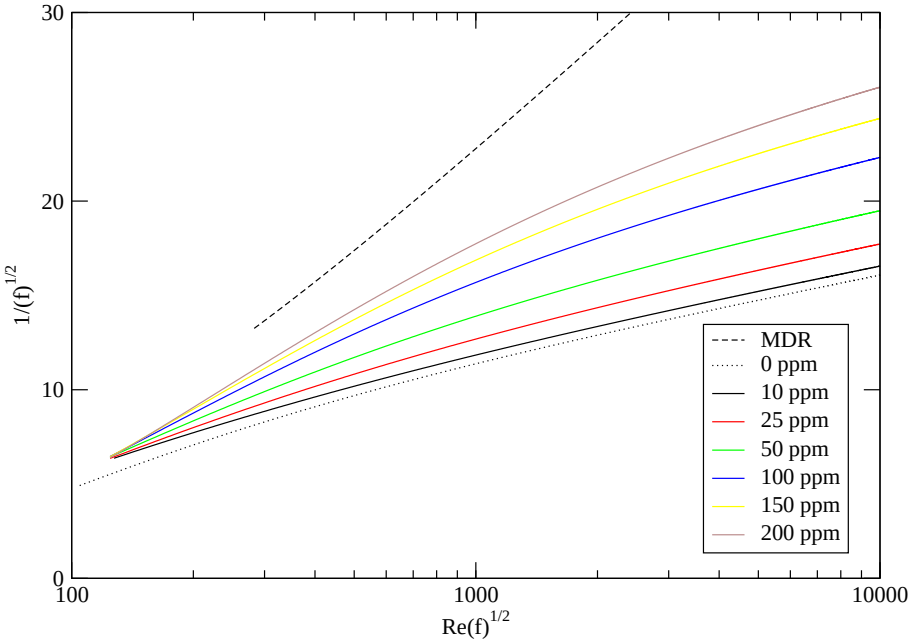


Figure 5.21: Theoretical friction factor relations at different xanthan gum concentrations obtained using Eq. (5.5).

The concentration dependence of the effective slip $\delta$ of xanthan gum is found by subtracting the zero concentration value of $1/\sqrt{f}$ from the polymer laden values at $Re\sqrt{f} = 10000$ in Fig. 5.21. The concentration dependence of the effective slip is presented in Fig. 5.22. The effective slip is well approx-

imated by a power law up to a concentration of about 100 ppm. The fitted exponent is 1.12. Recall that in Chapter 1 we quoted experimental results [2, 6, 7] that found power law relationships in the concentration dependence of the slope increment and effective slip. For the effective slip, Virk reported [6] an exponent of 1 while Sasaki reported [2] a value of about 0.72. The exponent of 1.12 from our result is comparable with these values.

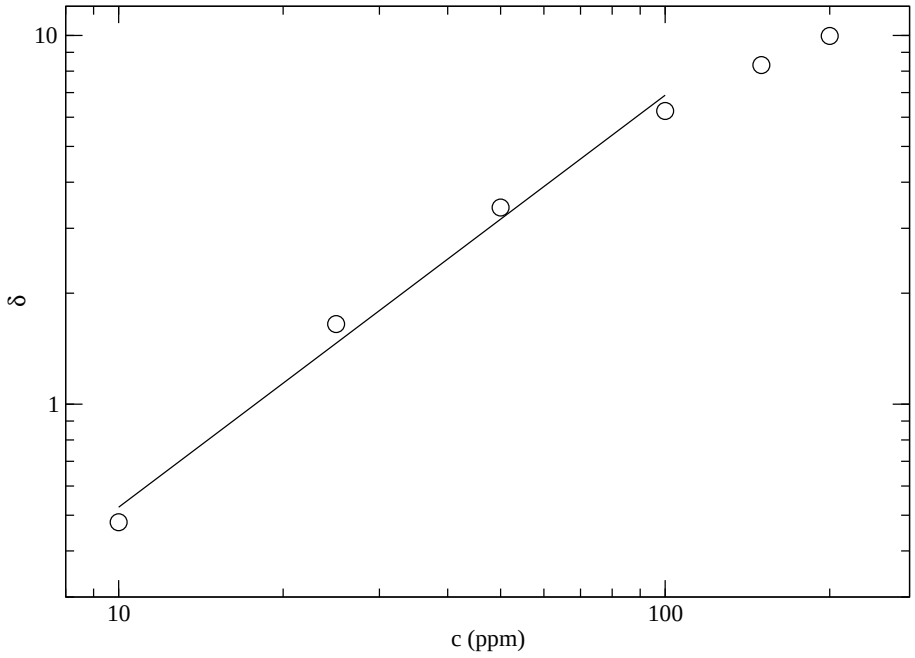


Figure 5.22: Concentration dependence of the effective slip for the data in Fig. 5.21. Solid line is a fitting of power law to the data up to 100 ppm.

# Chapter 6

# The Reynolds stress profile

In this section we show the results of $W^+$ from the theory. Figures 6.1 and 6.2 shows $W^+$ as a function of $y^+$ for flexible and rodlike polymers respectively. We observe that $W^+$ indeed decreases significantly as $\tilde{\nu}$ is increased, with the rate of decline greater for flexible polymer, as has been predicted. Furthermore, the maximum points on each $W^+$ profile trace out a nearly straight line. The maximum value of $W^+$ in each profile is plotted against $\tilde{\nu}$ in Fig. 6.3. Power law is observed at high $\tilde{\nu}$, with the scaling exponents given by $-2.01$ for flexible polymer and $-0.98$ for rodlike polymer, which is consistent with the prediction from our earlier analytical study. The value of $y^+$ at which $W^+$ attains maximum ($y_m^+$) is presented in Fig. 6.4. Power law is found in the intermediate $\tilde{\nu}$ regime, with the exponent 0.45 for flexible polymer and 0.37 for rodlike polymer. Finally, in Fig. 6.5 we check the relationship between the value of the maximum $W^+$ and the position $y_m^+$ at which it is maximum. A good linear fit is found, with $W_{max}^+ = 0.99 - 1.81 \times 10^{-4} y_m^+$ for flexible polymer and $W_{max}^+ = 1.01 - 2.30 \times 10^{-4} y_m^+$ for rodlike polymer. This linear relationship between the maximum value of the Reynolds stress profile and the position of the maximum is a new theoretical prediction. This

linear dependence of $W^+$ for flexible polymer is translated into a relationship for the dimensional Reynolds stress $W$ and compared to experimental data in Fig. 6.6. The relation seems to be plausible, and may be further tested by high precision Reynolds stress measurement for a large range of polymer concentrations.

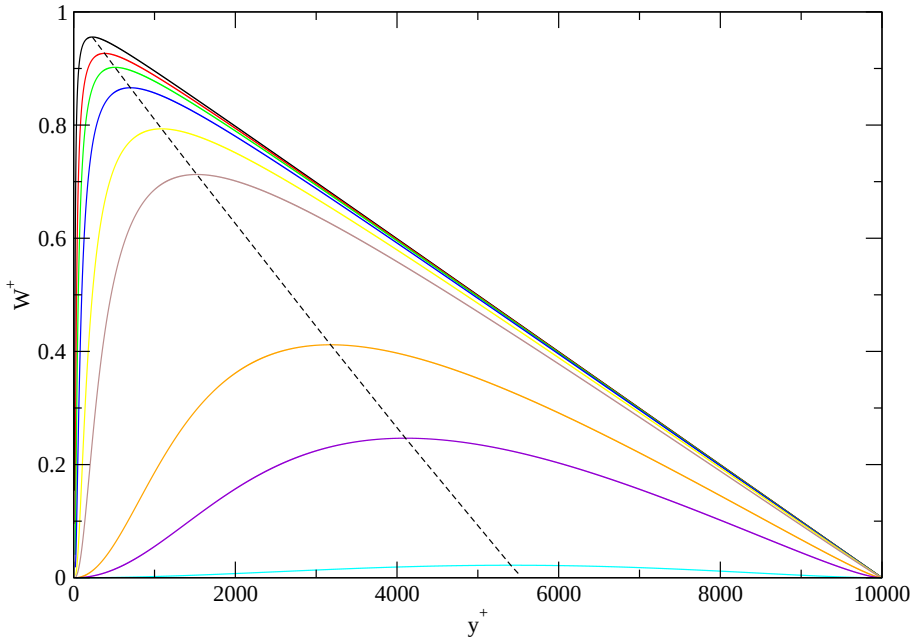


Figure 6.1: $W^+$ profile for flexible polymer. From top to bottom, $\tilde{\nu} = 1$, 5, 10, 20, 50, 100, 500, 1000 and 5000.

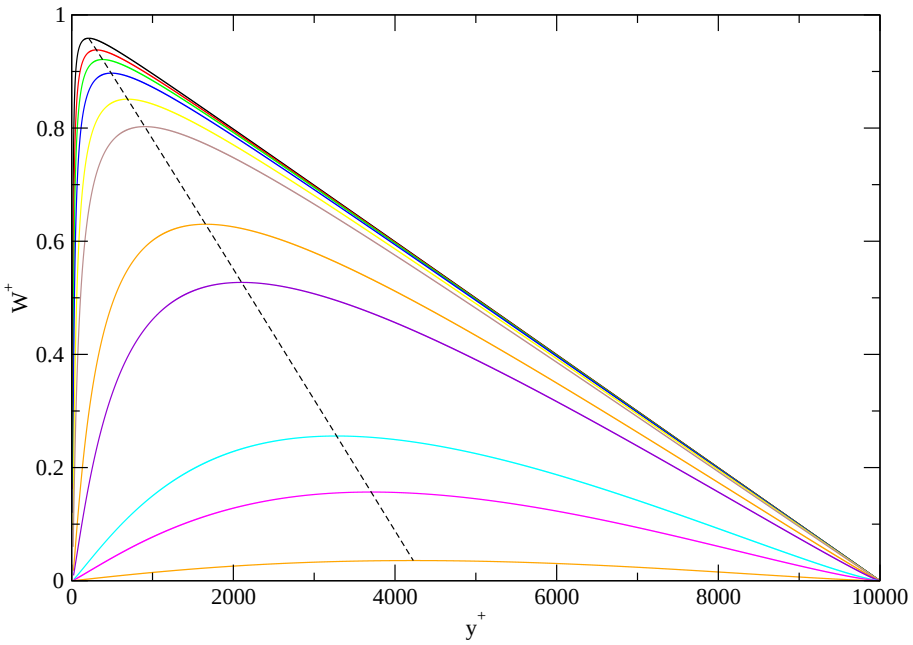


Figure 6.2: $W^+$ profile for rodlike polymer. From top to bottom, $\tilde{\nu} = 1$, 5, 10, 20, 50, 100, 500, 1000, 5000, 10000 and 50000.

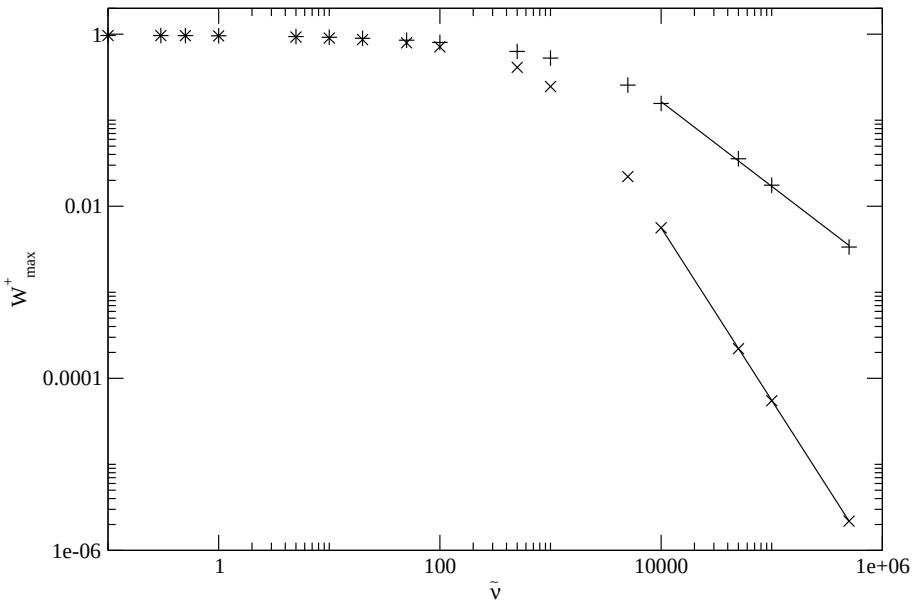


Figure 6.3: Maximum $W^+$ as a function of $\tilde{\nu}$. Crosses refer to flexible polymer and pluses to rodlike polymer. The scaling exponent at high $\tilde{\nu}$ is given by $-2.01$ for flexible polymer and $-0.98$ for rodlike polymer.

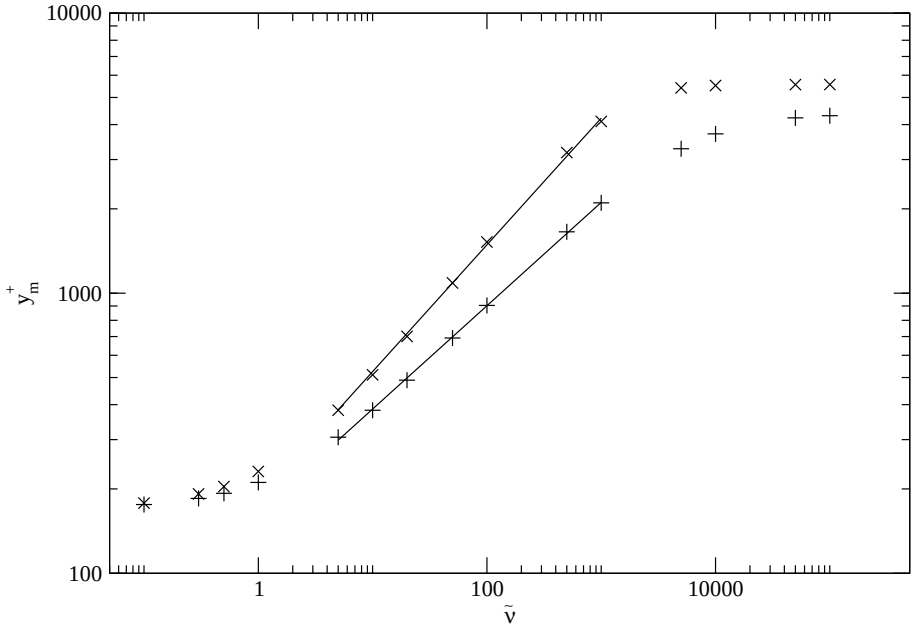


Figure 6.4: $y^+$ at maximum $W^+$ ($y_m^+$) as a function of $\tilde{\nu}$. Crosses refer to flexible polymer and pluses to rodlike polymer. The scaling exponent at intermediate $\tilde{\nu}$ is given by 0.45 for flexible polymer and 0.37 for rodlike polymer.

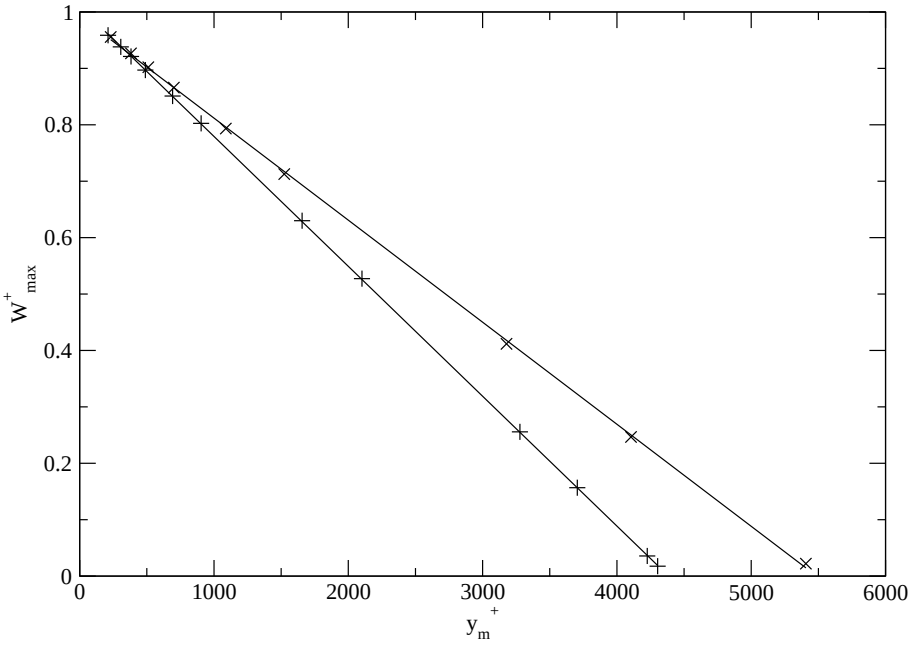


Figure 6.5: Maximum $W^+$ against position $y_m^+$. Crosses refer to flexible polymer and pluses to rodlike polymer. The linear fit gives $W_{max}^+ = 0.99 - 1.81 \times 10^{-4} y_m^+$ for flexible polymer and $W_{max}^+ = 1.01 - 2.30 \times 10^{-4} y_m^+$ for rodlike polymer.

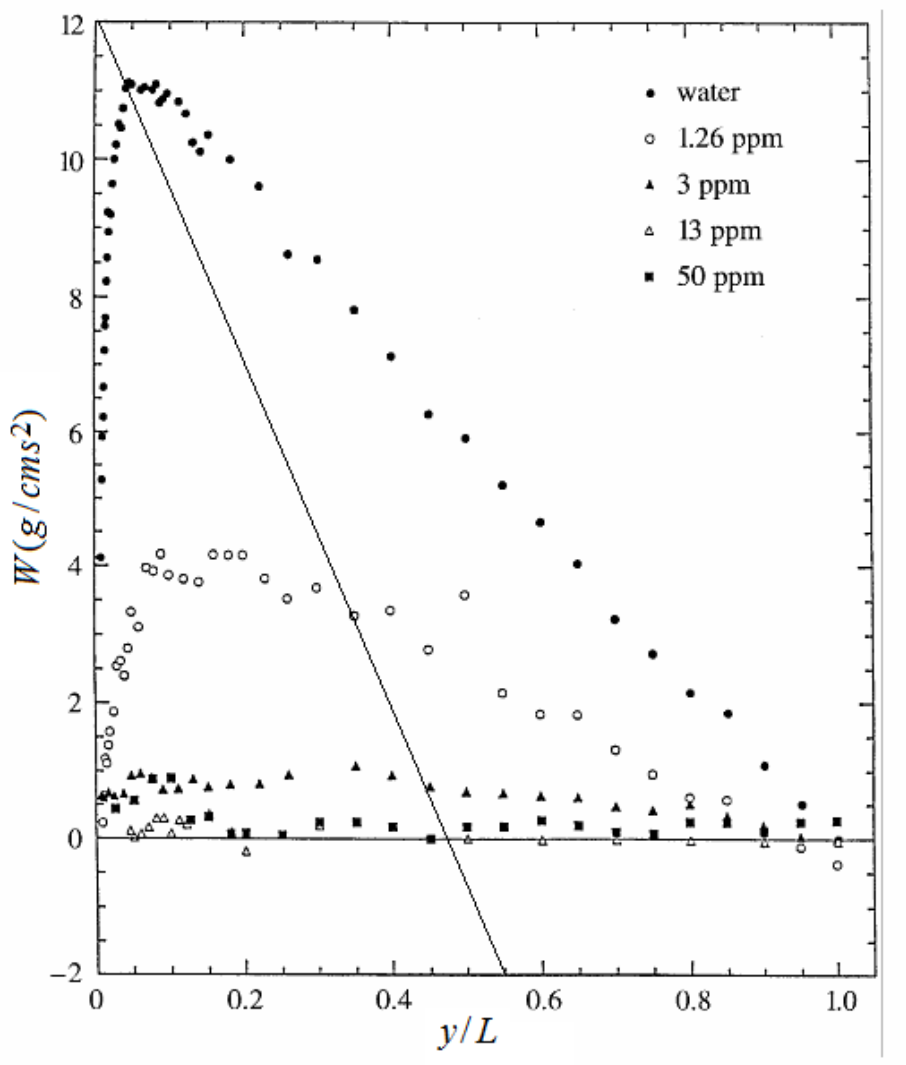


Figure 6.6: Comparison between the relation $W^+_{max} = 0.99 - 1.81 \times 10^{-4} y^+_m$ and experimental Reynolds stress profile.

# Chapter 7

# Percentage drag reduction

From the friction factor $f$, the percentage drag reduction is defined as,

$$DR \equiv (1 - \frac{f}{f_N}) \times 100\% \tag{7.1}$$

where $f_N$ is the friction factor of the Newtonian solvent where there is no polymer.

We present the percentage drag reduction computed from the theory in Figs. 7.1 and 7.2 for flexible and rodlike polymer respectively. In Fig. 7.1 it is found that the percentage drag reduction increases with $\tilde{\nu}$ and the Reynolds number. Saturation at high $\tilde{\nu}$ occurs at $\tilde{\nu} \approx 10$ at $Re = 4300$ to $\tilde{\nu} \approx 1000$ at $Re = 5 \times 10^5$. In Fig. 7.2, the percentage drag reduction also increases with $\tilde{\nu}$ and the Reynolds number, but the saturation occurs at a larger $\tilde{\nu}$ than in the flexible case. The amount of drag reduction at saturation is similar to that in flexible polymer, but it takes a larger $\tilde{\nu}$ to reach the saturated value. Saturation occurs at $\tilde{\nu} \approx 100$ at $Re = 4300$ to $\tilde{\nu} \approx 10000$ at $Re = 5 \times 10^5$. The same amount of drag reduction at saturation and the different rates at which saturation is attained for flexible and rodlike polymers explain the universality of the MDR asymptote and the weaker drag reducing power

usually attributed to rodlike polymers at intermediate concentrations.

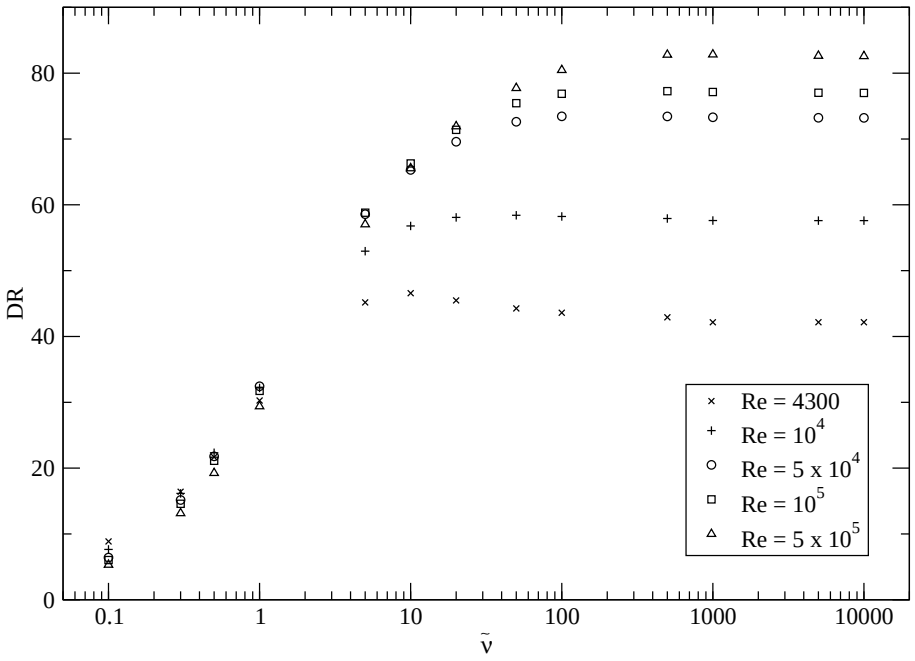


Figure 7.1: Percentage drag reduction against $\tilde{\nu}$ for flexible polymer at different Reynolds number.

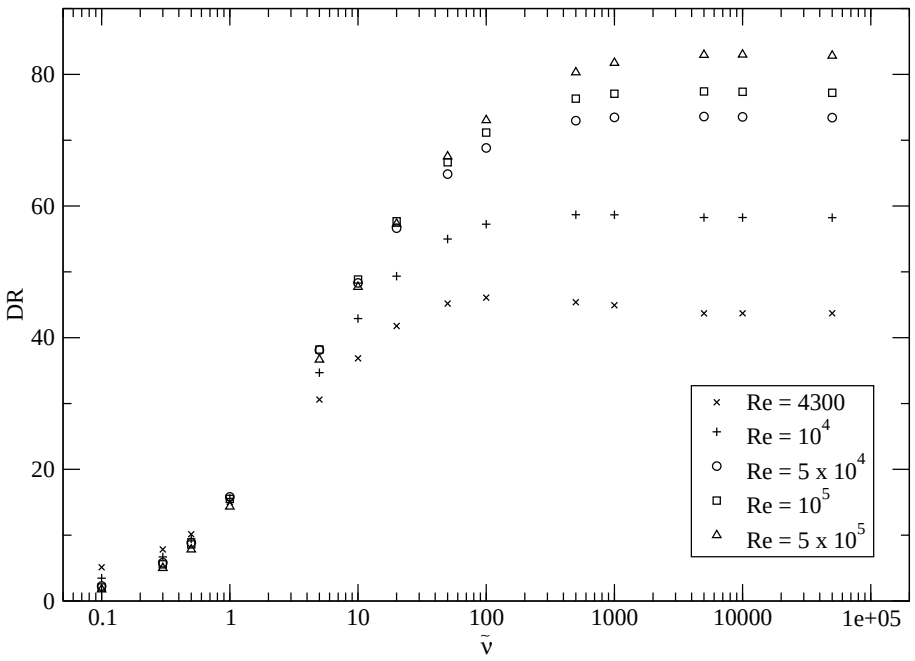


Figure 7.2: Percentage drag reduction against $\tilde{\nu}$ for rodlike polymer at different Reynolds number.

The $\tilde{\nu}$ dependence of the percentage drag reduction at different Reynolds number can be collapsed by normalizing the percentage drag reduction $DR$ by its maximum value $DR_m$, and rescaling $\tilde{\nu}$ by an intrinsic value of $\tilde{\nu}$ denoted as $[\tilde{\nu}]$. $[\tilde{\nu}]$ is the maximum drag reduction divided by the initial slope of the $DR$ vs $\tilde{\nu}$ graph, and therefore has the physical meaning of the $\tilde{\nu}$ required to reach the maximum drag reduction if the entire drag reduction profile is linear with the slope given by the initial slope. We can compute $[\tilde{\nu}]$ theoretically by first extracting the initial slope from the theory. From Eq. (2.93) we have,

$$U_{av}^{+} = (\frac{2}{f})^{1/2} \tag{7.2}$$

From Eqs. (1.2), (7.1) and (7.2), we can evaluate the initial slope $S_i$ as,

$$\begin{aligned} S_i &\equiv (\frac{\partial DR}{\partial \tilde{\nu}})_{\tilde{\nu}=0} = -\frac{1}{f_N}(\frac{\partial f}{\partial \tilde{\nu}})_{\tilde{\nu}=0} \\ &= \frac{8}{f_N(U_{av}^+)^3(R^+)^2}\int_{\delta^+}^{R^+}\int_{\delta^+}^{y^+}(\frac{\partial S_0^+(\hat{y})}{\partial \tilde{\nu}})_{\tilde{\nu}=0}(R^+ - y^+)d\hat{y}dy^+ \end{aligned} \quad (7.3)$$

The expression $(\partial S_0^+(\hat{y})/\partial\tilde{\nu})_{\tilde{\nu}=0}$ has already been evaluated in Eq. (4.15), therefore we can write,

$$\begin{aligned} S_i = \frac{8\zeta}{f_N(U_{av}^+)^3(R^+)^2}\int_{\delta^+}^{R^+}\int_{\delta^+}^{y^+}\frac{1}{(\hat{y})^2}\{[(\delta^+)^2 - \frac{1}{2\kappa_k^2}] \quad + \quad \frac{1}{2\kappa_k^2\sqrt{1+(1-\hat{y}/R^+)(2\kappa_k\hat{y})^2}}\} \\ \times d\hat{y}(R^+ - y^+)dy^+ \end{aligned} \quad (7.4)$$

where $\zeta = \delta^+\kappa_k/a$ for flexible polymer and $\zeta = (\delta^+\kappa_k/a)^2$ for rodlike polymer.

Consider integration of the variable $\hat{y}$, the first term in the curly bracket of Eq. (7.4) gives the integral,

$$\int_{\delta^+}^{y^+}\frac{1}{\hat{y}^2}[(\delta^+)^2 - \frac{1}{2\kappa_k^2}]d\hat{y} = -(\frac{1}{y^+} - \frac{1}{\delta^+})[(\delta^+)^2 - \frac{1}{2\kappa_k^2}] \quad (7.5)$$

Integration of $y^+$ on this term involves the following integral,

$$\begin{aligned} & -[(\delta^+)^2 - \frac{1}{2\kappa_k^2}]\int_{\delta^+}^{R^+}(\frac{1}{y^+} - \frac{1}{\delta^+})(R^+ - y^+)dy^+ \\ = \; & [(\delta^+)^2 - \frac{1}{2\kappa_k^2}]R^+\{\frac{R^+}{2\delta^+} - \ln\frac{R^+}{\delta^+} - \frac{\delta^+}{2R^+}\} \end{aligned} \quad (7.6)$$

Note that in the final result, the first term in the curly bracket dominates over the other terms since in turbulent flow $R^+ \gg \delta^+$.

Integration of the second term in the curly bracket of Eq. (7.4) involves the elliptic integral and is not easily solved, therefore it will be computed numerically. The coefficient $8\zeta/[f_N(U_{av}^+)^3(R^+)^2]$ in Eq. (7.3) can be simplified

as $U_{av}$, $f_N$ and $R^+$ are related.

Using Eq. (7.2),

$$\frac{8\zeta}{f_N(U_{av}^+)^3(R^+)^2} = \frac{2\sqrt{2f_N}\zeta}{(R^+)^2} \tag{7.7}$$

By Eq. (2.96), the results can be expressed in terms of $R^+$ and $Re$ instead,

$$\frac{8\zeta}{f_N(U_{av}^+)^3(R^+)^2} = \frac{8\zeta}{R^+Re} \tag{7.8}$$

The initial slope obtained is shown in Fig. 7.3, and with $DR_m$ calculated at each Reynolds number by using a sufficiently high $\tilde{\nu}$, we get $[\tilde{\nu}]$ in Fig. 7.4. With $[\tilde{\nu}]$ and the percentage drag reduction $DR_m$ we can plot $DR/DR_m$ against $x \equiv \tilde{\nu}/[\tilde{\nu}]$. The plots are shown in Figs. 7.5 and 7.6. From the two graphs we observe that there is a collapse of the data points for reasonably large Reynolds number. We obtained a good fit of the data using the following fitting form,

$$y = \frac{\alpha x^\beta}{1 + \alpha x^\beta} \tag{7.9}$$

where $\alpha$ and $\beta$ are fitting parameters.

From Fig. 7.5 we observe that for flexible polymer the fit matches well with the collapsed data point. The fitted values are $\alpha = 1.38$ and $\beta = 1$. For the rodlike case shown in Fig. 7.6, a good fit is obtained with $\alpha = 0.53$ and $\beta = 0.84$. These functional forms can be tested experimentally by measuring the viscosity dependence of the percentage drag reduction.

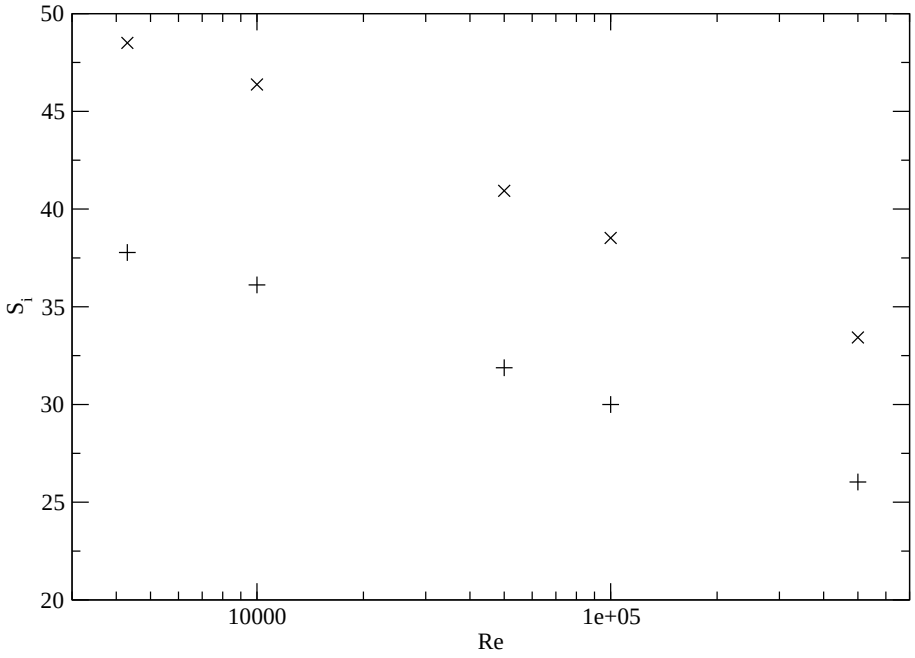


Figure 7.3: Initial slope $S_i$ against Reynolds number $Re$. Crosses refer to flexible polymer and plusses to rodlike polymer.

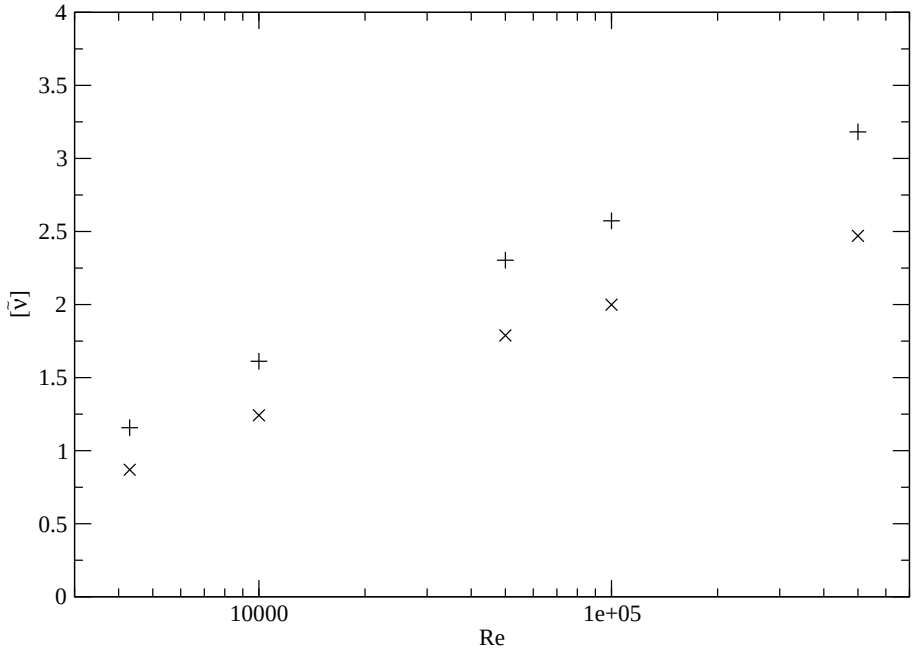


Figure 7.4: $[\tilde{\nu}]$ against Reynolds number $Re$. Crosses refer to flexible polymer and plusses to rodlike polymer.

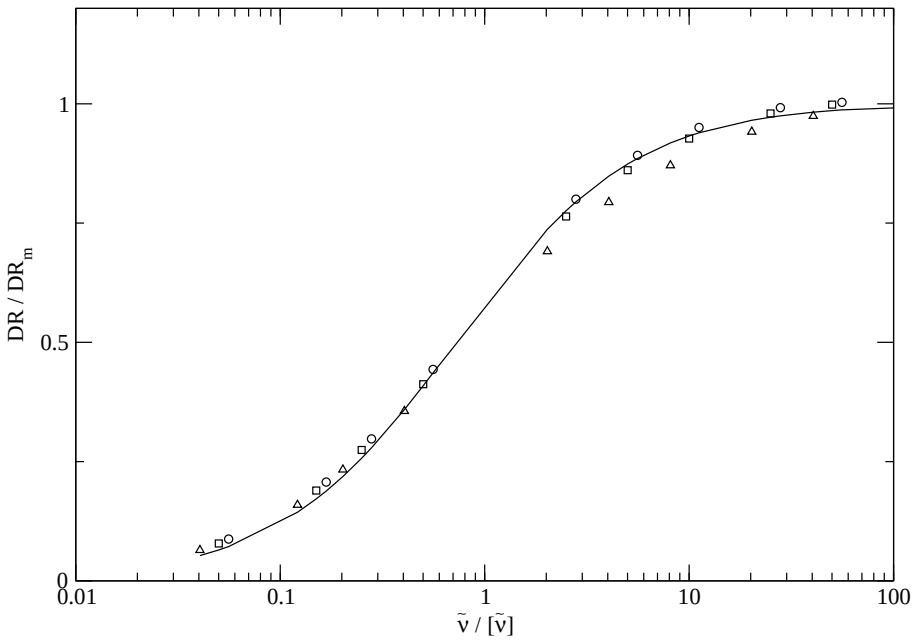


Figure 7.5: $DR/DR_m$ against $\tilde{\nu}/[\tilde{\nu}]$ for flexible polymer. Solid line is the fit Eq. (7.9). The symbols refer to different $Re$ as in Fig. 7.1.

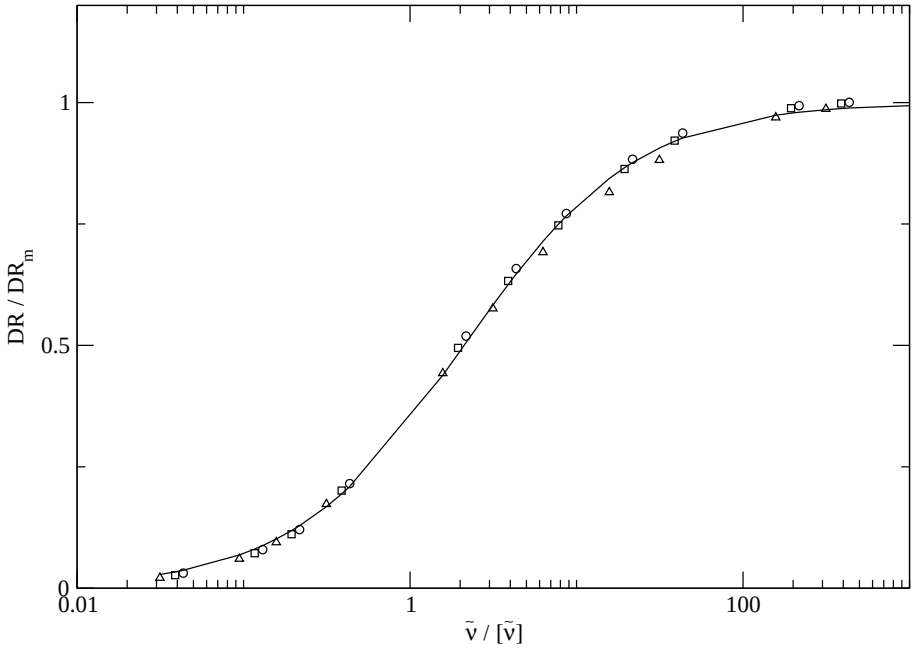


Figure 7.6: $DR/DR_m$ against $\tilde{\nu}/[\tilde{\nu}]$ for rodlike polymer. Solid line is the fit Eq. (7.9). The symbols refer to different $Re$ as in Fig. 7.1.

# Chapter 8

# Conclusion and future work

To conclude, we have used the theory to obtain a general set of equations for the Reynolds stress $W^+$ and the mean shear rate $S_0^+$, which will give back the Newtonian case with no polymer and MDR results when the appropriate limit is taken. We have shown analytically that the MDR asymptote attained at the high polymer concentration limit corresponds to $W^+ = 0$ and differs from the velocity profile that is maximized at every point. We have also shown that accounting for the far-from-wall region ($y^+ \approx R^+$) would have non-trivial effect on the solution of the MDR asymptote. Furthermore, the appearance of drag reduction has been explained using the equations at the small concentration limit.

We have also applied the theory to calculate the mean velocity and Reynolds stress profile for the entire cross-section of the pipe, the friction factor and the percentage drag reduction. The velocity profile of flexible polymer was found to follow the MDR asymptote outside the viscous sublayer, and then crosses over to the Newtonian plug. The velocity profile of rodlike polymer was found to interpolate smoothly between the Newtonian case without polymer and the MDR asymptote. The Reynolds stress pro-

file shows good qualitative agreement with experiment. The new theoretical prediction of a linear relationship between the maximum of the Reynolds stress profile and the position of the maximum matches reasonably well with the experimental data, though more precise measurements are required to verify it. The friction factor relation in Prandtl-Karman coordinates does not show a single log-law that covers a long range of $Re\sqrt{f}$, but effective log laws can be identified over range of $Re\sqrt{f}$ of around a decade. The friction factor does not show profound difference between the flexible and rodlike cases as observed in experiments. The slope increment and effective slip have been extracted. The percentage drag reduction has been obtained for different values of $\tilde{\nu}$. Using the concept of an intrinsic value of $\tilde{\nu}$, we were able to collapse the percentage drag reduction curves at different Reynolds number into a master curve which is well approximated by a functional form of $y = \alpha x^{\beta}/(1 + \alpha x^{\beta})$. These forms can be tested in future experiments.

Possible future work includes obtaining more concrete theoretical predictions for the concentration dependence of drag reduction. Using the viscosity-concentration relationship of any polymer, it is possible to derive polymer-specific theoretical predictions for the velocity profile, Reynolds stress, friction factor and percentage drag reduction. This has been done for the rodlike polymer xanthan gum in Chapter 5. We would like to apply the procedure to other polymers, especially flexible polymers like polyethylene oxide (PEO) and polyacrylamide (PAM). Theoretical results can then be obtained for the concentration dependence of the slope increment and compared to experiments.

# Bibliography


[1] B. Toms, Proc. Int'l Rheological Congress **2**, 135 (1948).

[2] S. Sasaki, J. Phys. Soc. Jap. **60**, 868 (1991).

[3] P. S. Virk, AIChE J. **21**, 625 (1975).

[4] P. S. Virk, J. Fluid Mech. **45**, 417 (1971).

[5] M. V. Zagarola and A. J. Smits, Phys. Rev. Lett. **78**, 239 (1997).

[6] P. S. Virk, Nature **253**, 109 (1975).

[7] P. Virk and H. Baher, Chem. Eng. Sci. **25**, 1183 (1970).

[8] M. D. Warholic, H. Massah, and T. J. Hanratty, Exp. Fluids **27**, 461 (1999), 10.1007/s003480050371.

[9] P. Ptasinski, F. Nieuwstadt, B. van den Brule, and M. Hulsen, Flow Turbul. Combust. **66**, 159 (2001), 10.1023/A:1017985826227.

[10] R. Benzi, E. De Angelis, V. S. L'vov, and I. Procaccia, Phys. Rev. Lett. **95**, 194502 (2005).

[11] J. L. Lumley, Annu. Rev. Fluid Mech. **1**, 367 (1969).

[12] U. Frisch and A. Kolmogorov, *Turbulence: the legacy of A.N. Kolmogorov*, Cambridge University Press, 1995.

[13] A. B. Metzner and A. P. Metzner, Rheol. Acta **9**, 174 (1970), 10.1007/BF01973476.

[14] M. T. Landhal, Drag reduction by polymer addition, in *Proceedings of the 13th International Congress of Theoretical and Applied Mechanics*, pages 177–199, Moscow, 1973, Springer.

[15] E. J. Hinch, Phys. Fluids **20**, S22 (1977).

[16] P. D. Gennes, Physica A **140**, 9 (1986).

[17] P. Pincus, Macromolecules **9**, 386 (1976).

[18] K. R. SREENIVASAN and C. M. WHITE, J. Fluid Mech. **409**, 149 (2000).

[19] R. H. Nadolink, *Friction reduction in dilute polystyrene solutions*, PhD thesis, University of California at San Diego, La Jolla, CA, 1987.

[20] N. S. Berman, Phys. Fluids **20**, s168 (1977).

[21] R. W. Patterson and F. H. Abernathy, J. Fluids Mech. **43**, 689 (1970).

[22] P. S. Virk, J. Fluid Mech. **45**, 225 (1971).

[23] B. Gampert and P. Wagner, Arch. Mech. **34**, 493 (1982).

[24] D. H. Lee and R. Akhavan, Scaling of polymer drag reduction with polymer and flow parameters in turbulent channel flow, in *Advances in Turbulence XII*, edited by B. Eckhardt, volume 132 of *Springer Proceedings Physics*, pages 359–362, Springer Berlin Heidelberg, 2009.

[25] V. S. L'vov, A. Pomyalov, I. Procaccia, and V. Tiberkevich, Phys. Rev. Lett. **92**, 244503 (2004).

[26] R. Benzi, E. S. C. Ching, T. S. Lo, V. S. L'vov, and I. Procaccia, Phys. Rev. E **72**, 016305 (2005).

[27] E. S. C. Ching, T. S. Lo, and I. Procaccia, Phys. Rev. E **74**, 026301 (2006).

[28] R. Benzi, E. De Angelis, V. S. L'vov, I. Procaccia, and V. Tiberkevich, J. Fluid Mech. **551**, 185 (2006).

[29] V. S. L'vov, A. Pomyalov, I. Procaccia, and V. Tiberkevich, Phys. Rev. E **71**, 016305 (2005).

[30] R. B. Bird, C. F. Curtiss, R. C. Armstrong, and O. Hassager, *Dynamics of Polymeric Fluids*, volume 2, Wiley, 1987.

[31] M. Doi and S. F. Edwards, *The Theory of Polymer Dynamics*, Oxford University Press, Oxford, 1988.

[32] C. A. Kim, D. S. Jo, H. J. Choi, C. B. Kim, and M. S. Jhon, Polym. Test. **20**, 43 (2000).

[33] J. I. Sohn, C. A. Kim, H. J. Choi, and M. S. Jhon, Carbohyd. Polym. **45**, 61 (2001).

[34] Y. Amarouchene et al., Phys. Fluids **20**, 065108 (2008).